ACCELERATED IMPLEMENTATION OF INTELLIGENT COMPACTION TECHNOLOGY FOR EMBANKMENT SUBGRADE SOILS, AGGREGATE BASE, AND ASPHALT PAVEMENT MATERIALS

Final Report ER10-01
US219, Springville, NY, Field Project
May 17 to 21, 2009

Prepared By

David J. White, Ph.D.
Pavana KR. Vennapusa, Ph.D.
Heath Gieselman
Jiake Zhang
Rachel Goldsmith
Luke Johanson
Stephen Quist

Earthworks Engineering Research Center (EERC)
Department of Civil Construction and Environmental Engineering
Iowa State University
2711 South Loop Drive, Suite 4600
Ames, IA 50010-8664
Phone: 515-294-1463
www.eerc.iastate.edu

January 30, 2010

TABLE OF CONTENTS

LIST OF FIGURES

LIST OF TABLES

ACKNOWLEDGMENTS

This study was funded by US FHWA research project DTFH61-07-C-R0032 “Accelerated Implementation of Intelligent Compaction Technology for Embankment Subgrade Soils, Aggregate Base, and Asphalt Pavement Materials”. George Chang from the Transtec Group, Inc. is the Principal Investigator for this research project. Robert D. Horan is the project facilitator and assisted with scheduling rollers for the project. Allen Declerk with Caterpillar, Inc., and Dave Dennison and Hans-Jurgen Wagner with Bomag Fayat Group provided IC rollers and field support during the project. Deeyvid Saez with Texas A&M University performed in-situ testing using Briaud Compaction Device and provided the results. Ronald Berube, P.E., with TransTech Systems, Inc., performed in-situ testing using Soil Density Gauge and provided the results. Several NYDOT personnel assisted with falling weight deflectometer testing, Troxler nuclear moisture-density gauge testing, and Zorn light weight deflectometer testing. Many other people assisted with the coordination and participated in the field demonstrations and their assistance and interest is greatly appreciated.

LIST OF SYMBOLS

a	Theoretical vibration amplitude
a_{max}	Maximum theoretical vibration amplitude
A_{Ω}	Acceleration at fundamental frequency
$A_{2\Omega}$	Acceleration at second order harmonic
$A_{0.5\Omega}$	Acceleration at sub-harmonic
A’	Machine acceleration
AFC	Automatic feedback control
b	machine internal loss coefficient used in MDP calculation
b_0	Intercept in a linear regression equation
b_1, b_2, b_3	Regression coefficients
B	Contact width of the drum
C	Semivariogram scale
C_0	Semivariogram nugget
$C+C_0$	Semivariogram sill
CBR	California bearing ratio
CBR_{300}	Weighted average CBR to a depth of 300 mm
CBR_{Base}	Weighted average CBR to a depth equal to the depth of the base material
CCV	Caterpillar compaction value
CMV	Compaction meter value
COV	Coefficient of variation (calculated as the ratio of mean and standard deviation)
DPI	Dynamic cone penetration index
d_0	measured settlement under plate
D_{10}	Particle size corresponding to 10% passing
D_{30}	Particle size corresponding to 30% passing
D_{60}	Particle size corresponding to 60% passing
E	Elastic modulus
E_{BCD}	Modulus determined from Briaud Compaction Device (BCD)
$E_{LWD\text{-}Z2}$	Elastic modulus determined from 200-mm plate Zorn light weight deflectometer
$E_{LWD\text{-}Z3}$	Elastic modulus determined from 300-mm plate Zorn light weight deflectometer
$E_{FWD\text{-}K3}$	Elastic modulus determined from 300-mm plate KUAB falling weight deflectometer
E_{V1}	Initial modulus from 300-mm diameter static plate load test
E_{V2}	Reload modulus from 300-mm diameter static plate load test
E_{VIB}	Vibratory modulus determined from the roller
f	Vibration frequency
F	Shape factor
F_s	Drum force
g	Acceleration of gravity
G_s	Specific gravity
GPS	Global positioning system
h	Separation distance
IC-MV	Intelligent compaction measurement value
LL	Liquid limit
m	machine internal loss coefficient used in MDP calculation

MDP	Caterpillar Machine drive power
MDP_{40}	See description in text
n	Number of test measurements
p	Number of regression parameters
P_g	Gross power needed to move the machine
PL	Plastic limit
PI	Plasticity index
r	Radius of the plate
R	Semivariogram range
R’	Radius of the roller drum
R^2	Coefficient of determination
R^2(adjusted)	Adjusted coefficient of determination (adjusted for number of parameters in multiple regression analysis)
RMV	Resonant meter value
v	Roller velocity
$w_{(H)}$	Moisture content determined from Humboldt nuclear gauge
$w_{(T)}$	Moisture content determined from Troxler nuclear gauge
$w_{(SDG)}$	Moisture content determined from Transtech’s Soil Density Gauge (SDG)
w_{opt}	Optimum moisture content
W	Roller weight
z_d	Drum displacement
α	Slope angle (roller pitch from a sensor)
μ	Statistical mean
σ	Statistical standard deviation
σ_0	Applied stress
η	Poisson’s ratio
$\gamma_{d(H)}$	Dry unit weight determined from Humboldt nuclear gauge (NG)
$\gamma_{d(T)}$	Dry unit weight determined from Troxler nuclear gauge (NG)
$\gamma_{d(SDG)}$	Dry unit weight determined from Transtech’s Soil Density Gauge (SDG)
γ_{dmax}	Maximum dry unit weight
$\gamma(h)$	Semivariogram

INTRODUCTION

The Iowa State University (ISU) research team performed field testing on the US219 project located near Springville, New York from May 17–21, 2009. Caterpillar and Bomag single drum intelligent compaction (IC) rollers were evaluated at this project. The project involved constructing and testing calibration and production areas with granular embankment subgrade and subbase materials (identified as Type I materials in the project proposal). An open house was conducted near the end of the investigation to disseminate results from current and previous IC projects. The New York department of transportation (DOT), contractor's personnel, and representatives from the IC roller manufacturers participated in the field testing phase of the project and the open house.

Vibratory smooth drum rollers were studied on this project. Caterpillar's CS683 IC roller was equipped with *machine drive power* (MDP) and *compaction meter value* (CMV) measurement systems, and Bomag's BW213-DH IC roller was equipped with the *vibratory modulus* (E_{VIB}) measurement system along with automatic feedback control (AFC). Both machines were equipped with real time kinematic (RTK) global positioning system (GPS) and proprietary on-board display and documentation systems.

The goals of this field investigation were similar to previous demonstration projects and included the following:

- document the impact of AFC operations on compaction uniformity,
- document machine vibration amplitude influence on compaction efficiency,
- evaluate impact of lift thickness on IC measurement values and compaction efficiency,
- develop correlations between IC measurement values (IC-MVs) to traditional in-situ test measurements,
- study IC roller measurement influence depth,
- compare IC results to tradition compaction operations,
- study IC measurement values in production compaction operations, and
- evaluate IC measurement values in terms of alternative specification options.

This report presents brief background information for the three IC-MVs evaluated in this study (MDP, CMV, and E_{VIB}), documents the results and analysis from the test bed studies, and documents the field demonstration activities. Geostatistical methods were used to quantify and characterize spatial non-uniformity of the embankment subgrade and subbase materials using spatially referenced IC-MV data. Regression analysis was performed to evaluate correlations between IC-MVs and in-situ soil properties (i.e., moisture-density, modulus, and California bearing ratio) determined using point measurements (Point MVs). Density and moisture content tests were performed using nuclear gauge devices manufactured by Humboldt and Troxler, and a non-nuclear gauge (Soil Density Gauge) manufactured by Transtech. Comparisons between the various measurements are documented in this report. Modulus measurements are obtained using Zorn light weight deflectometer (LWD)setup with 200 mm and 300 mm diameter plates, Briaud compaction device (BCD) setup with 150 mm diameter plate, KUAB falling weight deflectometer (FWD) setup with 300 mm diameter plate, and static plate load test (PLT) setup with 300 mm diameter plate. Each of these test measurements differ in the way the tests are

performed, in applied contact stresses during the test, and in the way load and deflection measurements are obtained. Correlations between modulus obtained from these different test methods are documented in this report.

Empirical correlations between IC-MVs and in-situ Point-MVs are first evaluated independently for each test bed which were obtained over a narrow measurement range and then combined in the end to develop site wide correlations capturing a wide measurement range. These results and correlations between different in-situ test measurements should be of significant interest to the pavement, geotechnical, and construction engineering community and are anticipated to serve as a good knowledge base for implementation of IC compaction monitoring technologies and various new in-situ testing methods into earthwork construction practice.

Another aspect of this study that should be of interest is the new data documenting performance of AFC. Some of the potential advantages cited in the literature (e.g., Adam and Kopf 2004) for using AFC for soil compaction are increased chances of rapid compaction (i.e., less passes) and improved uniformity of soil properties, although only limited data has been identified in the literature on this subject. For the study described herein, side-by-side test beds were constructed and evaluated using manual mode (with different amplitude settings) and AFC mode operations to obtain direct comparisons. The results of this evaluate should be of particular interest to contractors as it relates to the potential for compaction efficiency.

BACKGROUND

Caterpillar CS683 and Bomag BW213-DH vibratory smooth drum IC rollers were used on the project (Figure 1). A digital display unit employing proprietary software is mounted in the roller cabin for on-board visualization of roller position, IC-MVs, coverage information, amplitude/frequency settings, speed, etc. Some key features of the rollers are summarized in Table 1. Brief descriptions of the IC-MVs is provided in the following discussion.

Figure 1. Caterpillar CS683 (left) and Bomag BW213-H (right) vibratory smooth drum IC rollers

Table 1. Vibratory smooth drum IC roller features

Feature	Caterpillar CS683	Bomag BW 213-DH
Drum Geometry	2.13 m width and 1.52 m diameter	2.13 m width and 1.50 m diameter
Frequency (*f*)	30 Hz	28 Hz
Amplitude (*a*) Settings	Static, 0.90 mm (low amplitude), and 1.80 mm (high amplitude)	0, 0.7, 1.1, 1.7, 2.1 and 2.5 mm
IC-MV	MDP_{40} (shown as CCV in the output) and CMV	E_{VIB} (MPa)
Display Software	AccuGrade	BCM05
GPS coordinates	UTM Zone 15N (NAD83)	UTM Zone 15N (NAD83)
Output Documentation	Date/Time, Location (Northing/Easting/Elevation of left and right ends of the roller drum), Speed, CCV, CMV, RMV, Frequency, Amplitude, Direction (forward/backward), Vibration (On/Off)	Date/Time, Location (Northing/Easting/Elevation at center of the roller drum), E_{VIB}, Frequency, Amplitude, Speed, Jump
Output Export File	*.csv	*.csv
Automatic Feedback Control (AFC)	No	Yes

Machine Drive Power (MDP) Value

MDP technology relates mechanical performance of the roller during compaction to the properties of the compacted soil. Detailed background information on the MDP system is provided by White et al. (2005). Controlled field studies documented by White and Thompson (2008), Thompson and White (2008), and Vennapusa et al. (2009) verified that MDP values are empirically related to soil compaction characteristics (e.g., density, stiffness, and strength). MDP is calculated using Eq. 1.

$$MDP = P_g - Wv\left(\mathrm{Sin}\alpha + \frac{A'}{g}\right) - (mv + b) \quad (1)$$

Where MDP = machine drive power (kJ/s), P_g = gross power needed to move the machine (kJ/s), W = roller weight (kN), A' = machine acceleration (m/s^2), g = acceleration of gravity (m/s^2), α = slope angle (roller pitch from a sensor), v = roller velocity (m/s), and m (kJ/m) and b (kJ/s) = machine internal loss coefficients specific to a particular machine (White et al. 2005). MDP is a relative value referencing the material properties of the calibration surface, which is generally a hard compacted surface (MDP = 0 kJ/s). Positive MDP values therefore indicate material that is less compact than the calibration surface, while negative MDP values indicate material that is more compacted than the calibration surface (i.e. less roller drum sinkage). The MDP values

obtained from the machine were recalculated to range between 1 and 150 using Eq. 2 (referred to as MDP_{40}). In Eq. 3, the calibration surface with MDP = 0 kJ/s was scaled to MDP_{40} = 150 and a soft surface with MDP = 54.23 kJ/s (40000 lb-ft/s) was scaled to MDP_{40} = 1.

$$MDP_{40} = 54.23 - 0.355(MDP) \tag{2}$$

Compaction Meter Value (CMV) and Resonant Meter Value (RMV)

CMV is a dimensionless compaction parameter developed by Geodynamik that depends on roller dimensions, (i.e., drum diameter and weight) and roller operation parameters (e.g., frequency, amplitude, speed), and is determined using the dynamic roller response (Sandström 1994). It is calculated using Eq. 3, where C is a constant (300), $A_{2\Omega}$ = the acceleration of the first harmonic component of the vibration, A_{Ω} = the acceleration of the fundamental component of the vibration (Sandström and Pettersson 2004). Correlation studies relating CMV to soil dry unit weight, strength, and stiffness are documented in the literature (e.g., Floss et al. 1983, Samaras et al. 1991, Brandl and Adam 1997, Thompson and White 2008, White and Thompson 2008).

$$CMV = C \cdot \frac{A_{2\Omega}}{A_{\Omega}} \tag{3}$$

RMV provides an indication of the drum behavior (e.g. continuous contact, partial uplift, double jump, rocking motion, and chaotic motion) and is calculated using Eq. 4, where $A_{0.5\Omega}$ = subharmonic acceleration amplitude caused by jumping (the drum skips every other cycle). It is important to note that the drum behavior affects the CMV measurements (Brandl and Adam 1997) and therefore must be interpreted in conjunction with the RMV measurements (Vennapusa et al. 2010). More discussion on effect of drum behavior on CMV measurements is provided later in this report.

$$RMV = C \cdot \frac{A_{0.5\Omega}}{A_{\Omega}} \tag{4}$$

Vibratory Modulus (E_{VIB}) Value

The vibratory modulus (E_{VIB}) value is calculated using the one-degree-of-freedom lumped parameter model theory and Lundeberg's theoretical solution (Lundberg 1939) for a rigid cylinder on an elastic half-space. A detailed description of the E_{VIB} measurement technology is provided by Kröber et al. (2001). Previous studies (Krober 1998 and Krober et al. 2001) reported that the E_{VIB} value is related to the modulus determined from a static plate load test. The drum force (F_s) and displacement (z_d) behaviour is related to E_{VIB} (see Eq. 5) using Lundberg's analytical solution. According to Hertz (1895), the contact width of a cylindrical drum (B) can be calculated using the geometry of the drum, applied force, and the material properties (see Eq. 6). The two equations (Eqs. 5 and 6) are numerically solved to determine the E_{VIB} value.

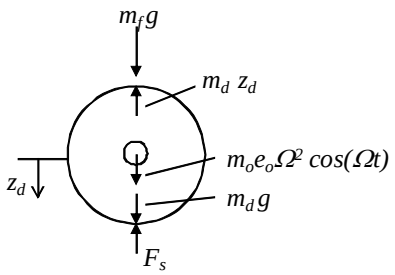

Figure 2. One-degree-of-freedom lumped parameter model representation of vibratory compactor (reproduced from Kröber et al. 2001)

$$z_d = \frac{\left(1-\eta^2\right)}{E_{VIB}} \cdot \frac{F_s}{L} \cdot \frac{2}{\pi} \cdot \left(1.8864 + \ln\frac{L}{B}\right) \tag{5}$$

$$\text{where } B = \sqrt{\frac{16}{\pi} \cdot \frac{R'(1-\eta^2)}{E_{VIB}} \cdot \frac{F_s}{L}} \tag{6}$$

Where, η = Poisson's ratio of the material, L = length of the drum, B = contact width of the drum, and R' = radius of the drum.

The automatic feedback control (AFC) system employed by Bomag uses a concept of counter-rotating eccentric mass assembly that is directionally vectored to vary the vertical excitation force on the soil (see Figure 3). If the counter-rotating masses are opposite each other in their rotation cycles, the eccentric force is zero. On the other hand, when the counter-rotating masses pass each other, the eccentric force is at maximum. The AFC system automatically adjusts the amplitude (by adjusting the vectors) depending on the pre-selected settings or the drum behavior (see Figure 3). Two different AFC settings are available as described below.

(1) Pre-selected target E_{VIB} and a maximum amplitude a_{max} value: In this setting, the vibration amplitude is reduced below the a_{max} value when $E_{VIB} \geq$ target E_{VIB}, and the amplitude is at the a_{max} value when $E_{VIB} <$ target E_{VIB}.
(2) Pre-selected a_{max} value: In this setting, the vibration amplitude is controlled based on the drum double jump behavior (described more in detail below) as measured by the *jump* value. When the jump value increases above 0, the amplitude is lowered to 0.6 mm.

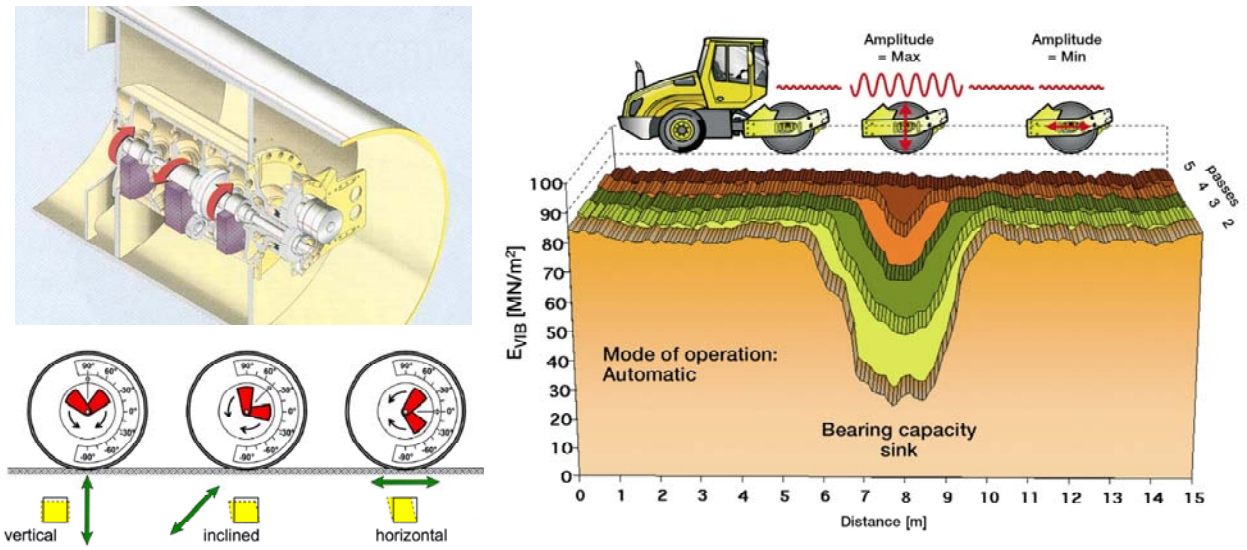

Figure 3. Bomag roller eccentric mass assembly and vectoring to vary the vertical excitation force (left) and principle of Bomag's automatic feedback control (AFC) system (right) (courtesy of Bomag)

Influence of Drum Behavior and Soil Stiffness on IC-MVs

Previous experimental and numerical investigations (e.g., Adam and Kopf 2004) on roller drum-soil interaction identified five different drum behavior modes which are dependent on the soil stiffness and roller operational settings (i.e., amplitude, frequency, and speed). These five modes include: continuous contact, partial uplift, double jump, rocking motion, and chaotic motion (see Figure 4). The accelerometer based IC-MVs (i.e., CMV, RMV, E_{VIB}) are influenced by these different drum modes (see Figure 5).

For CMV measurement technology the drum jump behavior is assessed using the RMV measurements. RMV is described earlier in this report. According to Adam and Kopf (2004), RMV = 0 indicates that the drum is in a continuous contact or partial uplift mode. For RMV > 0, the drum enters double jump mode and transitions into rocking and chaotic modes with increasing soil stiffness. Based on numerical studies, Adam and Kopf (2004) demonstrated the change in CMV relative to soil stiffness and drum behavior as shown in Figure 5. For E_{VIB} measurement technology, the drum behavior is assessed using the *Jump* value. *Jump* = 0 indicates the drum is in continuous contact or partial uplift mode and *Jump* > 0 (1 or 2) indicates the drum is in either in double jump, rocking, or chaotic mode (personal communication with Bomag manufacturer representative). The effect of increasing soil stiffness and drum behavior on E_{VIB} value is illustrated in Figure 5.

AFC systems should help control the drum behavior to prevent drum double jumping by automatically adjusting the vibration amplitude and/or frequency. The AFC system for E_{VIB} measurement technology is described earlier in this report. Although not used on this project, results from an AFC system for the CMV measurement system (using RMV measurements) is documented in White *et al.* (2008).

drum motion	Interaction drum-soil	operating condition	soil contact force	application of CCC	soil stiffness	roller speed	drum ampli-tude
periodic	continuous contact	CONT. CONTACT		yes	low	fast	small
	periodic loss of contact	PARTIAL UPLIFT		yes			
		DOUBLE JUMP		yes			
		ROCKING MOTION		no			
chaotic	non-periodic loss of contact	CHAOTIC MOTION		no	high	slow	large

Figure 4. Influence of soil modulus and drum behavior on IC-MVs (from Adam and Kopf 2004)

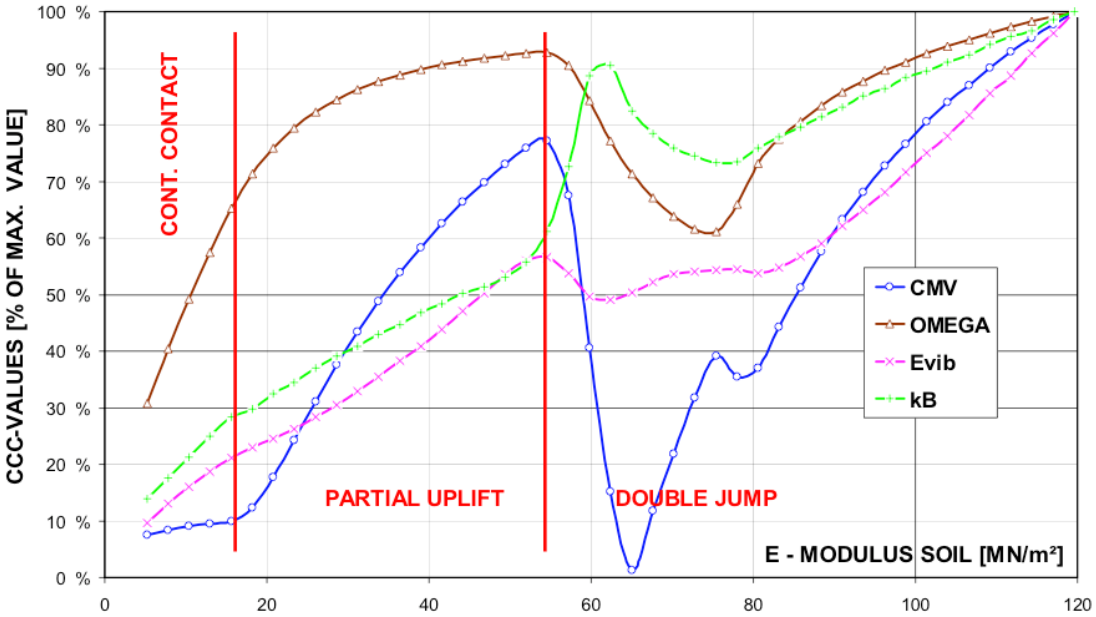

Figure 5. Influence of drum behavior on IC-MVs relative to soil modulus (based on numerical simulations from Adam and Kopf 2004)

Overview of Project Compaction Specifications

New York state DOT 2002 standard specifications were reportedly implemented on the project (https://www.nysdot.gov/main/business-center/engineering/specifications/2002-standard-specifications). In this specification, uniform compactive effort (number of passes and travel

speed) is required for fill compaction. Embankment fill and gravel subbase materials are required to be compacted to at least 95% of the standard Proctor maximum dry density. Quality assurance (QA) tests to check relative compaction are however not required. The decision to performed field QA is based on field observations by the project engineer.

ANALYSIS METHODS

Regression Analysis

Simple linear regression relationships between IC-MVs and in-situ point measurement values (Point MV) were developed by spatially pairing the data obtained from the test beds. The analysis was performed by considering Point-MVs as "true" independent variables and IC-MVs as dependent variables using the models shown in Eqs. 7 to 9, where b_0 = intercept and b_1, b_2 = regression parameters.

$$\text{Linear model: } IC\text{–}MV = b_0 + b_1 \cdot Point\,MV \tag{7}$$

$$\text{Non-linear logarithmic model: } IC\text{–}MV = b_0 + b_1 \cdot \ln(Point\,MV) \tag{8}$$

$$\text{Non-linear power model: } IC\text{–}MV = b_1 (Point\,MV)^{b_2} \tag{9}$$

Statistical significance of the independent variable was assessed based on *p*- and *t*-values. The selected criteria for identifying the significance of a parameter included: *p*-value < 0.05 = significant, < 0.10 = possibly significant, > 0.10 = not significant, and *t*-value < -2 or > +2 = significant. The best fit model is determined based on the strength of the regression relationships assessed by the coefficient of determination (i.e., R^2) values. For the analysis and discussion in this report, an R^2 value ≥ 0.5 is considered acceptable following the guidelines from European specifications. A statistical prediction interval approach for determining "target" values from the regression relationships would account for R^2 values in the relationships (see NCHRP 21-09). A regression relationship with lower R^2 values would result in higher target value and a regression relationship with higher R^2 value will result in lower target values.

Multiple regression analysis results to statistically assess the influence of vibration amplitude are presented in this report. Multiple regression analysis is performed by incorporating amplitude as an independent variable into a general multiple linear regression model as shown in Eq. 10 where b_0 = intercept, b_1 and b_2 = regression coefficients, and *a* = amplitude (mm). The statistical significance of amplitude was assessed based on *p*- and *t*- values using the criteria described above.

$$IC\text{–}MV = b_0 + b_1 \cdot Point\,MV + b_2 \cdot a \tag{10}$$

For the multiple regression analysis, the R^2 values have been adjusted for the number of regression parameters using Eq. 11. The adjusted R^2 from multiple regression analysis is used to compare with R^2 from simple linear regression analysis to assess which regression model best describes the data.

$$R^2(\text{adjusted}) = \frac{R^2(n-1)}{n-p} \quad (11)$$

Geostatistical Analysis

Spatially referenced IC measurement values provide an opportunity to quantify "non-uniformity" of compacted fill materials. Vennapusa *et al.* (2010) demonstrated the use of semivariogram analysis in combination with conventional statistical analysis to evaluate non-uniformity in QC/QA during earthwork construction. A semivariogram is a plot of the average squared differences between data values as a function of separation distance, and is a common tool used in geostatistical studies to describe spatial variation. A typical semivariogram plot is presented in Figure 6. The semivariogram $\gamma(h)$ is defined as one-half of the average squared differences between data values that are separated at a distance h (Isaaks and Srivastava 1989). If this calculation is repeated for many different values of h (as the sample data will support) the result can be graphically presented as experimental semivariogram shown as circles in Figure 6. More details on experimental semivariogram calculation procedure are available elsewhere in the literature (e.g., Clark and Harper 2002, Isaaks and Srivastava 1989).

To obtain an algebraic expression for the relationship between separation distance and experimental semivariogram, a theoretical model is fit to the data. Some commonly used models include linear, spherical, exponential, and Gaussian models. A spherical model was used for data analysis in this report. Arithmetic expression of the spherical model and the spherical variogram are shown in Figure 6. Three parameters are used to construct a theoretical semivariogram: sill ($C+C_0$), range (R), and nugget (C_0). These parameters are briefly described in Figure 6. More discussion on the theoretical models can be found elsewhere in the literature (e.g., Clark and Harper 2002, Isaaks and Srivastava 1989). For the results presented in this section, the sill, range, and nugget values during theoretical model fitting were determined by checking the models for "goodness" using the modified Cressie goodness fit method (see Clark and Harper 2002) and cross-validation process (see Isaaks and Srivastava 1989). From a theoretical semivariogram model, a low "sill" and longer "range of influence" represent best conditions for uniformity, while the opposite represents an increasingly non-uniform condition.

Some of the results presented in this report revealed nested structures with short-range and long-range components in the experimental semivariograms. Nested structures have been observed in geological applications where different physical processes are responsible for spatial variations at different scale (see Chiles and Delfiner 1999). For the cases with nested structures, nested spherical variograms combining two spherical models (with two sill values and two range values) are fit to the experimental semivariogram data. This report is the first application of this approach for IC data.

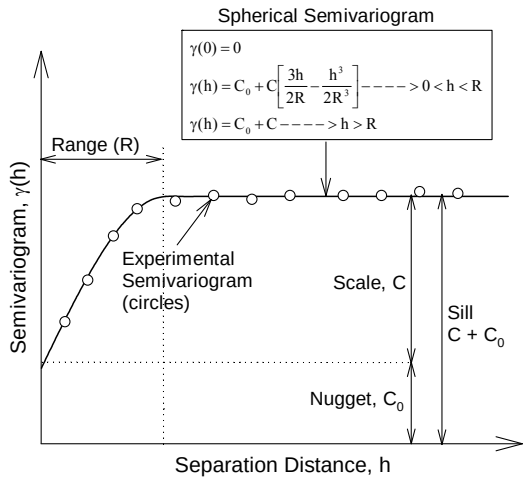

Range, R: As the separation distance between pairs increase, the corresponding semivariogram value will also generally increase. Eventually, however, an increase in the distance no longer causes a corresponding increase in the semivariogram, i.e., where the semivariogram reaches a plateau. The distance at which the semivariogram reaches this plateau is called as range. Longer range values suggest greater spatial continuity or relatively larger (more spatially coherent) "hot spots".

Sill, $C+C_0$: The plateau that the semivariogram reaches at the range is called the sill. A semivariogram generally has a sill that is approximately equal to the variance of the data.

Nugget, C_0: Though the value of the semivariogram at h = 0 is strictly zero, several factors, such as sampling error and very short scale variability, may cause sample values separated by extremely short distances to be quite dissimilar. This causes a discontinuity at the origin of the semivariogram and is described as nugget effect. (Isaaks and Srivastava, 1989)

Figure 6. Description of a typical experimental and spherical semivariogram and its parameters

EXPERIMENTAL TESTING

Description of Test Beds

A total of ten test beds including two different materials (i.e., embankment subgrade and subbase materials) were studied. A summary of test beds with material conditions and tests performed is provided in Table 2. A summary of soil index properties is provided in Table 3. Details regarding construction and testing of each test bed are provided in the discussion later and in test bed summary sheets in the Appendix. The following specific objectives were targeted at different test beds evaluated in this study:

- Capture data over wide measurement range to develop IC-MV and different Point-MV correlations – TBs1, 2, 3, 4, 5, 6, 8, 9, and 10.
- Demonstrate the usefulness of using IC-MV maps for selection of QA test locations – TBs1, 2, 7, and 9.
- Demonstrate the usefulness of using IC-MV maps to differentiate underlying support conditions – TB2 (test bed is partially underlain by shredded rubber tire fill)
- Explore geostatistical methods to quantify and characterize spatial non-uniformity of embankment materials – TBs1 and 2.
- Evaluate AFC mode operations in comparison with manual mode operations – TBs 3, 5, and 10.
- Evaluate the influence of amplitude on IC-MVs – TBs 3, 4, 5, and 8.
- Provide hands-on experience to NYDOT and contractor personnel – TBs 6, 7, and 9
- Evaluate impact of lift thickness on IC-MVs and compaction efficiency – TB10
- Evaluate compaction influence depth – TB10

Table 2. Summary of test beds and in-situ testing

TB	Material	Date	Machine(s)	Pass	Theoretical Amplitude (mm)/ Speed (km/h)*	Notes/In-situ Test Measurements
1	Embankment (underlain by tire fill at < 1m depth)	05/17	Caterpillar	1	Static, 4	CBR, $E_{LWD\text{-}Z2}$ after Pass 3
				2	0.90, 4	
				3	0.90, 4	
2	Embankment (partially underlain by tire fill at < 1m depth)	05/18	Caterpillar	1	Static, 4	CBR, $E_{LWD\text{-}Z2}$, $w_{(H)}$, $\gamma_{d(H)}$, and E_{BCD} after Pass 2
				2	0.90, 4	
3	Embankment	05/18	Bomag	1	0.70, 4	$E_{LWD\text{-}Z2}$ and $E_{LWD\text{-}Z3}$ after Pass 2
				2	AFC a_{max} = 1.90 (E_{VIB} = 150MPa), 4	
				3	0.70 mm, 4	
				4	1.50 mm, 4	
4	Gravel Subbase (Lane 2)	05/18	Caterpillar	1-8	Static, 4	$E_{LWD\text{-}Z3}$, CBR, $w_{(H)}$, and $\gamma_{d(H)}$ after Pass 0 and 8.
	Gravel Subbase (Lane 3)			1-8	0.90, 4	
5	Gravel Subbase (Lane 4)	05/18	Bomag	1-8	AFC a_{max} = 1.10 and (E_{VIB} = 150 MPa), 4	$E_{LWD\text{-}Z3}$, CBR, $w_{(H)}$, and $\gamma_{d(H)}$ after Pass 0 and 8. $w_{(T)}$, and $\gamma_{d(T)}$ after Pass 0. $w_{(SDG)}$, and $\gamma_{d(SDG)}$ after Pass 8.
	Gravel Subbase (Lane 5)				0.70 mm, 4	
6	Gravel Subbase (Production)	05/19	Caterpillar	1-2	0.90, 4	$E_{LWD\text{-}Z3}$, $w_{(H)}$, $\gamma_{d(H)}$, and E_{BCD} after pass 6
7			Bomag	3-6	0.70, 4	
8	Embankment (same area as TB3)	05/19	Caterpillar	5	0.90, 4	$E_{FWD\text{-}K3}$, E_{V1}, and E_{V2} after Pass 6
				6	Static, 4	
9	Gravel Subbase (Production by Contractor)	05/19	Caterpillar	Variable	0.90, 4	$E_{LWD\text{-}Z3}$, CBR, $w_{(H)}$, $\gamma_{d(H)}$, and E_{BCD} after final pass
10	Embankment (1m and 2m Trenches)	05/20 to 05/21	Caterpillar (Lane 1)	1-8	0.90, 4	$E_{LWD\text{-}Z3}$, CBR, $w_{(H)}$, $\gamma_{d(H)}$, $w_{(SDG)}$, $\gamma_{d(SDG)}$ and E_{BCD} after Pass 0, 1, 2, 4, 8 and 10
				9-10	0.90, 2	
			Bomag (Lane 2)	1-8	AFC a_{max} = 1.10 and (E_{VIB} = 150 MPa), 4	
				9-10	AFC a_{max} = 2.50 and (E_{VIB} = 150 MPa), 2	
			Bomag (Lane 3)	1-8	0.70, 4	
				9-10	0.70, 2	

Note: * - nominal.

Table 3. Summary of soil index properties

Parameter	Embankment Material	Aggregate Base
Standard Proctor Test Results		
γ_{dmax} (kN/m^3)	20.46	21.20
w_{opt}	8.6	8.0
Relative Density Test Results (oven-dry material)		
γ_{dmin} (kN/m^3)	Not Performed	15.95
γ_{dmax} (kN/m^3)		20.01
Gravel Content (%) (> 4.75mm)	24	46
Sand Content (%) (4.75mm – 75μm)	55	44
Silt Content (%) (75μm – 2μm)	15	7
Clay Content (%) (< 2μm)	6	3
D_{10} (mm)	0.0083	0.075
D_{30} (mm)	0.193	1.09
D_{60} (mm)	1.54	6.98
Coefficient of Uniformity, c_u	185.5	93.1
Coefficient of Curvature, c_c	2.9	2.3
Liquid Limit, LL (%)	16	15
Plastic Limit, PL (%)	Non-Plastic	
AASHTO Classification	A-1-b	A-1-a
USCS Classification	SM	GW
Specific Gravity, G_s (Assumed)	2.70	2.75

In-situ Testing Methods

Eight different in-situ testing methods were employed in this study to evaluate the in-situ soil engineering properties (Figure 7): (a) Zorn light weight deflectometer setup with 200 and 300 mm plate diameters to determine elastic modulus ($E_{LWD\text{-}Z2}$ for 200 mm plate diameter and $E_{LWD\text{-}Z3}$ for 300 mm plate diameter), (b) Dynamic Cone Penetrometer (DCP) to determine California bearing Ratio (CBR), (c) Briaud's compaction device (BCD) setup with 150 mm diameter plate to determine soil elastic modulus (E_{BCD}), (d) calibrated Humboldt nuclear gauge (NG(H))to measure moisture content ($w_{(H)}$) and dry unit weight ($\gamma_{d(H)}$), (e) calibrated Troxler nuclear gauge (NG(T))to measure moisture content ($w_{(T)}$) and dry unit weight ($\gamma_{d(T)}$), (f) Transtech soil density gauge (SDG) to measure moisture content ($w_{(SDG)}$) and dry unit weight ($\gamma_{d(SDG)}$), (g) 300-mm diameter two-segmented plate KUAB falling weight deflectometer (FWD) to determine elastic modulus ($E_{FWD\text{-}K3}$), and (h) 300-mm plate diameter static plate load test (PLT) to determine initial (E_{V1}) and re-load modulus (E_{V2}). LWD (200 mm plate), DCP, NG(H),

and PLT tests were conducted by the ISU research team, LWD (300 mm plate), FWD, and NG(T) tests were conducted by New York (NYDOT) personnel, BCD tests were conducted by Texas A&M research personnel, and SDG tests were conducted by Transtech personnel. SDG results were analyzed by Transtech personnel to determine the $\gamma_{d(SDG)}$ and $w_{(SDG)}$ values. The BCD device is described in Briaud et al. (2006) and the results were analyzed by Texas A&M research personnel to determine E_{BCD} values.

LWD tests were performed following manufacturer recommendations (Zorn 2003) and the E_{LWD} values were determined using Eq. 12, where E = elastic modulus (MPa), d_0 = measured settlement (mm), η = Poisson's ratio, σ_0 = applied stress (MPa), r = radius of the plate (mm), F = shape factor depending on stress distribution (assumed as 8/3) (see Vennapusa and White 2009).

$$E = \frac{(1-\eta^2)\sigma_0 r}{d_0} \times F \tag{12}$$

To help differentiate between the 300 mm LWD and 200 mm LWD measurements the following terminology is followed in this report:

- $E_{LWD\text{-}Z2}$: Elastic modulus determined by Zorn 200 mm diameter LWD
- $E_{LWD\text{-}Z3}$: Elastic modulus determined by Zorn 300 mm diameter LWD

FWD testing was performed by applying one seating drop using a nominal force of about 27 kN followed by three test drops each at a nominal force of about 45, 60, and 80 kN. The actual applied force was recorded using a load cell. The deflections were measured using geophones placed at the center of the plate and at 0.30, 0.46, 0.61, 0.91, 1.22, 1.52, and 1.83 m offsets from the center of the plate. A composite modulus value ($E_{FWD\text{-}K3}$) was calculated using measured deflection at the center of the plate using Eq. 12. Shape factor F = 2 was assumed in the calculations as the plate used for testing was a segmented plate (assume to produce uniform contact stress distribution).

DCP tests were performed in accordance with ASTM D6951-03 to determine dynamic cone penetration index (DPI) and calculate CBR using Eq. 13. The DCP test results are presented in this report as CBR point values or CBR depth profiles. When the data is presented as point values, the data represents a weighted average CBR of the compaction layer depth or depth indicated in the subscript (e.g., CBR_{300} indicates weighted average CBR to a depth of 300 mm and CBR_{Base} indicates weighted average CBR to the depth equal to the thickness of the base layer).

$$CBR = \frac{292}{DPI^{1.12}} \tag{13}$$

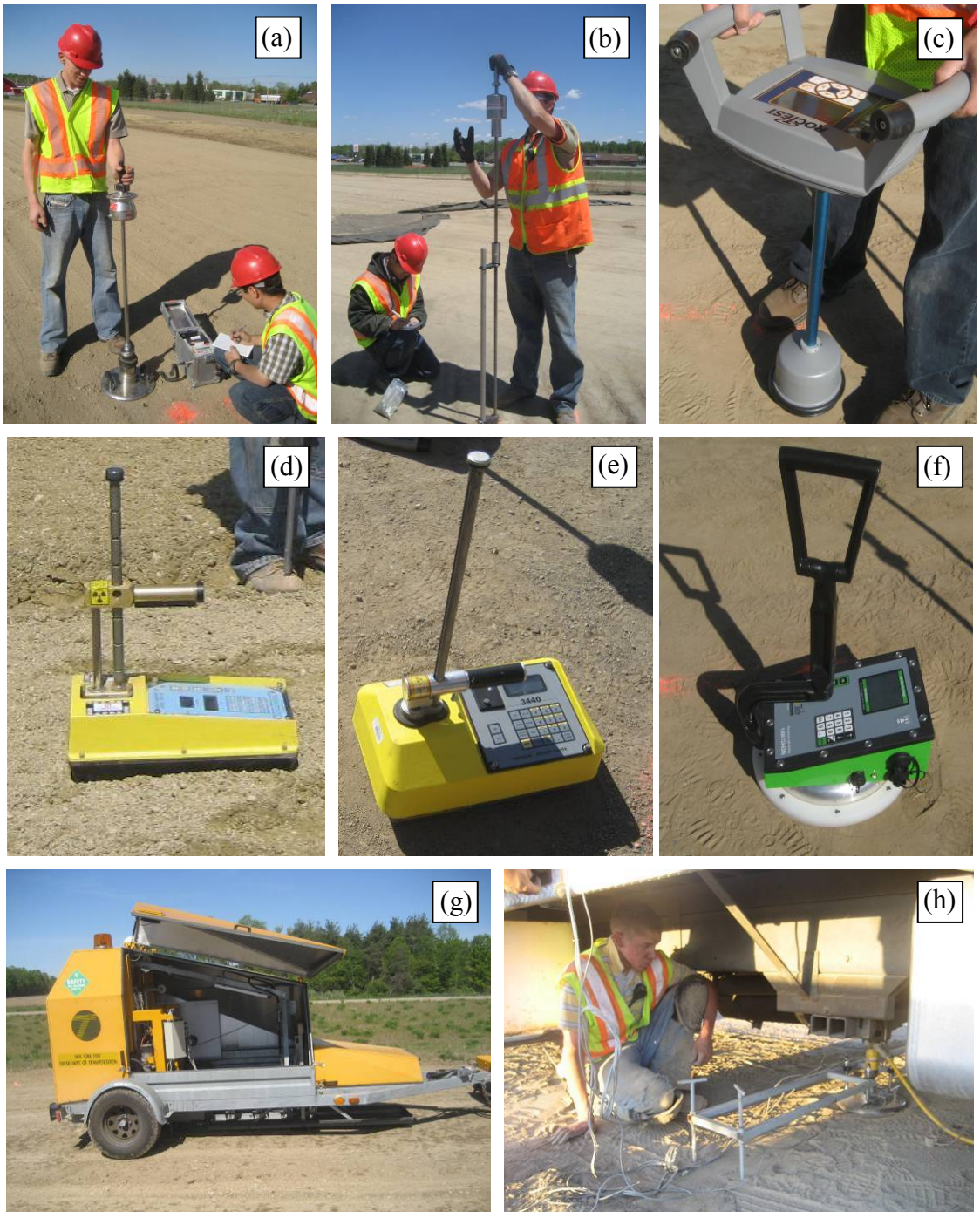

Figure 7. In-situ testing methods used on the project: (a) Zorn light weight deflectometer, (b) dynamic cone penetrometer, (c) Briaud compaction device, (d) Humboldt nuclear gauge, (e) Troxler nuclear gauge, (f) Transtech's soil density gauge, (g) KUAB falling weight deflectometer, (h) static plate load test

Static PLT's were conducted by applying a static load on 300 mm diameter plate against a 6.2kN capacity reaction force. The applied load was measured using a 90-kN load cell and deformations were measured using three 50-mm linear voltage displacement transducers (LVDTs). The load and deformation readings were continuously recorded during the test using a data logger. The E_{V1} and E_{V2} values were determined from Eq. 12 using deflection values at 0.1 and 0.2 MPa applied contact stresses for embankment subgrade materials and at 0.2 and 0.4 MPa contact stresses for base materials, as illustrated in Figure 8.

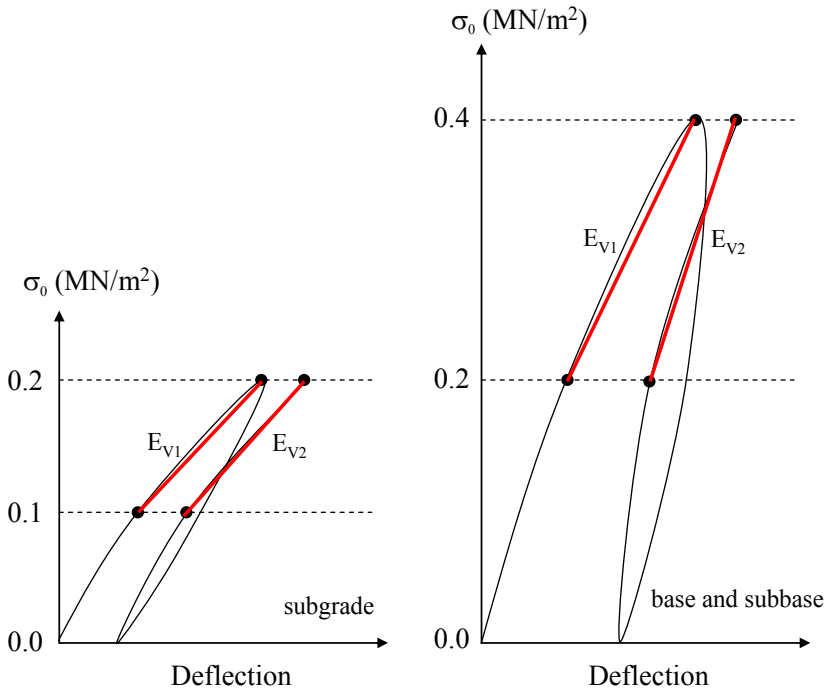

Figure 8. E_{V1} and E_{V2} determination procedure from static PLT for subgrade and base materials

EXPERIMENTAL TEST RESULTS

TB1 Embankment Material – Caterpillar

Test bed conditions, IC-MV mapping, and Point-MV testing

TB1 consisted of compacted embankment granular subgrade material (Figure 9) with plan dimensions of approximately 18 m x 200 m. Reportedly, the embankment material was underlain by shredded rubber tires at depths < 1m below grade. The area was divided into eight roller lanes and compacted with three roller passes using the Caterpillar IC roller. MDP_{40} and CMV IC-MVs were obtained from the roller. Pass 1 was made in static mode and passes 2 and 3 were made using low amplitude (a = 0.90 mm, f = 30 Hz) settings (see Table 2). Point-MVs ($E_{LWD\text{-}Z2}$, CBR_{300}) were obtained at 10 test locations after pass 3. The test locations were selected using the IC-MV map (at low, medium, and high IC-MV locations).

IC-MV maps from the three roller passes are shown in Figure 10. The spatial orientations of the IC-MV maps for passes 1 and 2 are slightly different from that of pass 3 because of an incorrect GPS setting used for passes 1 and 2. The correct GPS setting was used for pass 3. Histograms of CMV and MDP_{40} IC-MVs are presented in Figure 11. Point-MV locations are shown (as circles with point location number) on the pass 3 spatial map (Figure 10). DCP-CBR depth profiles along with surface $E_{LWD\text{-}Z2}$ measurements at each test location are presented in Figure 12. $E_{LWD\text{-}Z2}$ measurements at two test locations (locations 8 and 9) were above the upper measurement range of the device (>200 MPa) and therefore were not included in the regression analysis presented below.

Figure 9. TB1 embankment material area and pictures of in-situ testing and roller used for mapping the area

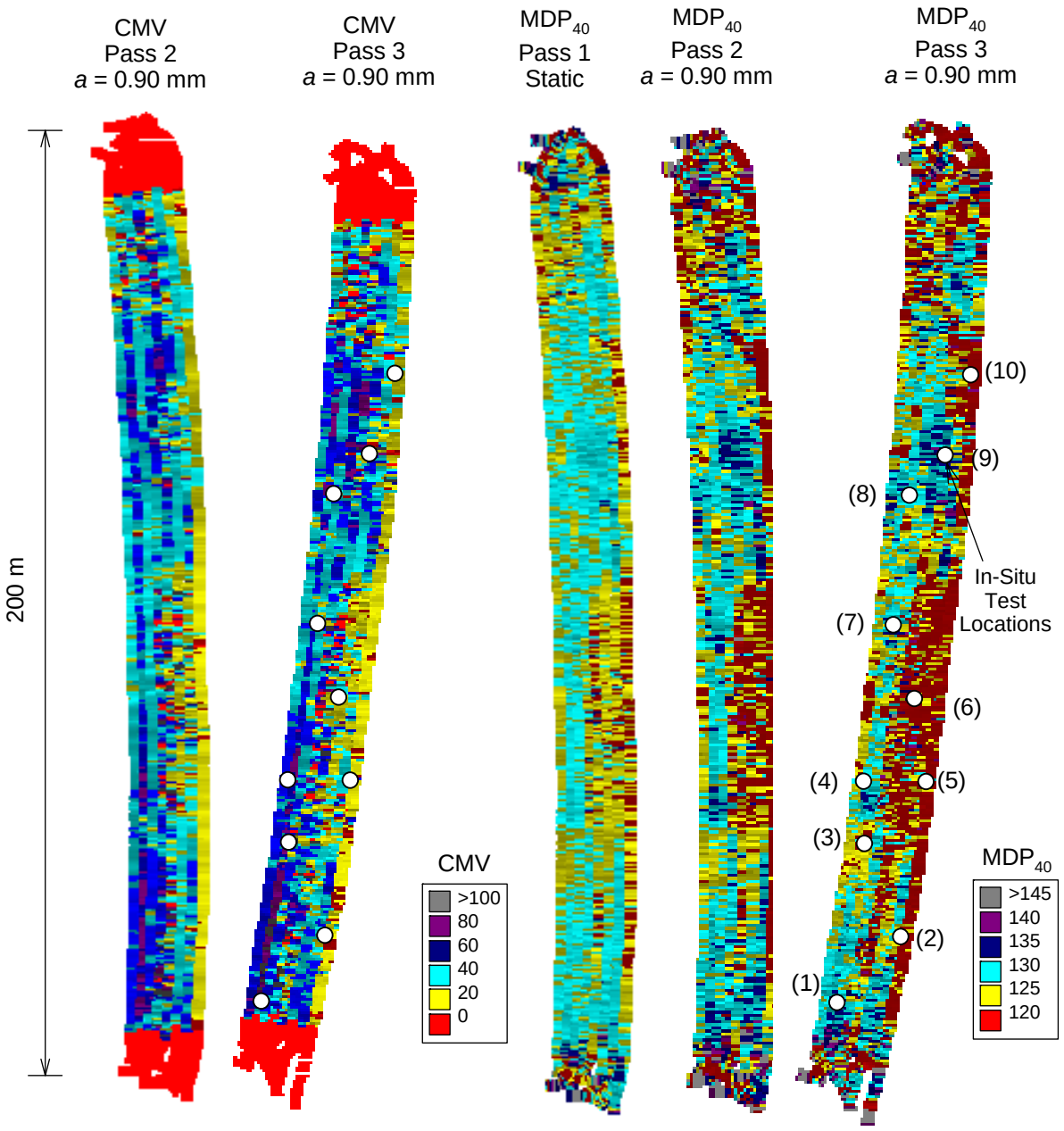

Figure 10. CMV and MDP_{40} spatial maps for three roller passes – TB1 embankment material

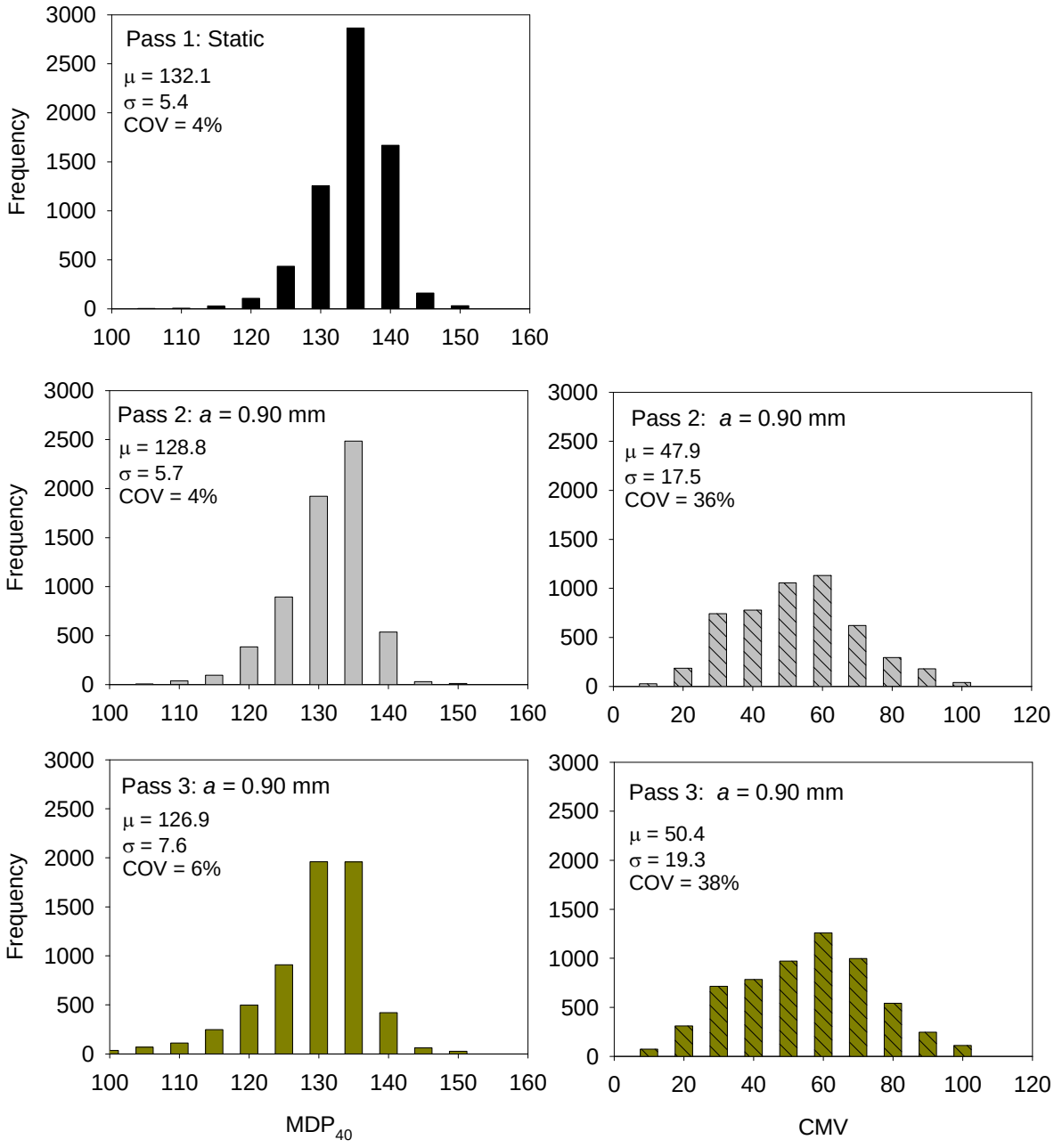

Figure 11. CMV and MDP_{40} histograms for passes 1 through 3 – TB1 embankment material

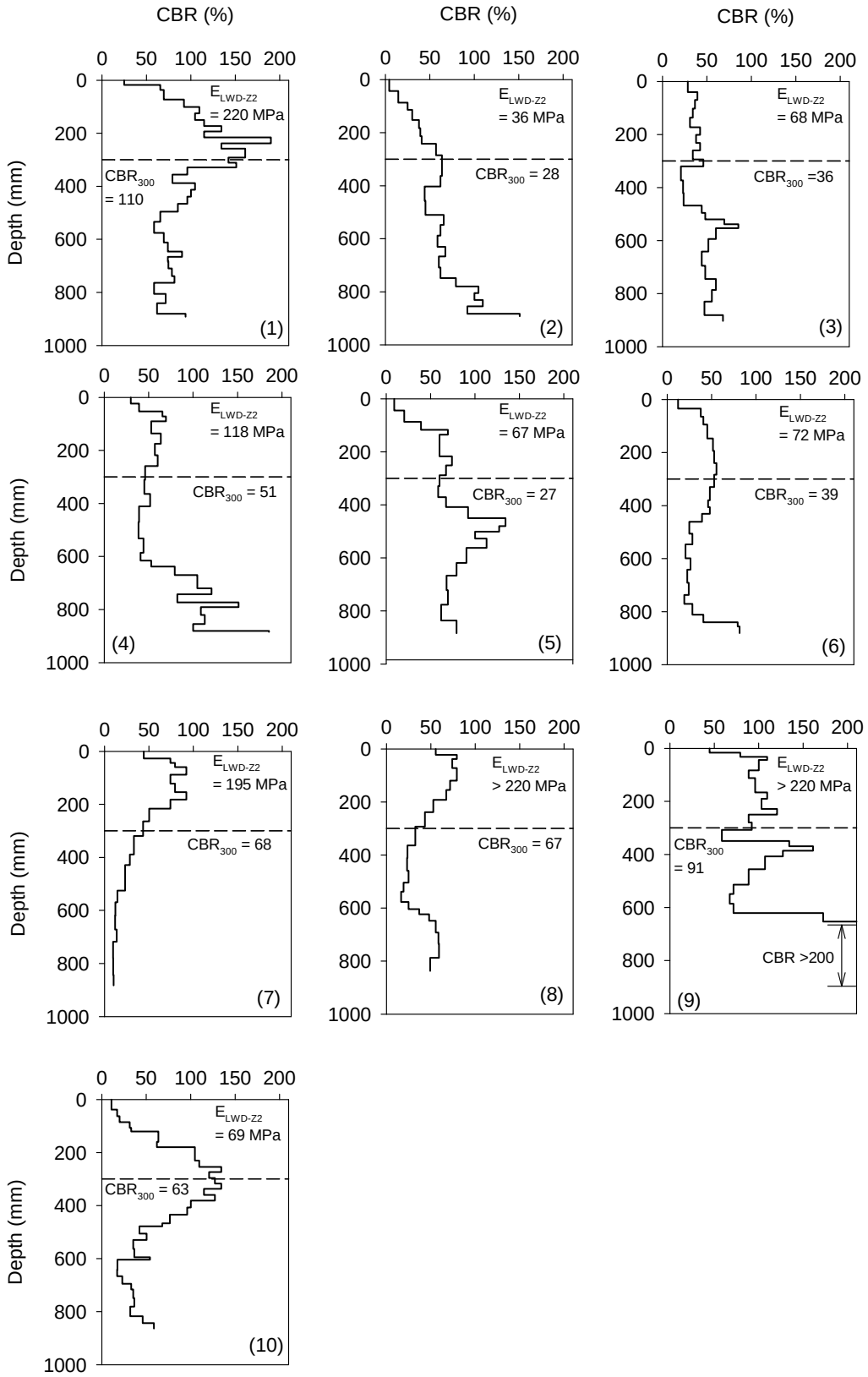

Figure 12. DCP-CBR profiles and $E_{LWD\text{-}Z2}$ measurements after pass 3 – TB1 embankment material

Regression Analysis between IC-MVs and Point-MVs

Regression analysis results between IC-MVs and Point-MVs are presented in Figure 13 and the relationships are summarized in Table 4. Non-linear power relationships showed the best fit for all Point-MVs. The R^2 values of the relationships varied from 0.27 to 0.86. All relationships except the CMV vs. CBR_{300} relationship yielded $R^2 > 0.5$.

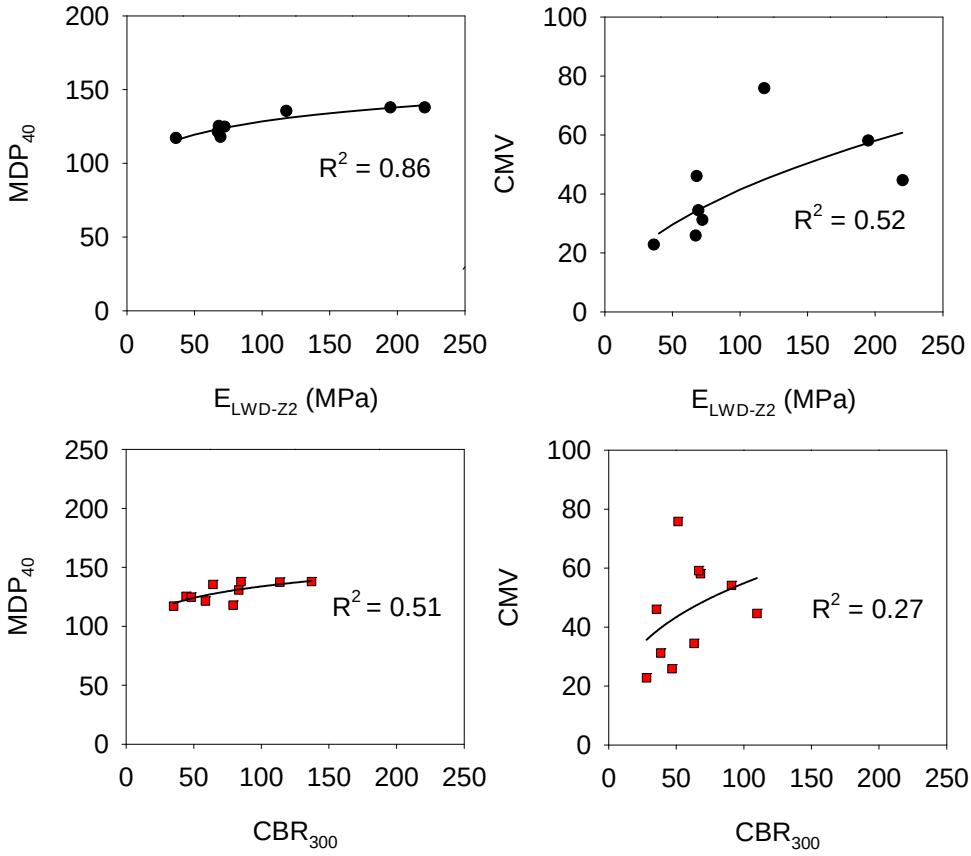

Figure 13. Regression relationships between IC-MVs and Point MVs – TB1 embankment material (nominal settings: *a* = 0.90 mm, *f* = 30 Hz)

Table 4. Summary of regression analysis – TB1 embankment material

Relationship	a (mm)	n	R^2
$MDP_{40} = 79.59\ (E_{LWD\text{-}Z2})^{0.10}$	0.90	8	0.86
$MDP_{40} = 82.91\ (CBR_{300})^{0.11}$	0.90	10	0.51
$CMV = 4.44\ (E_{LWD\text{-}Z2})^{0.49}$	0.90	8	0.52
$CMV = 6.09\ (CBR_{300})^{0.48}$	0.90	10	0.27

Geostatistical Analysis of IC-MVs

Semivariograms of IC-MVs for passes 1, 2, and 3 are presented in Figure 14 and a summary of the spatial statistics (i.e., nugget, sill, and range) are provided in Table 5. The experimental semivariograms of the MDP_{40} values showed a nested spatial structure with short-range and long-range components. A nested spherical variogram was fit to the experimental semivariogram data. The CMV experimental semivariograms did not exhibit nested structures. For MDP_{40} semivariograms, it is possible that the long-range spatial structure is linked to the spatial variation in underlying layer support conditions while the short-range spatial structure is a result of soil properties close to the surface. These concepts have not previously been evaluated and could provide an important step in understanding the spatial variability associated with IC data. Again, the embankment material in this area was reportedly underlain by shredded rubber tire fill at depths < 1m below grade.

The MDP_{40} and CMV semivariograms showed increasing non-uniform conditions (as indicated with increasing sill values) with increasing roller passes. This is also reflected by higher standard deviation (σ) values with increasing roller passes. Increasing spatial variability with increasing roller passes may be a result of localized areas of material decomposition (likely dilation) as the test bed had been compacted before IC rolling, but was not evaluated as part of the test plan. This occurrence should be studied further on future projects.

Summary of Key Findings

Measurements from TB1 involved obtaining IC-MV maps using static and low amplitude settings and Point-MVs ($E_{LWD\text{-}Z2}$ and CBR_{300}) at select locations over a plan area of about 18 m x 200 m. The embankment material was underlain by shredded rubber tires at depths < 1m below the grade. Regression analysis was performed using the IC-MVs and Point-MVs by spatially pairing the data, and geostatistical analysis was performed using the GPS referenced IC-MV data obtained for each pass. Following is a summary of key findings from analysis of the TB1 measurements:

- Regression analysis results between IC-MVs and Point-MVs showed non-linear power relationships with R^2 values ranging from 0.27 to 0.86. All relationships except CMV vs. CBR_{300} produced $R^2 > 0.5$.
- The MDP_{40} semivariograms exhibited a nested spatial structure with short-range and long-range components, while the CMV semivariograms did not. Additional studies are needed to better understand this finding.
- The MDP_{40} and CMV semivariograms showed increased non-uniform conditions (as indicated with increasing sill values standard deviation values) with increasing roller passes. Additional studies are needed to better understand this finding.

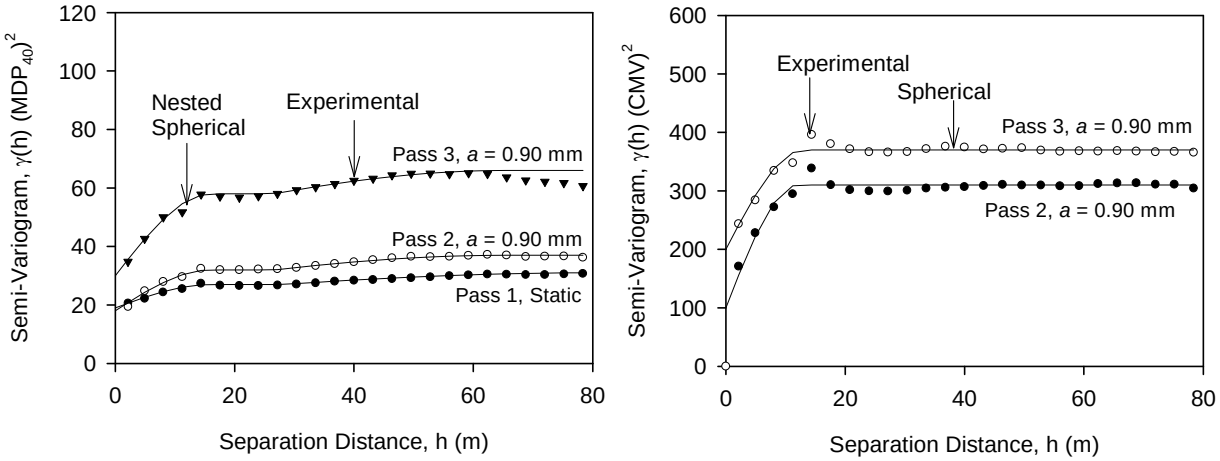

Figure 14. Semivariograms of roller MVs for different passes – TB1 embankment material

Table 5. Summary of univariate and spatial statistics – TB1 embankment material

				Univariate Statistics			Spatial Statistics				
Pass	**MV**	**n**	***a* (mm)**	**μ**	**σ**	**COV (%)**	**Nugget**	**Sill$_1$**	**Range$_1$**	**Sill$_2$**	**Range$_2$**
1	MDP_{40}	6579	Static	132.1	5.4	4	19	27	16	31	80
2	MDP_{40}	6240	0.9	128.8	5.7	4	18	32	16	37	65
2	CMV	6240	0.9	47.9	17.5	36	100	310	12	—	—
3	MDP_{40}	6008	0.9	126.9	7.6	6	30	58	16	66	65
3	CMV	6008	0.9	50.4	19.3	38	200	370	13	—	—
3	E_{LWD-Z2}	10	NA	144.8	104.4	72	Not enough measurements				
3	CBR_{300}	10		59.9	25.5	43					

TB2 Embankment Material – Caterpillar

Test bed conditions, IC-MV mapping, and Point-MV testing

This test bed consisted of compacted embankment granular subgrade material with plan dimensions of approximately 18 m x 71 m. The test bed was connected to the south end of TB1. Reportedly, the embankment material in this area was underlain by rubber tire fill at depths < 1m below grade in the northern half of the test bed (see note on Figure 15). The area was divided into eight roller lanes and compacted with two passes using the Caterpillar IC roller. MDP_{40} and CMV IC-MVs were obtained from the roller. The roller was operated in static mode for Pass 1 vibratory mode with low amplitude (a = 0.90 mm, f = 30 Hz) for pass 2 (see Table 2). Following mapping passes, Point-MVs (E_{LWD-Z2}, DCP-CBR, $w_{(H)}$, $w_{(SDG)}$, $\gamma_{d(H)}$ and $\gamma_{d(SDG)}$) were obtained at 7 test locations selected using the IC-MV map.

IC-MV maps from the two roller passes are shown in Figure 15. Histograms of IC-MVs for each pass are presented in Figure 16. Point-MV locations are shown (as circles with point location number) on pass 2 spatial map (Figure 15). DCP-CBR depth profiles along with $E_{LWD\text{-}Z2}$, $w_{(H)}$, $w_{(SDG)}$, $\gamma_{d(H)}$ and $\gamma_{d(SDG)}$ measurements at the surface of each test location are presented in Figure 17. An $E_{LWD\text{-}Z2}$ measurement at one test location (location 2) was above the upper measurement range of the device (> 200 MPa) and therefore was not included in the regression analysis presented below.

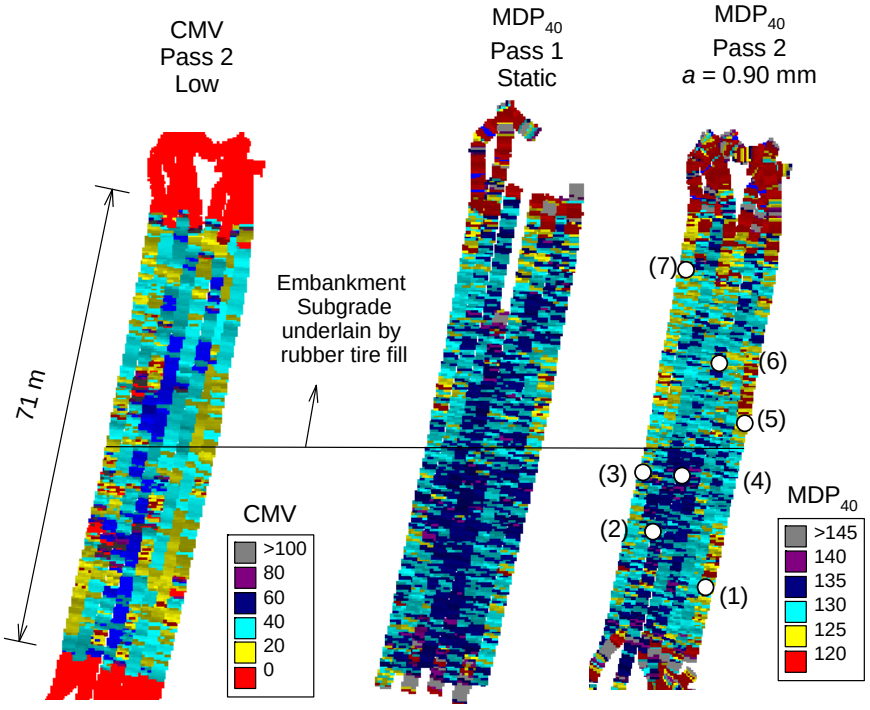

Figure 15. CMV and MDP_{40} spatial maps with different machine amplitude settings – TB2 embankment material

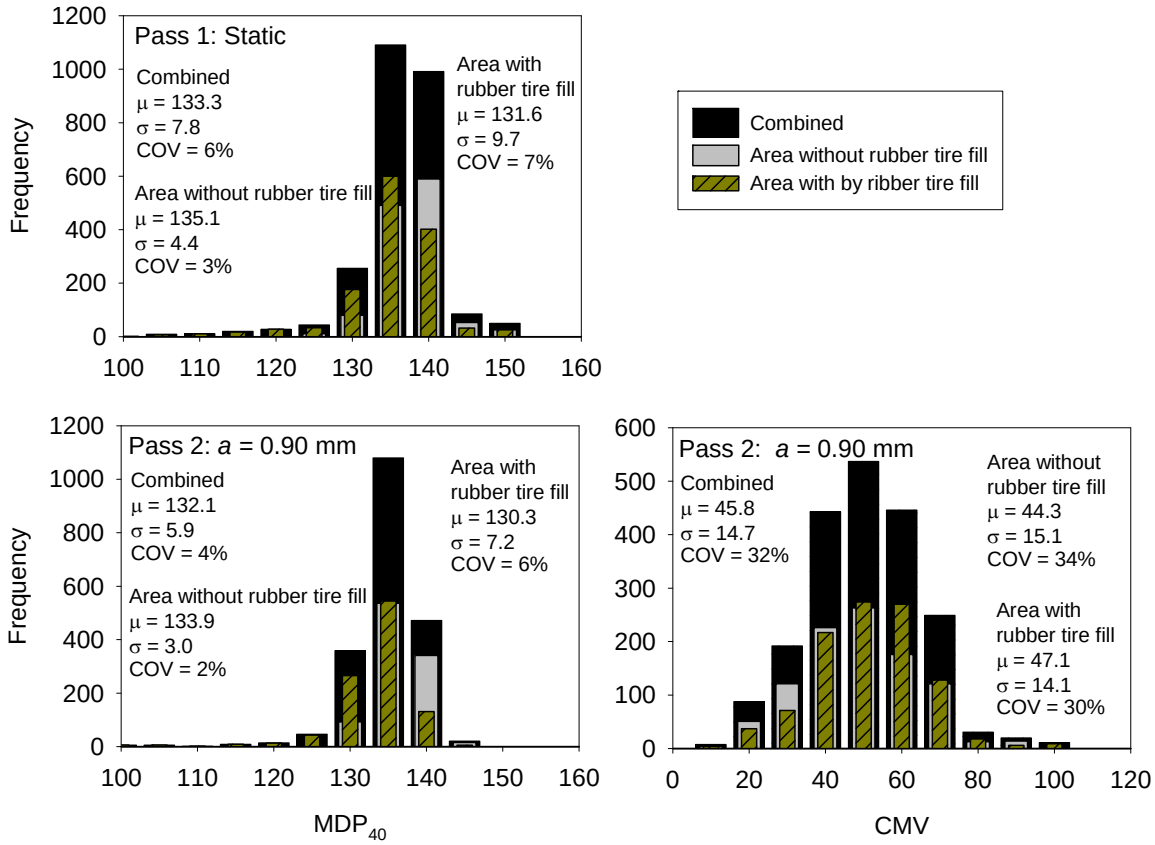

Figure 16. CMV and MDP_{40} histograms – TB2 embankment material

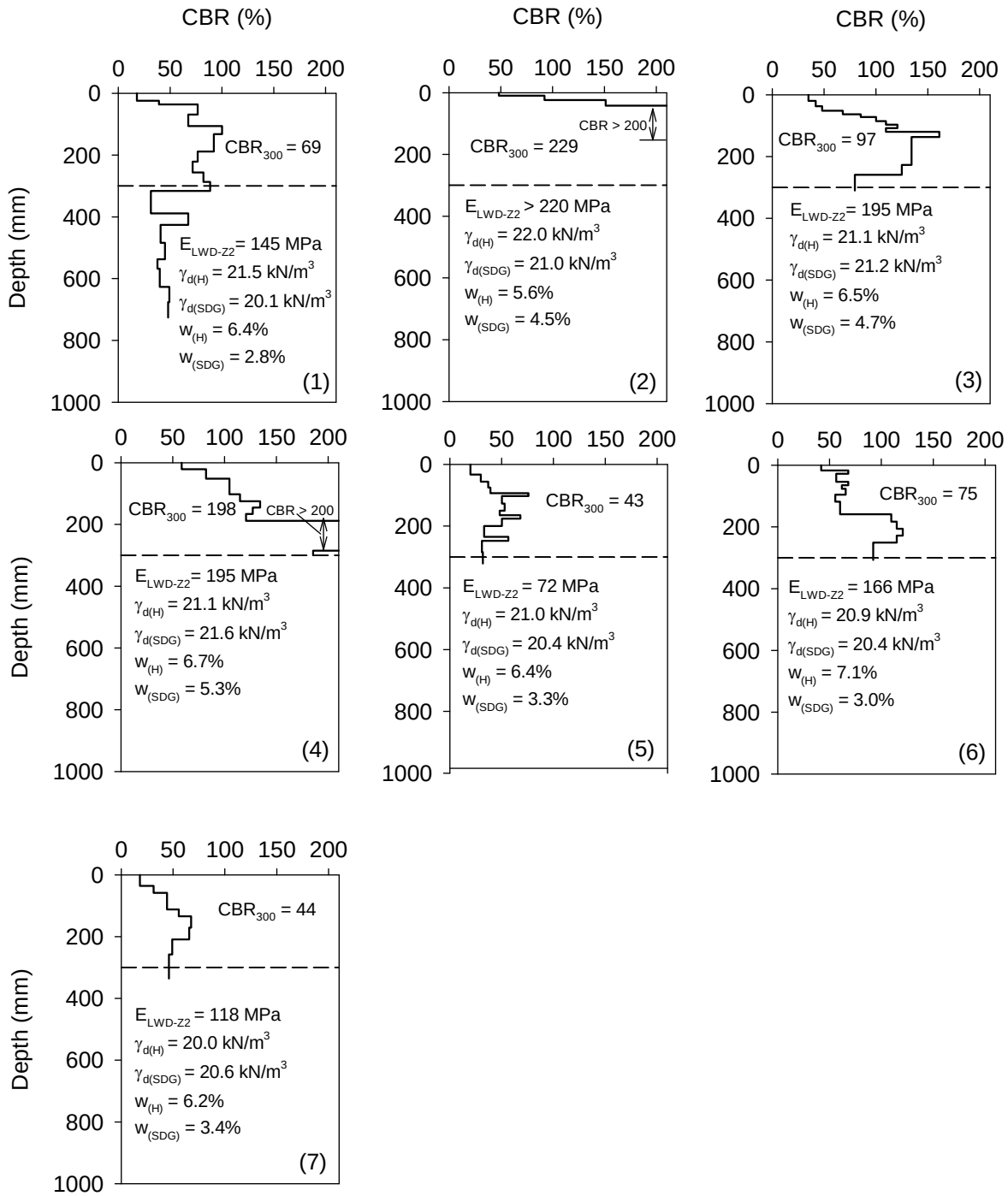

Figure 17. DCP-CBR profiles – TB2 embankment material

Regression Analysis between IC-MVs and Point-MVs

Regression analysis results between IC-MVs and Point-MVs are presented in Figure 18 and the relationships are summarized in Table 6. Simple linear relationships showed the best fit for all the relationships with R^2 values ranging from 0.15 to 0.85. Relationships between IC-MVs

and $E_{LWD\text{-}Z2}$ and CBR_{300} Point-MVs produced better R^2 values (0.41 to 0.85) than between IC-MVs and γ_d Point-MVs (0.26 to 0.52). The relationship between IC-MVs and $w_{(SDG)}$ produced R^2 = 0.48 to 0.50 while $w_{(H)}$ did not show a statistically significant relationship.

Geostatistical Analysis of IC-MVs

Semivariograms of IC-MVs for passes 1 and 2 are presented in Figure 19 and a summary of the spatial statistics (i.e., nugget, sill, and range) are provided in Table 7. A spherical variogram was fit to the experimental semivariogram data. The semivariograms are presented separately for the areas with and without underlying rubber tire fill. The MDP_{40} spatial statistics (sill = 9 and 35 in areas with and without tire fill) and univariate statistics (COV = 2% and 6% in areas with and without tire fill, respectively) indicate greater non-uniformity in the areas with the tire fill compared to the areas without the tire fill. In contrary, CMV statistics showed slightly higher non-uniformity in the areas without tire fill.

Summary of Key Findings

Measurements from TB 2 involved IC-MV mapping using static and low amplitude settings and Point-MVs ($E_{LWD\text{-}Z2}$, CBR_{300}, $w_{(H)}$, $w_{(SDG)}$, $\gamma_{d(H)}$ and $\gamma_{d(SDG)}$) at select locations over a plan area of about 18 m x 71 m. For about half of the test bed, the embankment material was underlain by shredded rubber tires at depths < 1m below the grade. Regression analysis was performed between IC-MVs and Point-MVs by spatially pairing the data, and geostatistical analysis was performed using the GPS referenced IC-MV data. Following is a summary of key findings from these analyses:

- Regression analysis results between IC-MVs and Point-MVs showed simple linear relationships with R^2 values varying from 0.15 to 0.85. Relationships between IC-MVs and $E_{LWD\text{-}Z2}$ and CBR_{300} Point-MVs yielded better R^2 values (0.41 to 0.85) than between IC-MVs and γ_d Point-MVs (0.26 to 0.52).
- The MDP_{40} spatial statistics (sill = 9 and 35 in areas with and without tire fill) and univariate statistics (COV = 2% and 6% in areas with and without tire fill, respectively) indicate increased non-uniformity in the areas with the tire fill compared to the areas without the tire fill. In contrary, CMV statistics showed slightly higher non-uniformity in the areas without the tire fill.

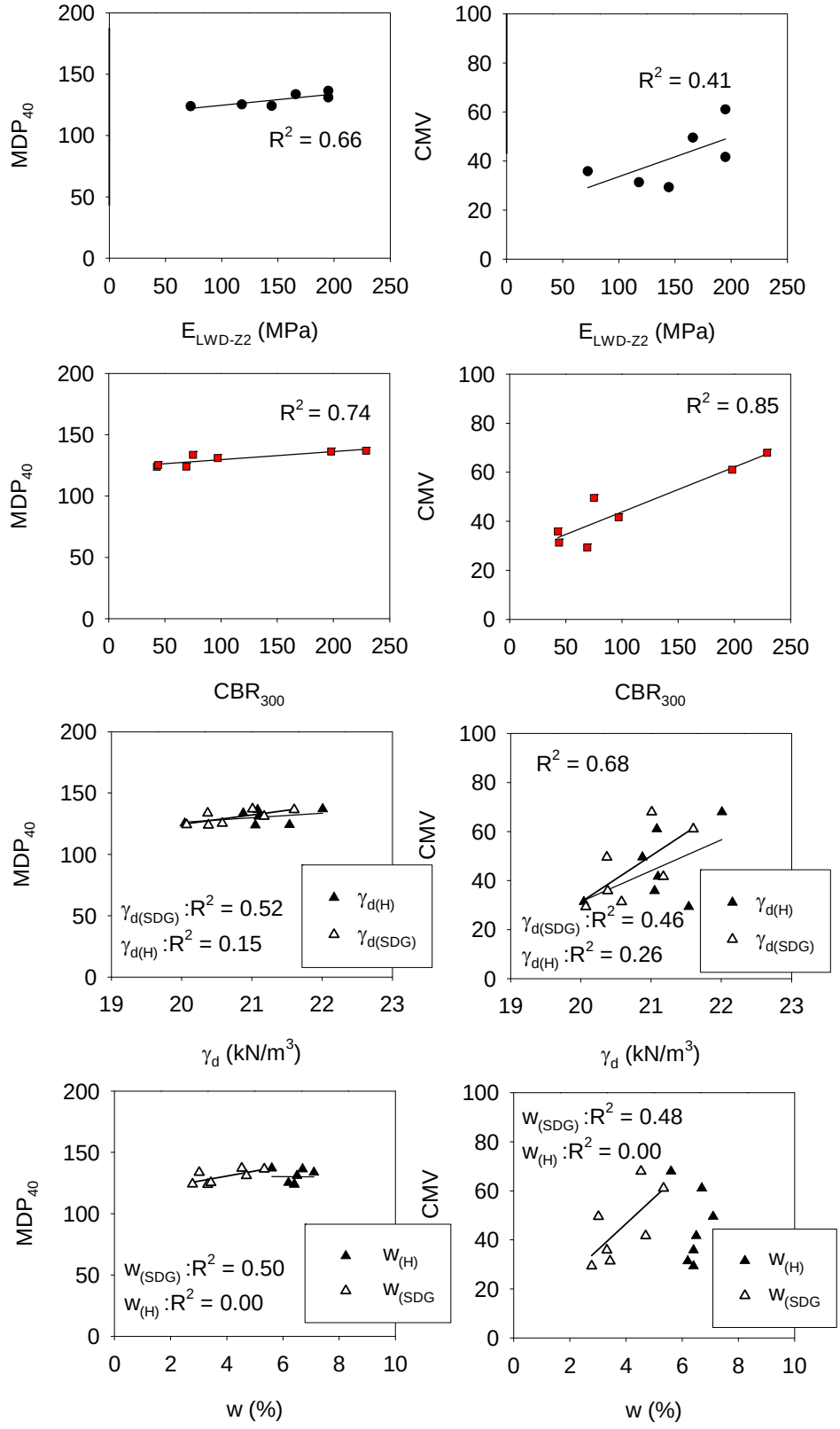

Figure 18. Regression relationships between roller MVs and in-situ point measurements – TB2 embankment material (Pass 2 nominal settings: *a* = 0.90 mm, *f* = 30 Hz, *v* = 4 km/h)

Table 6. Summary of regression analysis – TB2 embankment material

Relationship	a (mm)	n	R^2
$MDP_{40} = 115.5 + 0.09\ (E_{LWD\text{-}Z2})$	0.90	6	0.66
$MDP_{40} = 123.1 + 0.07\ (CBR_{300})$	0.90	7	0.74
$MDP_{40} = 51.6 + 3.72\ (\gamma_{d(H)})$	0.90	7	0.15
$MDP_{40} = -29.4 + 7.69\ (\gamma_{d(SDG)})$	0.90	7	0.52
$MDP_{40} = 114.1 + 4.16\ (w_{(SDG)})$	0.90	7	0.50
$CMV = 17.3 + 0.16\ (E_{LWD\text{-}Z2})$	0.90	7	0.41
$CMV = 25.4 + 0.18\ (CBR_{300})$	0.90	7	0.85
$CMV = -221.4 + 12.63\ (\gamma_{d(H)})$	0.90	7	0.26
$CMV = 4.14 + 10.60\ (w_{(SDG)})$	0.90	7	0.48
$CMV = -345.8 + 18.85\ (\gamma_{d(SDG)})$	0.90	7	0.46

Note: No statistically significant relationship between IC-MVs and $w_{(H)}$

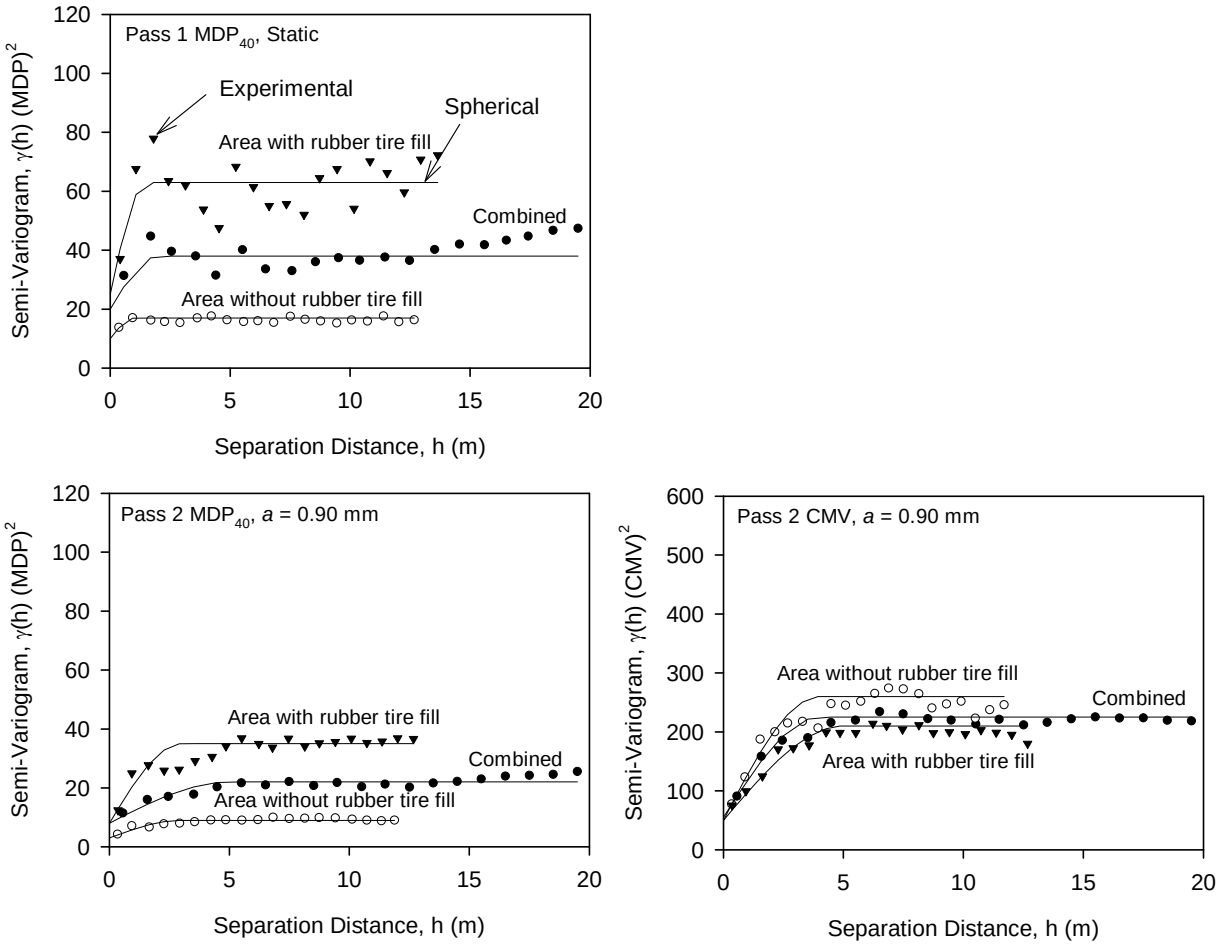

Figure 19. Semivariograms of roller MVs for different passes – TB2 embankment material

Table 7. Summary of univariate and spatial statistics – TB2 embankment material

TB Area	Pass	Measurement	n	*a* (mm)	Univariate Statistics μ	σ	COV (%)	Spatial Statistics Nugget	Sill	Range
Combined	1	MDP_{40}	2618	Static	133.3	7.8	6	20	38	2
	2	MDP_{40}	2025	0.9	132.1	5.9	4	8	22	5
	2	CMV	2025	0.9	45.8	14.7	32	55	225	4
	2	E_{LWD-Z2}	7	0.9	169.8	71.6	42			
	2	CBR_{300}	7	0.9	107.8	74.9	69			
	2	$\gamma_{d(H)}$	7	0.9	21.1	0.6	3	Not enough measurements		
	2	$\gamma_{d(SDG)}$	7	0.9	20.7	0.5	3			
	2	$w_{(H)}$	7	0.9	6.4	0.5	7			
	2	$w_{(SDG)}$	7	0.9	3.9	10	25			
Area without tire fill	1	MDP_{40}	1257	Static	135.1	4.4	3	10	17	1
	2	MDP_{40}	991	0.9	133.9	3.0	2	3	9	3
	2	CMV	991	0.9	44.3	15.1	34	50	270	4
	2	E_{LWD-Z2}	4	0.9	208.2	64.8	31			
	2	CBR_{300}	4	0.9	148.1	77.1	52			
	2	$\gamma_{d(H)}$	4	0.9	21.4	0.4	2	Not enough measurements		
	2	$\gamma_{d(SDG)}$	4	0.9	21.0	0.6	3			
	2	$w_{(H)}$	4	0.9	6.3	0.5	7			
	2	$w_{(SDG)}$	4	0.9	4.3	1.1	25			
Area with tire fill	1	MDP_{40}	1361	Static	131.6	9.7	7	25	63	1.5
	2	MDP_{40}	1034	0.9	130.3	7.2	6	8	35	3
	2	CMV	1034	0.9	47.1	14.1	30	50	210	5
	2	E_{LWD-Z2}	3	0.9	118.7	47	40			
	2	CBR_{300}	3	0.9	54.1	18.3	34			
	2	$\gamma_{d(H)}$	3	0.9	20.7	0.5	3	Not enough measurements		
	2	$\gamma_{d(SDG)}$	3	0.9	20.4	0.1	1			
	2	$w_{(H)}$	3	0.9	6.6	0.5	7			
	2	$w_{(SDG)}$	3	0.9	3.3	0.2	7			

TB 3/8 Embankment Material – Bomag and Caterpillar

Test bed conditions, IC-MV mapping, and Point-MV testing

This test bed consisted of compacted embankment granular subgrade material with plan dimensions of approximately 10 m x 105 m (Figure 20). The area was first mapped using the

Bomag IC roller (TB3) in a manual low amplitude mode (pass 1: a = 0.70 mm, f = 28 Hz) and then in AFC mode (pass 2: a_{max}= 1.90 mm, f = 28 Hz) using setting (2) (recall that using setting (2) the vibration amplitude is controlled to prevent roller jumping). Point-MVs ($E_{LWD\text{-}Z2}$ and $E_{LWD\text{-}Z3}$) were obtained along lane 3 at 62 test locations after pass 2. Following testing, lane 3 was rolled with two additional passes using manual low (pass 3: a = 0.70 mm, f = 28 Hz) and medium (pass 4: a = 1.50 mm, f = 28 Hz) amplitude settings.

Lane 3 was subsequently mapped using the Caterpillar IC roller (TB8) in static mode (designated as pass 5 following the Bomag roller passes) and low amplitude mode (pass 6: a = 0.90 mm, f = 30 Hz). See Table 2 for a summary of roller passes and machine settings. Following pass 6, FWD test measurements were obtained at 88 test locations and static PLT measurements were obtained at 23 test locations along lane 3.

E_{VIB} spatial maps for passes 1 to 4 are shown in Figure 21. Lane 3 E_{VIB}, *jump*, and amplitude measurements are presented for passes 1 to 4 in Figure 22. E_{VIB} measurement values for passes 2, 3, and 4 on lane 3 are compared with in-situ Point MVs obtained after pass 2 in Figure 23. Results presented in Figure 23 indicate that the E_{VIB} measurement values are amplitude dependent. For pass 2 performed in AFC mode (Figure 22), the amplitude values varied from 1.3 to 1.9 mm for E_{VIB} > 160 MPa and the amplitude values varied from 0.6 to 1.3 mm for E_{VIB} < 160 MPa. Roller jumping was observed (as shown with *Jump* > 0) at several short intervals along the length of the test bed for pass 2. No roller jumping was observed for passes 1 and 3 performed in manual a = 0.70 mm mode. Roller jumping was observed for pass 4 performed in manual a = 1.50 mm mode at many locations along the lane. As discussed earlier in the background section of this report, drum jumping behavior is linked to ground stiffness and vibration amplitude and affects the E_{VIB} measurement values. In this study roller jumping (*Jump* > 0) reduced the E_{VIB} values, for example between the 70 to 80 m marks on the test bed the jumping E_{VIB} values are generally < 150 MPa whereas with no jumping, E_{VIB} values are > 220 MPa. Considering the drum jumping behavior observed for pass 4 with a = 1.50 mm, it appears that pass 2 performed in AFC mode with a_{max} = 1.90 mm effectively controlled the roller jumping by reducing the amplitude at many locations along the lane. In some segments though, jumping was still observed even in AFC mode.

The Point-MVs shown in Figure 23 more closely follow the pass 3 E_{VIB} values compared to the pass 2 and 4 results. Of all the Point-MVs, $E_{FWD\text{-}K3}$ measurements tracked best with the E_{VIB} values from pass 3. The $E_{LWD\text{-}Z2}$ and $E_{LWD\text{-}Z3}$ measurements exceeded the upper measurement range of the devices at 20 and 22 test locations, respectively (e.g., between 70 and 85 m distance) along the lane and therefore are not shown in Figure 23.

MDP_{40} spatial maps and linear correlation plots for total pass numbers 5 and 6 are shown in Figure 24 and Figure 25, respectively. MDP_{40} values were not affected by the amplitude setting on this test bed. Roller drum jumping was observed by the roller operator during pass 6. RMV measurements were not available in the output files, however, and the CMV measurements could not be interpreted for this set of passes. It is not known why the CMV values were not recorded during this set of measurement runs. TheMDP_{40} measurement values for passes 5 and 6 are compared with in-situ Point MVs obtained after passes 2 and 6 in Figure 26.

Regression Analysis between IC-MVs and Point-MVs

Regression analysis results between E_{VIB} and Point-MVs are presented in Figure 27 and the relationships are summarized in Table 8. Simple linear relationships showed the best fit for all the relationships. E_{VIB} relationships with E_{V1} and E_{FWD-K3} showed good correlations with $R^2 > 0.6$, while with E_{LWD-Z2}, E_{LWD-Z3}, and E_{V2} showed relatively low R^2 values (0.15 to 0.37).

Regression analysis results between MDP_{40} and Point-MVs are presented in Figure 28 and the relationships are summarized in Table 9. No statistically significant relationships were observed between E_{LWD-Z2}, E_{LWD-Z3}, and E_{V2} Point-MVs and MDP_{40}. MDP_{40} relationship with E_{V1} and E_{FWD-K3} produced relatively low R^2 values (0.10 to 0.26). MDP_{40} obtained in static and low amplitude settings were similar along the test strip and showed a correlation with $R^2 = 0.5$.

Weak correlations observed in this test bed are attributed to: (a) the narrow range of measurements over which the correlations were performed (note that the test bed consisted of very stiff compacted embankment material), and (b) the differences in measurement influence depths between IC-MVs and different Point-MVs.

Figure 20. TB 3/8 embankment material area and testing on lane 3

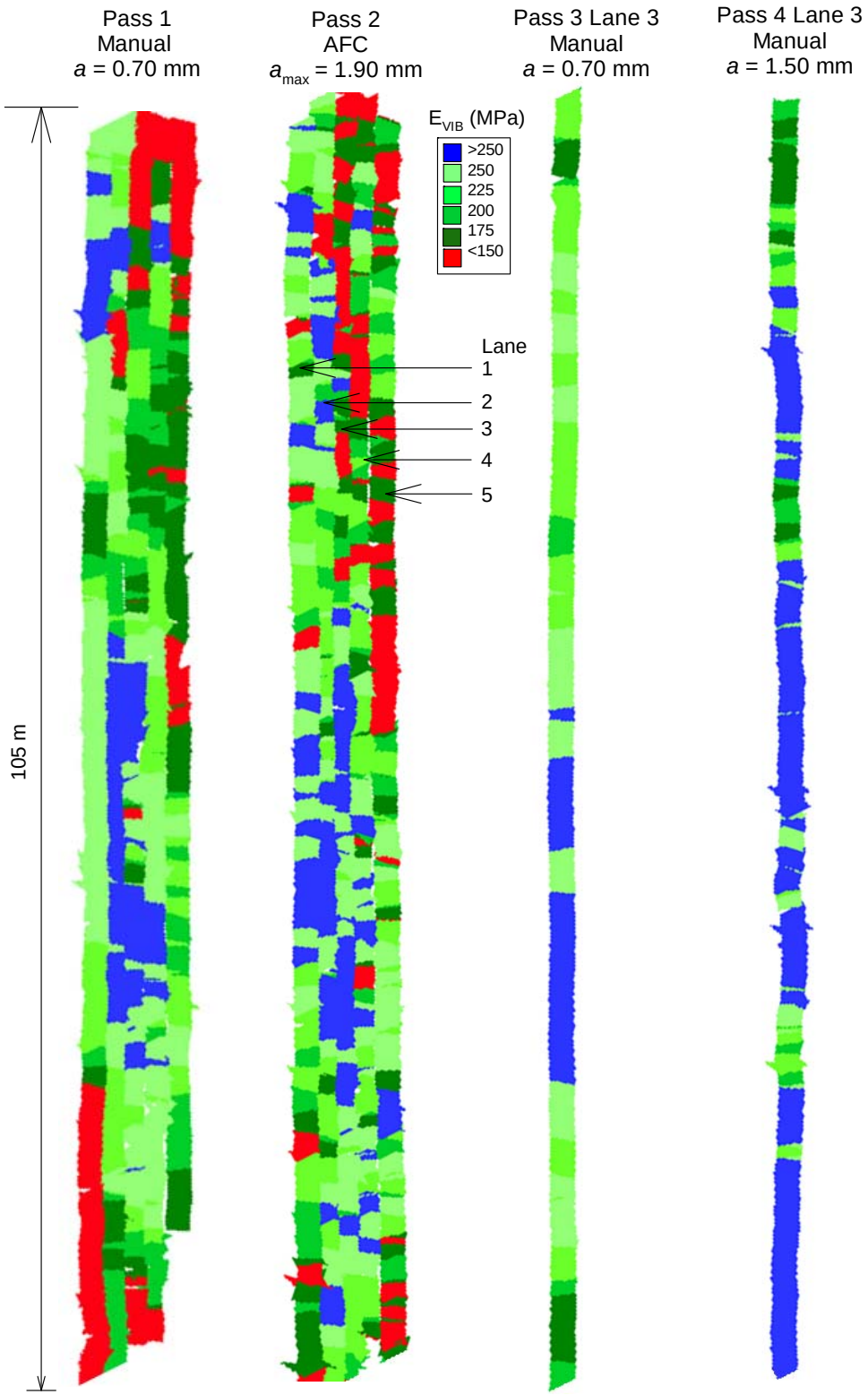

Figure 21. E_{VIB} spatial maps with different machine amplitude settings in manual and AFC mode – TB3 embankment material

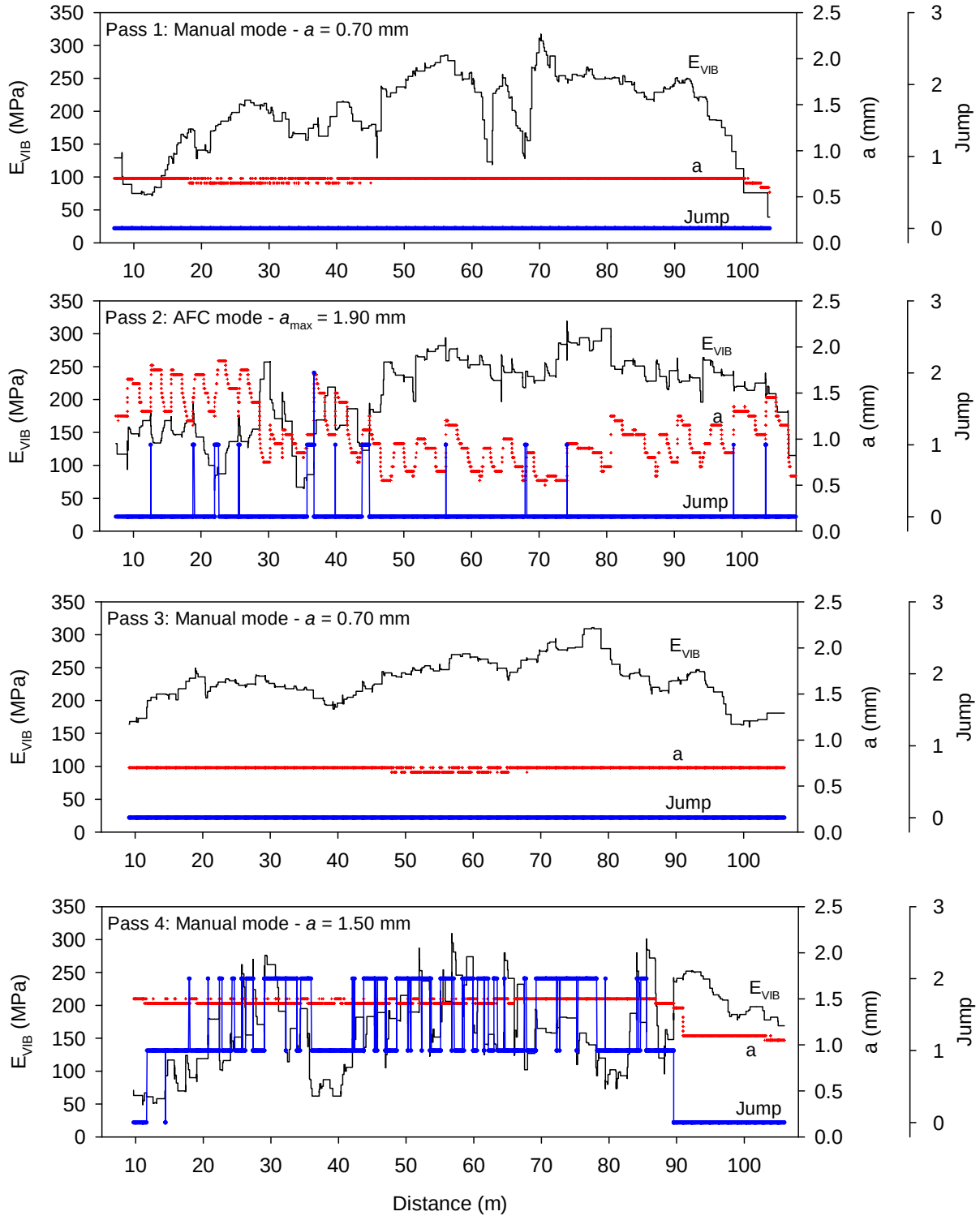

Figure 22. E_{VIB} and jump measurements from each pass on lane 3 – TB3 embankment material

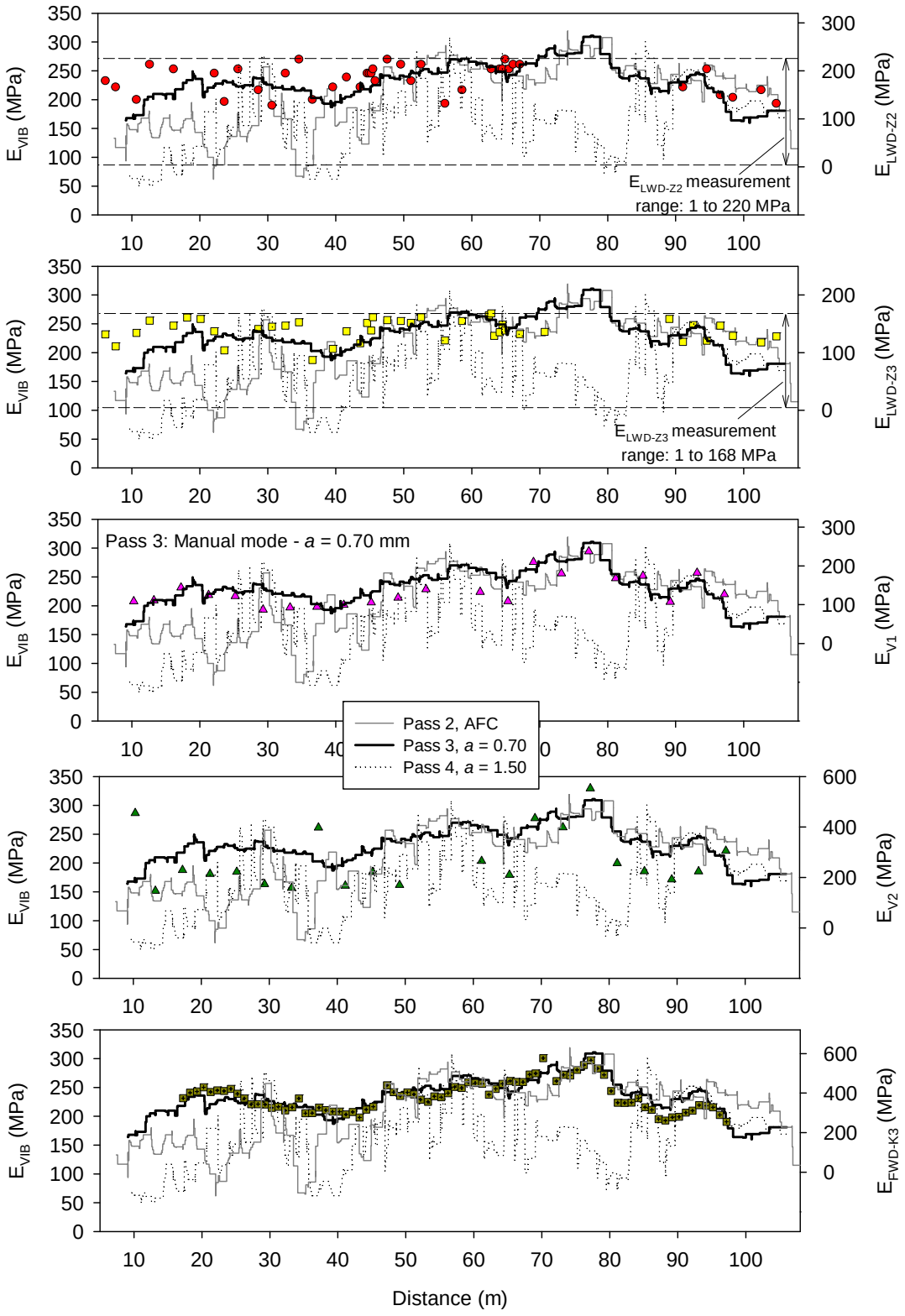

Figure 23. Comparison between E_{VIB} (pass 3) and Point-MVs on lane 3 – TB3 embankment material

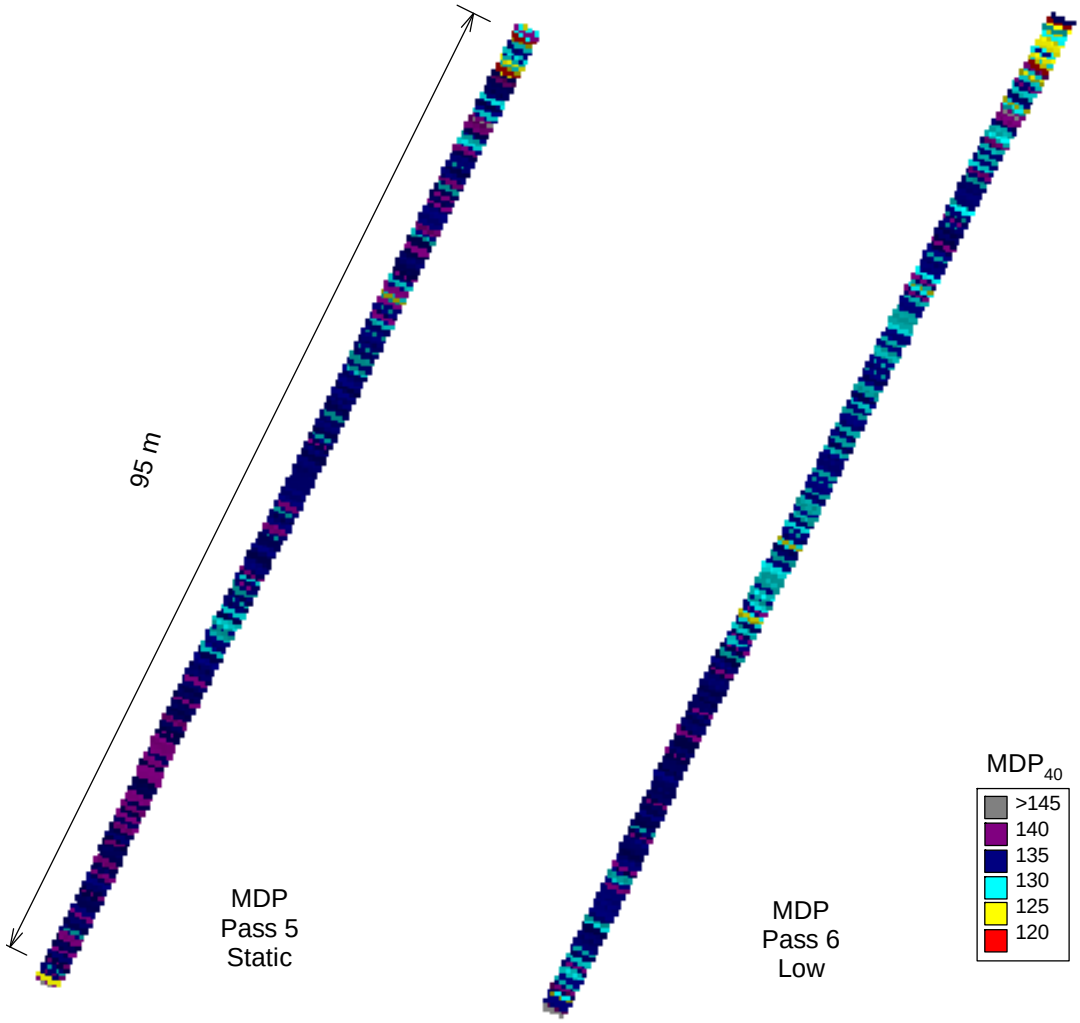

Figure 24. MDP spatial maps for two roller passes on TB8 embankment material

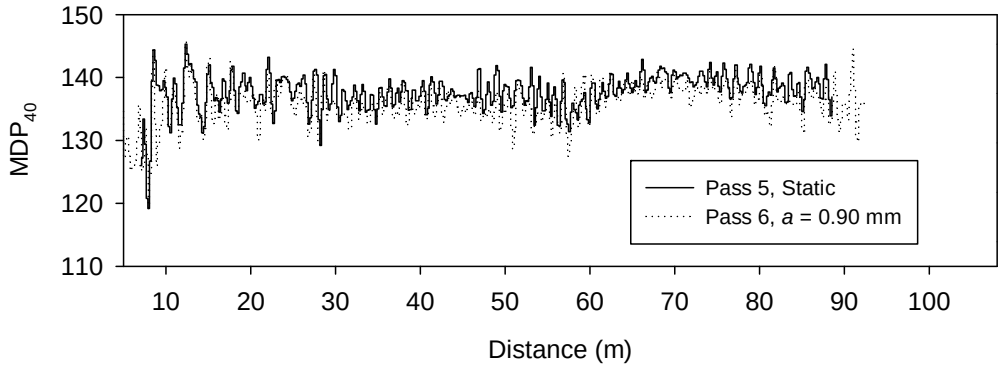

Figure 25. MDP measurements from passes 1 and 2 on lane 3 – TB8 embankment material

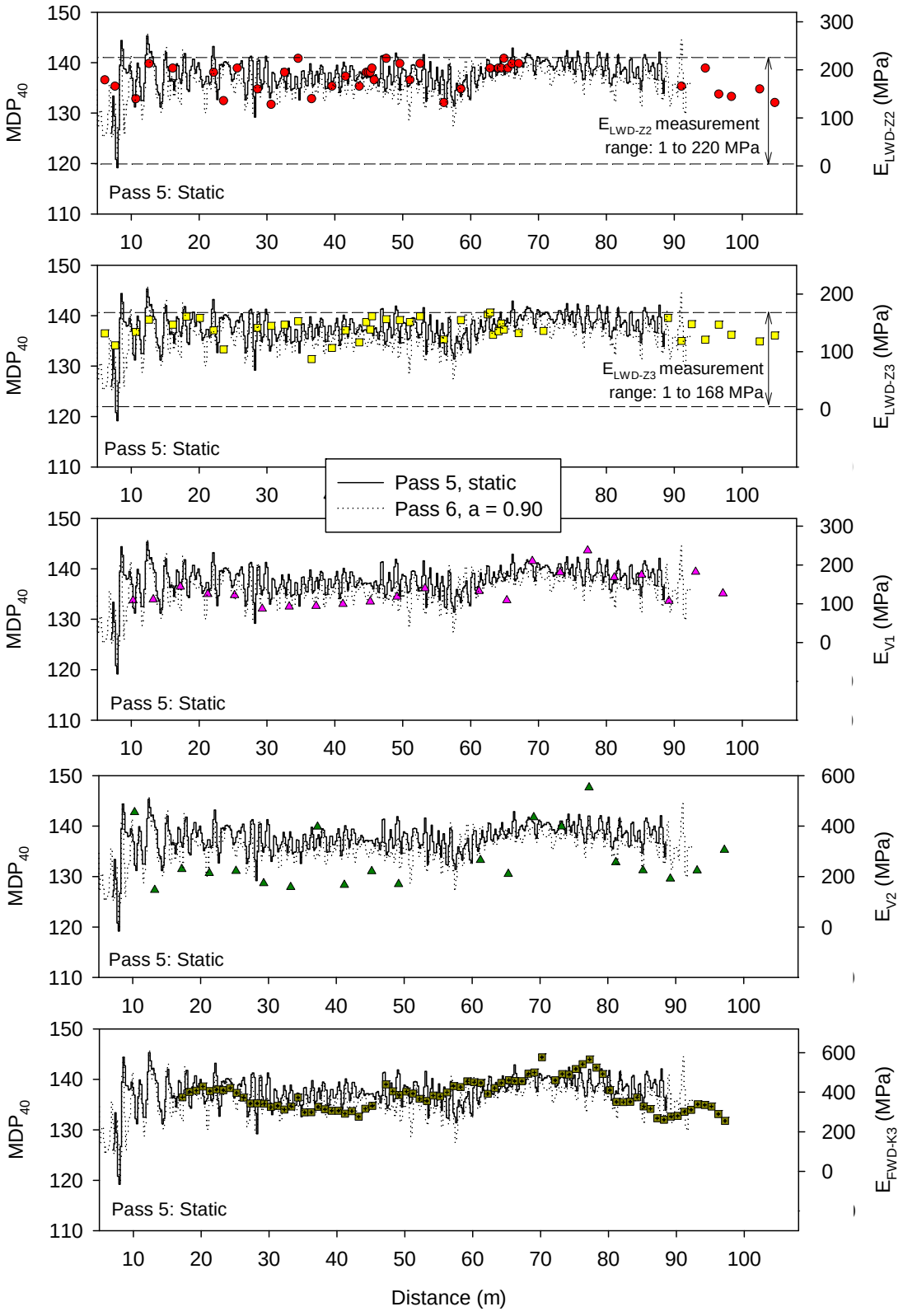

Figure 26. Comparison between MDP_{40} (pass 5) and Point-MVs on lane 3 – TB8 embankment material

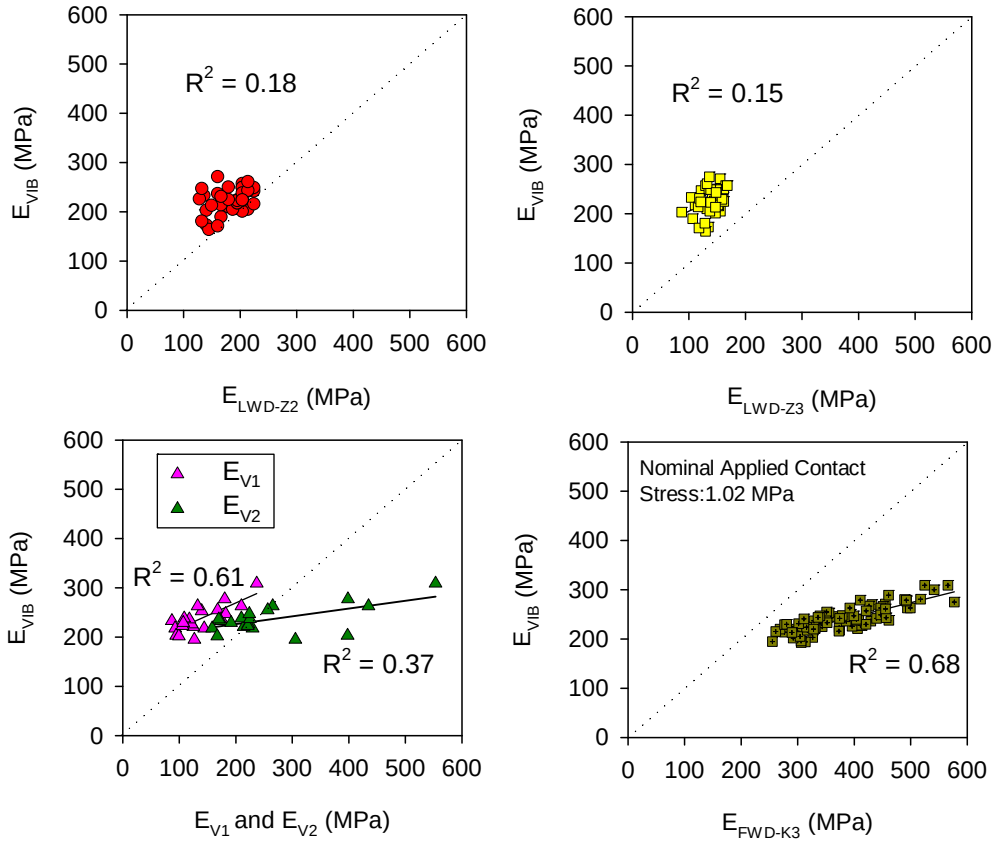

Figure 27. Regression relationships between E_{VIB} and Point-MVs – TB3 embankment material (Pass 3 nominal settings: *a* = 0.70 mm, *f* = 28 Hz, *v* = 4 km/h)

Table 8. Summary of regression analysis – TB3 embankment material

Relationship	a (mm)	n	R^2
$E_{VIB} = 158.2 + 0.36\ (E_{LWD\text{-}Z2})$	0.70	40	0.18
$E_{VIB} = 149.9 + 0.55\ (E_{LWD\text{-}Z3})$	0.70	42	0.15
$E_{VIB} = 166.5 + 0.51\ (E_{V1})$	0.70	20	0.61
$E_{VIB} = 194.6 + 0.16\ (E_{V2})$	0.70	20	0.37
$E_{VIB} = 131.0 + 0.29\ (E_{FWD\text{-}K3})$	0.70	79	0.68

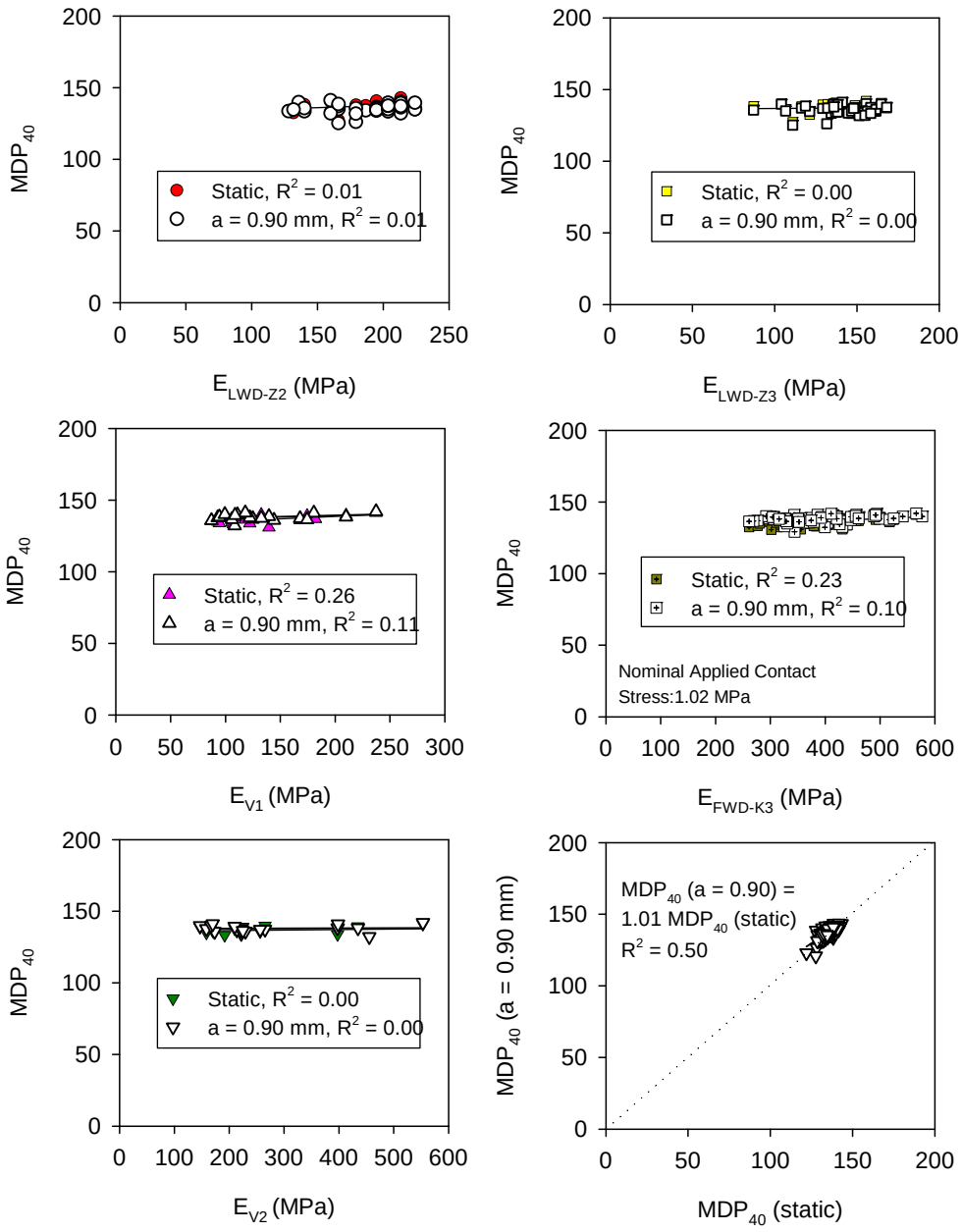

Figure 28. Regression relationships between MDP_{40} and Point-MVs – TB8 embankment material

Table 9. Summary of regression analysis – TB8 embankment material

Relationship	a (mm)	n	R^2
$MDP_{40} = 131.9 + 0.03\ (E_{V1})$	Static	21	0.26
$MDP_{40} = 130.3 + 0.02\ (E_{FWD-K3})$	Static	75	0.23
$MDP_{40} = 135.6 + 0.02\ (E_{V1})$	0.90	21	0.11
$MDP_{40} = 133.8 + 0.01\ (E_{FWD-K3})$	0.90	75	0.10

Note: no statistically significant relationship between E_{LWD-Z2}, E_{LWD-Z3}, and E_{V2} Point MVs and MDP_{40}

Summary of Key Findings

Measurements from TBs 3 and 8 involved obtaining E_{VIB} IC-MVs in manual and AFC mode settings, MDP_{40} IC-MVs in static and low amplitude settings, and Point-MVs ($E_{LWD\text{-}Z2}$, $E_{LWD\text{-}Z3}$, $E_{FWD\text{-}K3}$, E_{V1}, and E_{V2}), along a 100 m long test strip. Comparisons are made between AFC mode and manual mode operations to assess how drum jumping behavior is controlled using the AFC mode and the impact of jumping on E_{VIB} values. Regression analysis was performed between IC-MVs obtained in manual constant amplitude settings and Point-MVs by spatially pairing the data. Following is a summary of key findings from these analyses:

- E_{VIB} measurements values obtained in different amplitude settings indicated that the values are amplitude dependent.
- Roller jumping was not observed for passes performed in manual a = 0.70 mm mode for the Bomag IC roller. Roller jumping was observed for a pass performed in manual a = 1.50 mm mode at many locations along the test bed. For a pass performed in AFC mode (using a_{max} = 1.90 setting), the amplitude values varied between 1.3 to 1.9 mm for E_{VIB} > 160 MPa and the amplitude values varied between 0.6 and 1.3 mm for E_{VIB} < 160 MPa. Roller jumping was observed at several segmented sections when operated in AFC mode.
- The Point-MVs tracked well with E_{VIB} values obtained in manual a = 0.70 mm setting compared to other higher amplitude settings. Of all the Point-MVs, $E_{FWD\text{-}K3}$ produced the best correlation with E_{VIB} values.
- Regression analyses yielded good correlations with $R^2 > 0.6$ between E_{VIB} and E_{V1} and $E_{FWD\text{-}K3}$ Point-MVs, and relatively weak correlations with R^2 values (0.15 to 0.37) for $E_{LWD\text{-}Z2}$, $E_{LWD\text{-}Z3}$, and E_{V2} Point-MVs.
- No statistically significant relationships were observed between $E_{LWD\text{-}Z2}$, $E_{LWD\text{-}Z3}$, and E_{V2} Point-MVs and MDP_{40}. MDP_{40} relationships with E_{V1} and $E_{FWD\text{-}K3}$ showed relatively low R^2 values (0.10 to 0.26). Weak correlations are attributed to: (a) narrow range of measurements over which the correlations were performed, and (b) potential differences in measurement influence depths.
- MDP_{40} obtained in static and low amplitude settings were similar along the test strip and showed a correlation with R^2= 0.5.

TBs 4 and 5 Gravel Subbase Calibration Test Strips – Caterpillar and Bomag

Test beds construction and in-situ testing – TB4 (Lanes 2 and 3)

TB 4 consisted of approximately 200 to 250 mm thick loosely placed aggregate subbase material over a geosynthetic separation material underlain by granular embankment material (Figure 29). Two side-by-side lanes (lanes 2 and 3) were selected for this test bed and were compacted with eight roller passes using the Caterpillar IC roller. Lane 2 was compacted in static mode while lane 3 was compacted using the low amplitude setting (a = 0.90 mm and f = 30 Hz). The length of each testing lane was about 100 m. A summary of nominal machine settings is provided in Table 2. DCP-CBR, $w_{(H)}$, $w_{(SDG)}$, $\gamma_{d(H)}$, and $\gamma_{d(SDG)}$ Point-MVs were obtained at13 test locations along each lane prior to compaction and after pass 8. $E_{LWD\text{-}Z3}$, E_{BCD} and $E_{FWD\text{-}K3}$ Point-MVs were obtained at 13 test locations along each lane after pass 8 only. $E_{FWD\text{-}K3}$ tests performed at 11 locations along lane 3 yielded deflections that are greater than the upper

measurement range of the deflection sensors and were not reported in the output file. As a result $E_{FWD\text{-}K3}$ measurements were available for only two point locations within lane 3. The moisture content of the subbase material was relatively uniform (6 to 7%) for this test bed.

Figure 29. Construction of TBs 4 and 5 gravel subbase material calibration test strips

IC-MVs and Point-MVs – TB4 (Lanes 2 and 3)

Spatial IC-MV (MDP_{40} and CMV) maps for each pass on lanes 2 and 3 are provided in Figure 30 and Figure 31, respectively. IC-MV plots for lanes 2 and 3 for passes 1, 2, 4, 6, and 8 are provided in Figure 32. IC-MV plots in Figure 32 indicate that the MVs are repeatable and there is an increase in the IC-MVs with increasing roller passes indicating compaction.

Average IC-MV and Point-MV compaction curves for lanes 2 and 3 are presented in Figure 33. The average MDP_{40}, CMV, CBR, and γ_d measurements generally increased with increasing roller pass indicating compaction. DCP-CBR depth profiles obtained at pass 0 and 8 from each point location on lanes 2 and 3 are provided in Figure 34 and Figure 35, respectively. Average MDP_{40} values for lane 2 compacted in static mode are on-average higher than the MDP_{40} values on lane 3 compacted in low amplitude vibration mode. The average $E_{LWD\text{-}Z3}$ and $E_{FWD\text{-}K3}$ values on lane 2 after pass 8 are also higher than lane 3 (note that the average $E_{FWD\text{-}K3}$ measurement for lane 2 is based on 13 measurements while for lane 3 is based on only 2 measurements). However, the

average relative compaction values are similar for lanes 2 and 3 after pass 8 (100 to 101% using $\gamma_{d(H)}$ about 103% using $\gamma_{d(SDG)}$ measurements).

IC-MV plots in comparison with Point-MVs along lanes 2 and 3 after pass 8 are provided in Figure 36 to Figure 38. Regression analysis between IC-MVs and Point-MVs by spatially pairing the nearest point data is presented in Figure 39 to Figure 41, and the relationships are summarized in Table 10. Regression relationships generally showed weak correlations with R^2 values ranging from 0.0 to 0.48. The narrow range of measurements for this test bed contributed to low R^2 values.

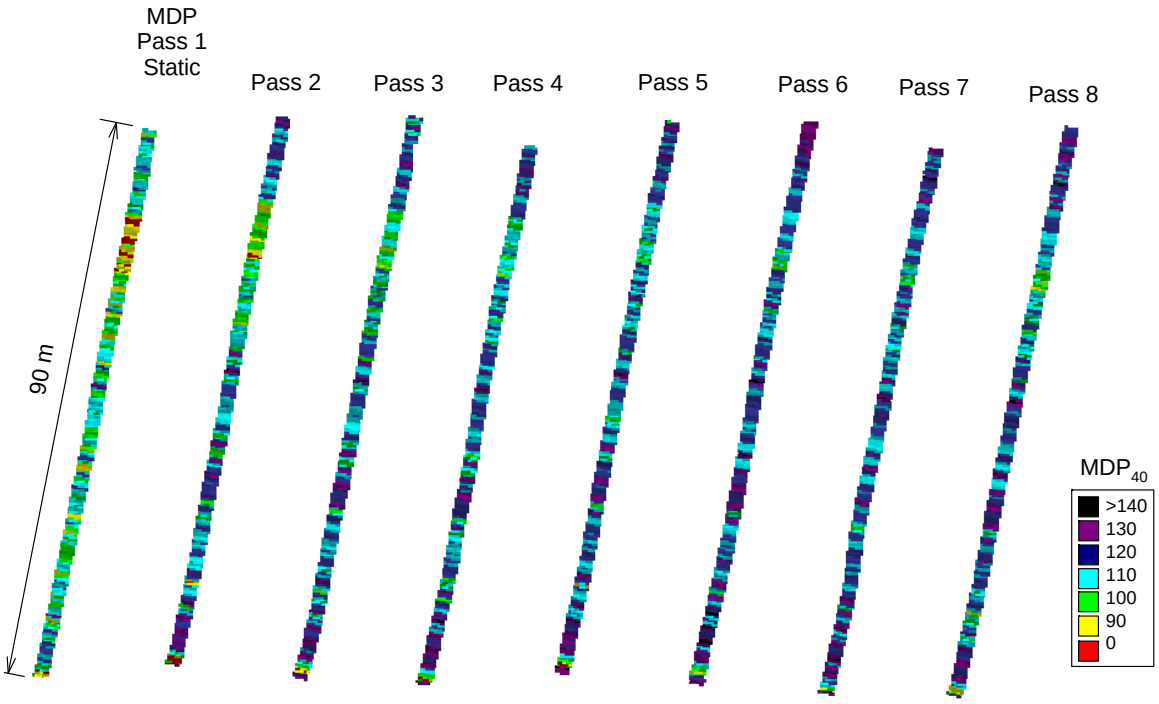

Figure 30. MDP_{40} maps on lane 2 for passes 1 to 8 made in static mode – TB4 gravel subbase material

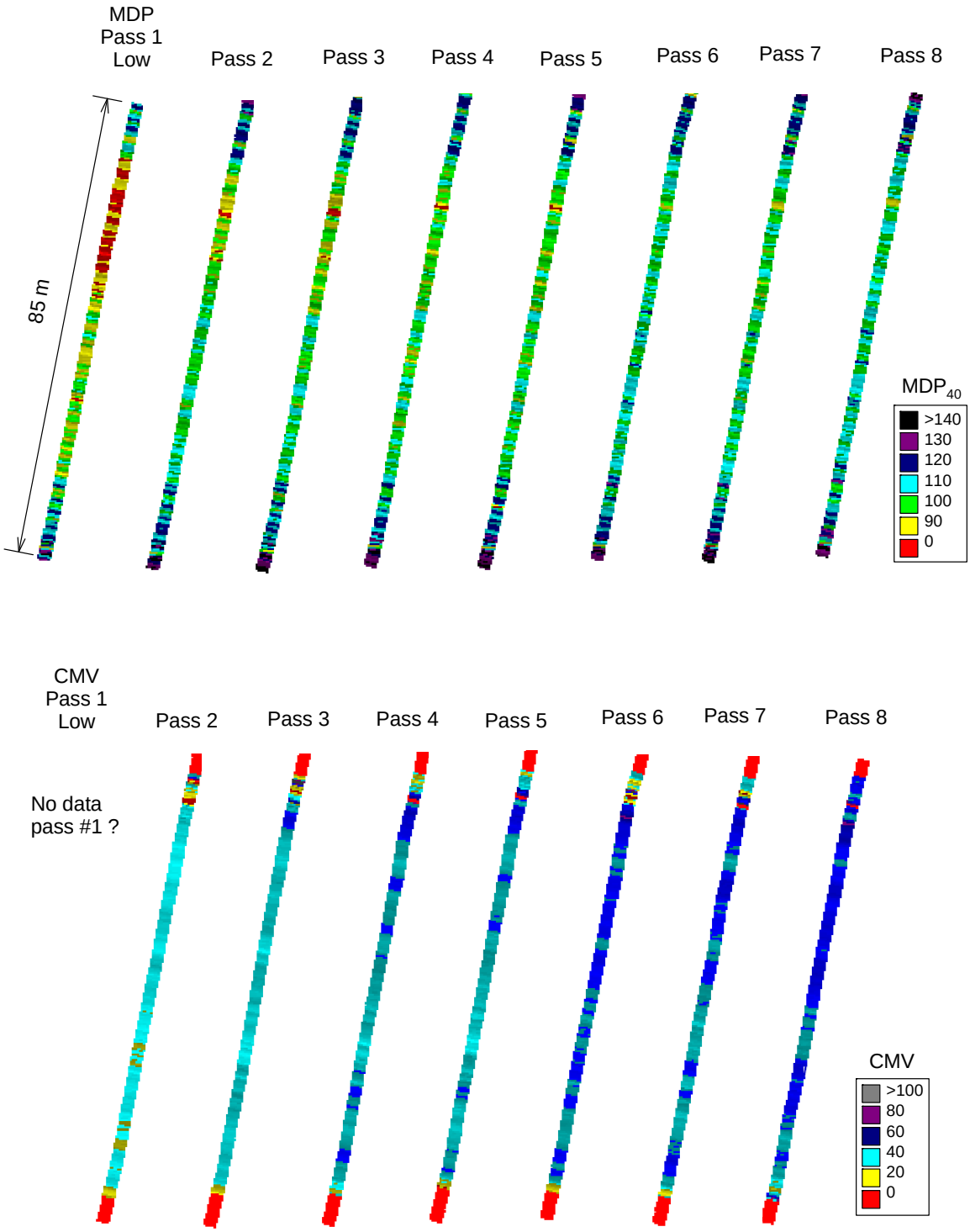

Figure 31. MDP_{40} (top) and CMV (bottom) maps on lane 3 for passes 1 to 8 made with *a* = 0.90 mm setting – TB4 gravel subbase material

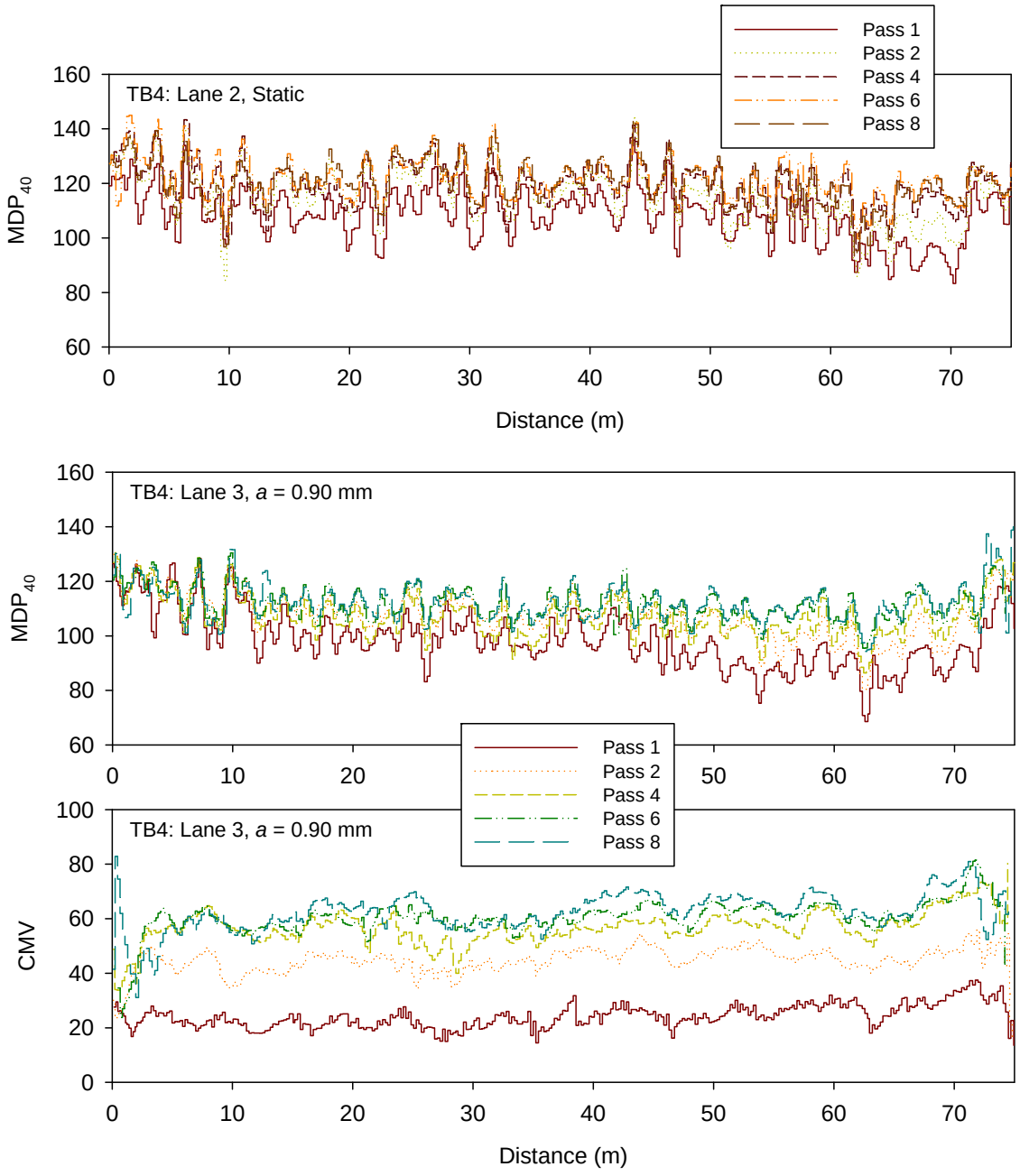

Figure 32. MDP_{40} and CMV plots on lanes 2 and 3 for different roller passes – TB4 gravel subbase material

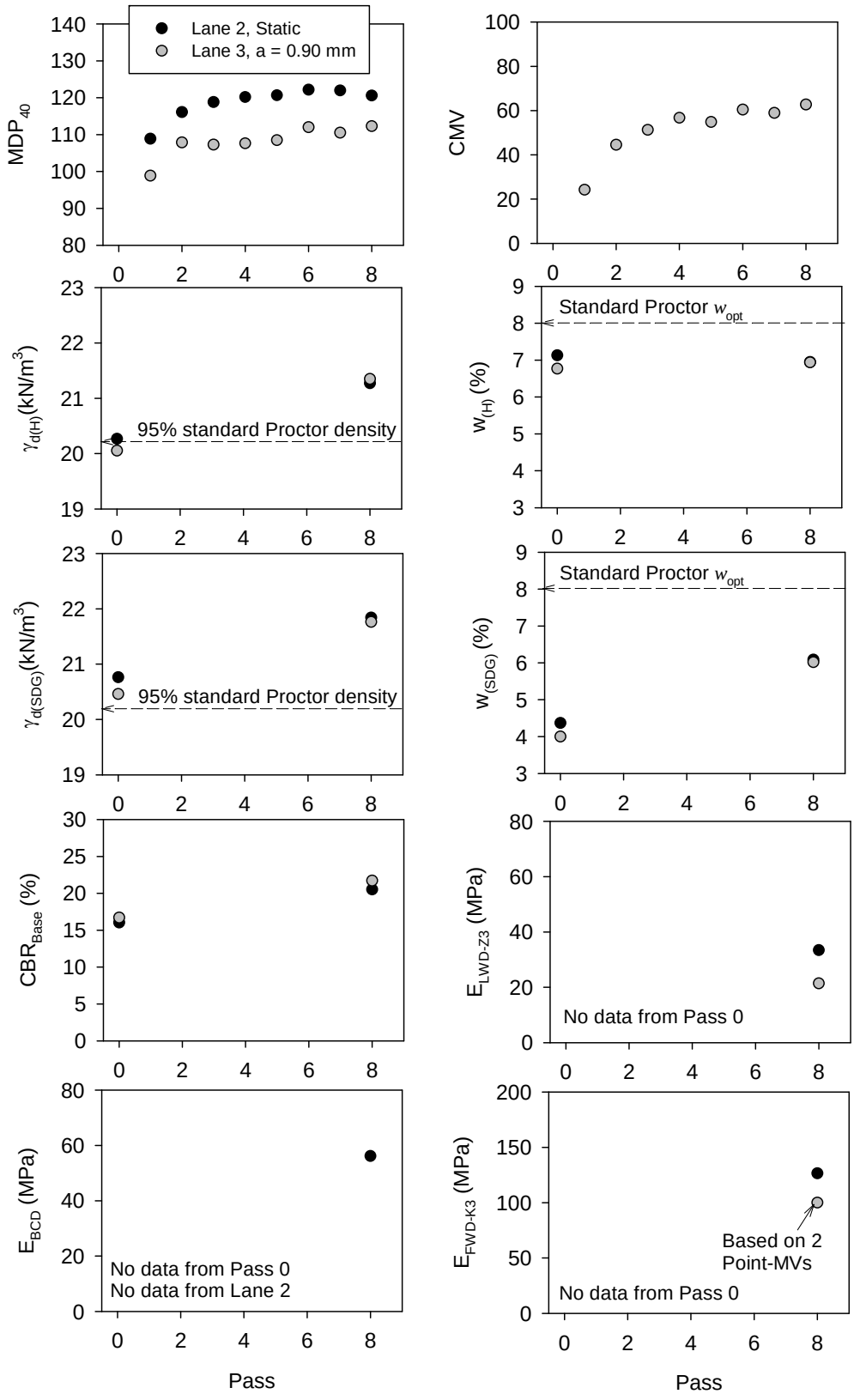

Figure 33. Average IC-MV and Point-MV compaction curves on lanes 2 and 3 – TB4 gravel subbase material

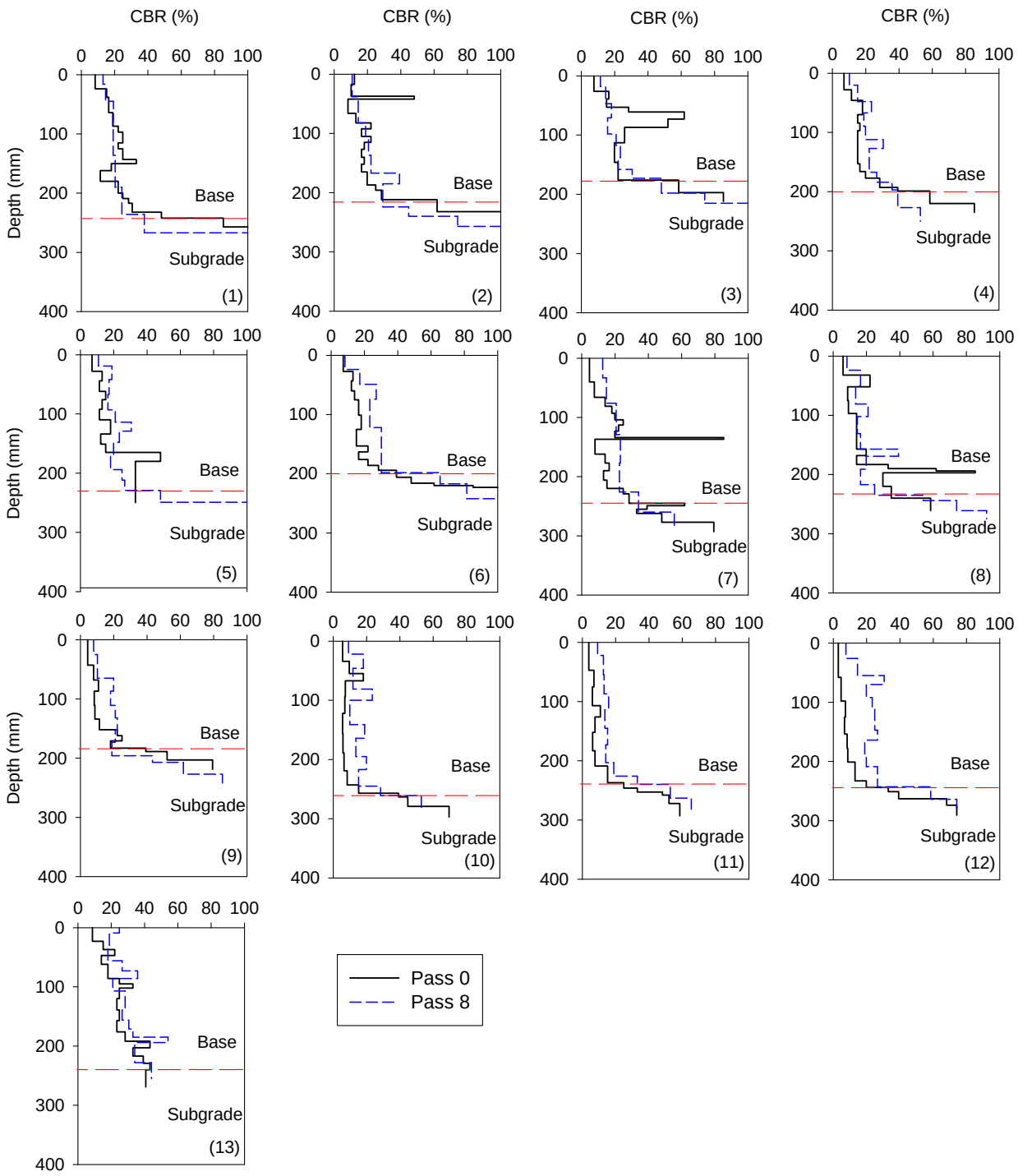

Figure 34. DCP-CBR depth profiles before compaction and after eight roller passes on lane 2 – TB4 gravel subbase material

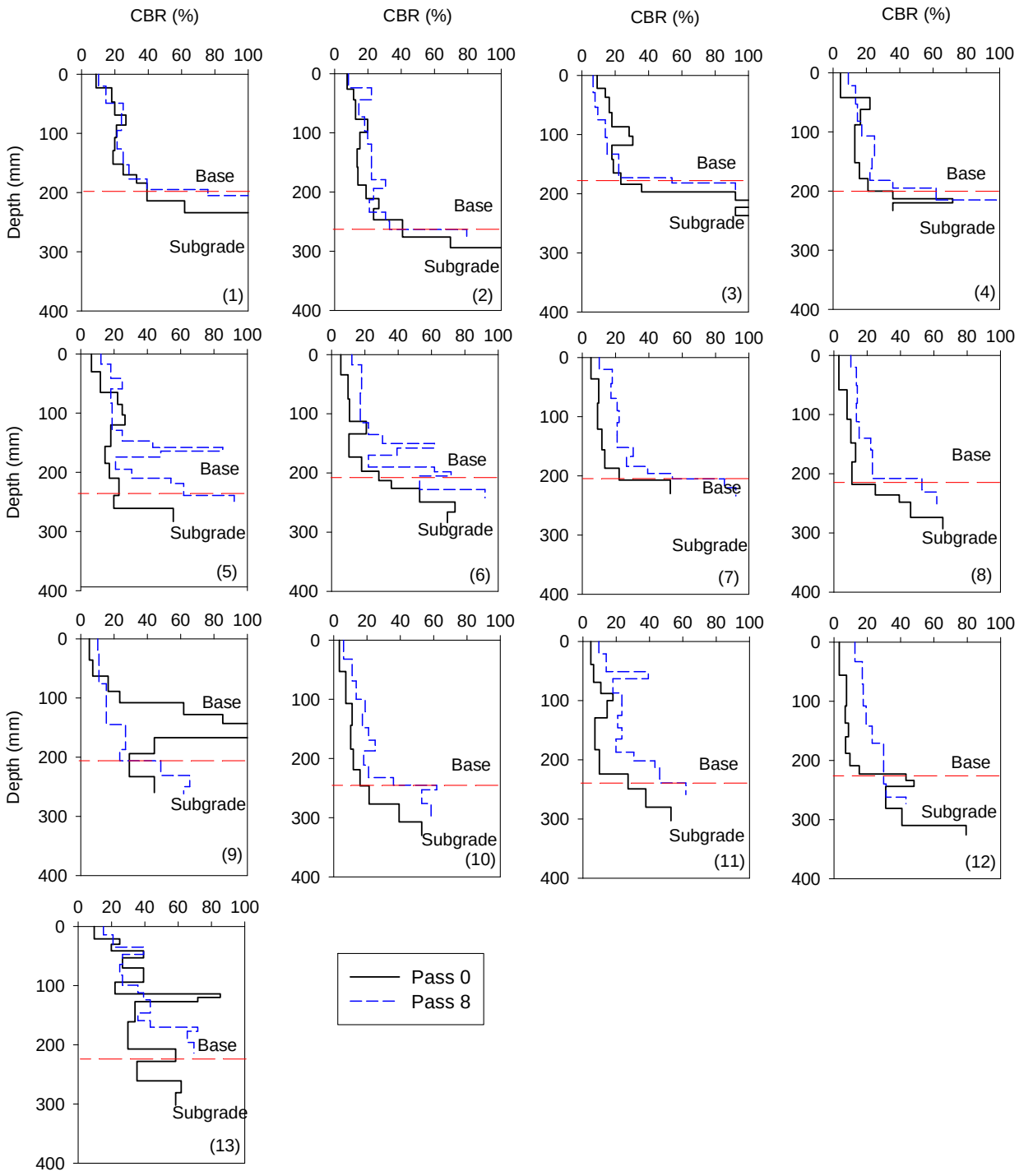

Figure 35. DCP-CBR depth profiles before compaction and after eight roller passes on lane 3 – TB4 gravel subbase material

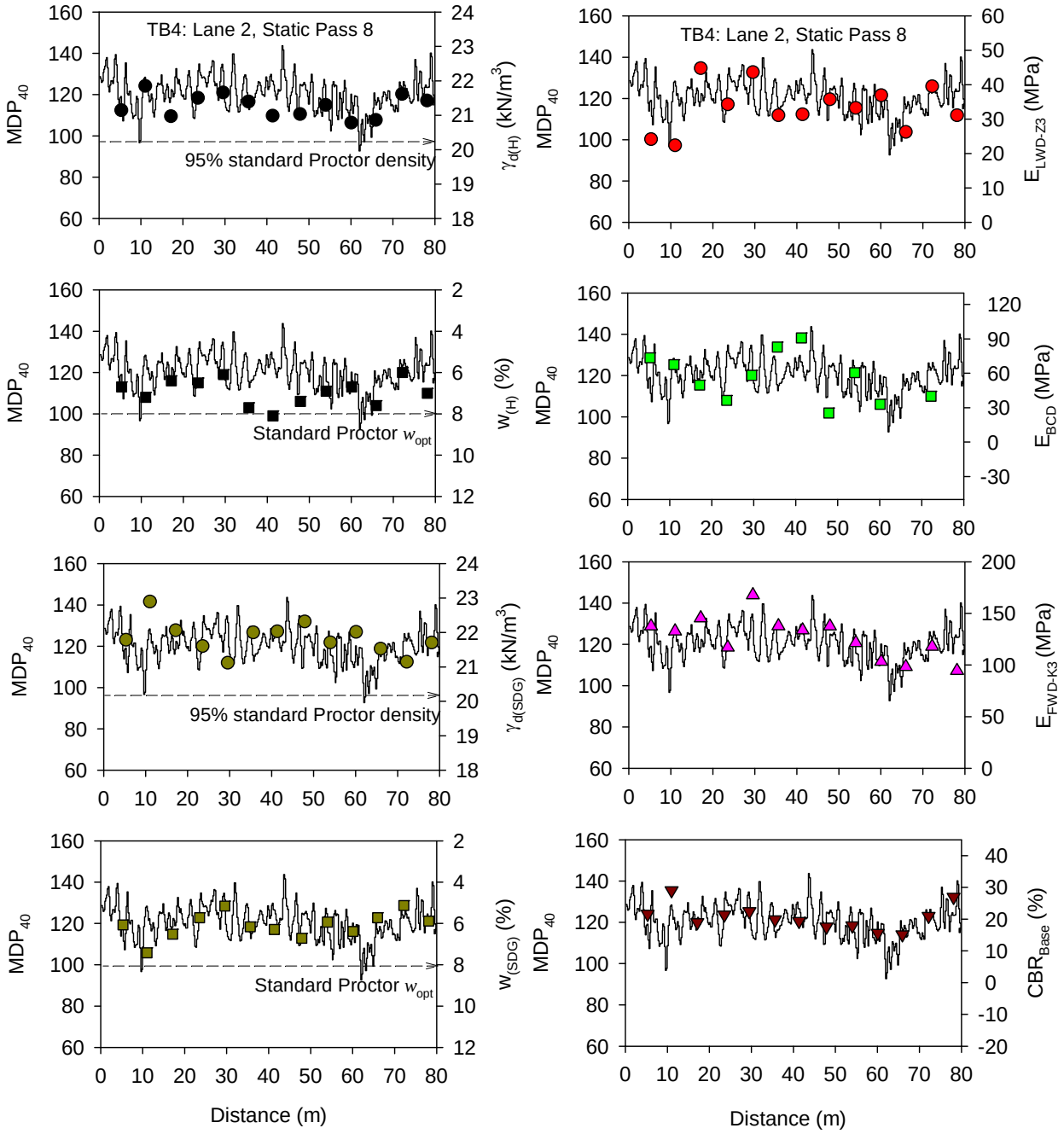

Figure 36. Comparison between MDP_{40} and Point-MVs on lane 2 (static pass 8) – TB4 gravel subbase material

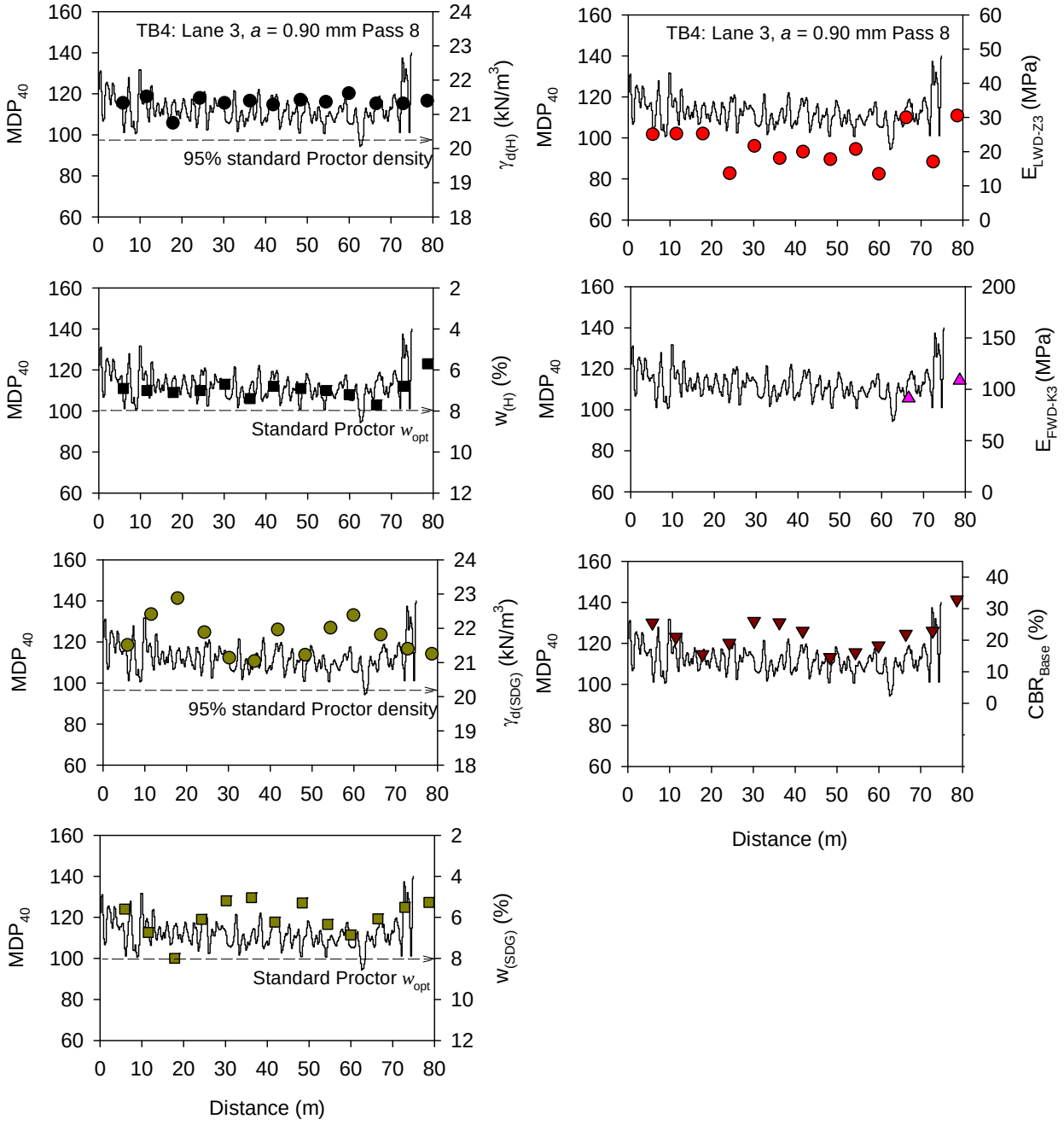

Figure 37. Comparison between MDP_{40} and Point-MVs on lane 3 (a = 0.90 mm pass 8) – TB4 gravel subbase material

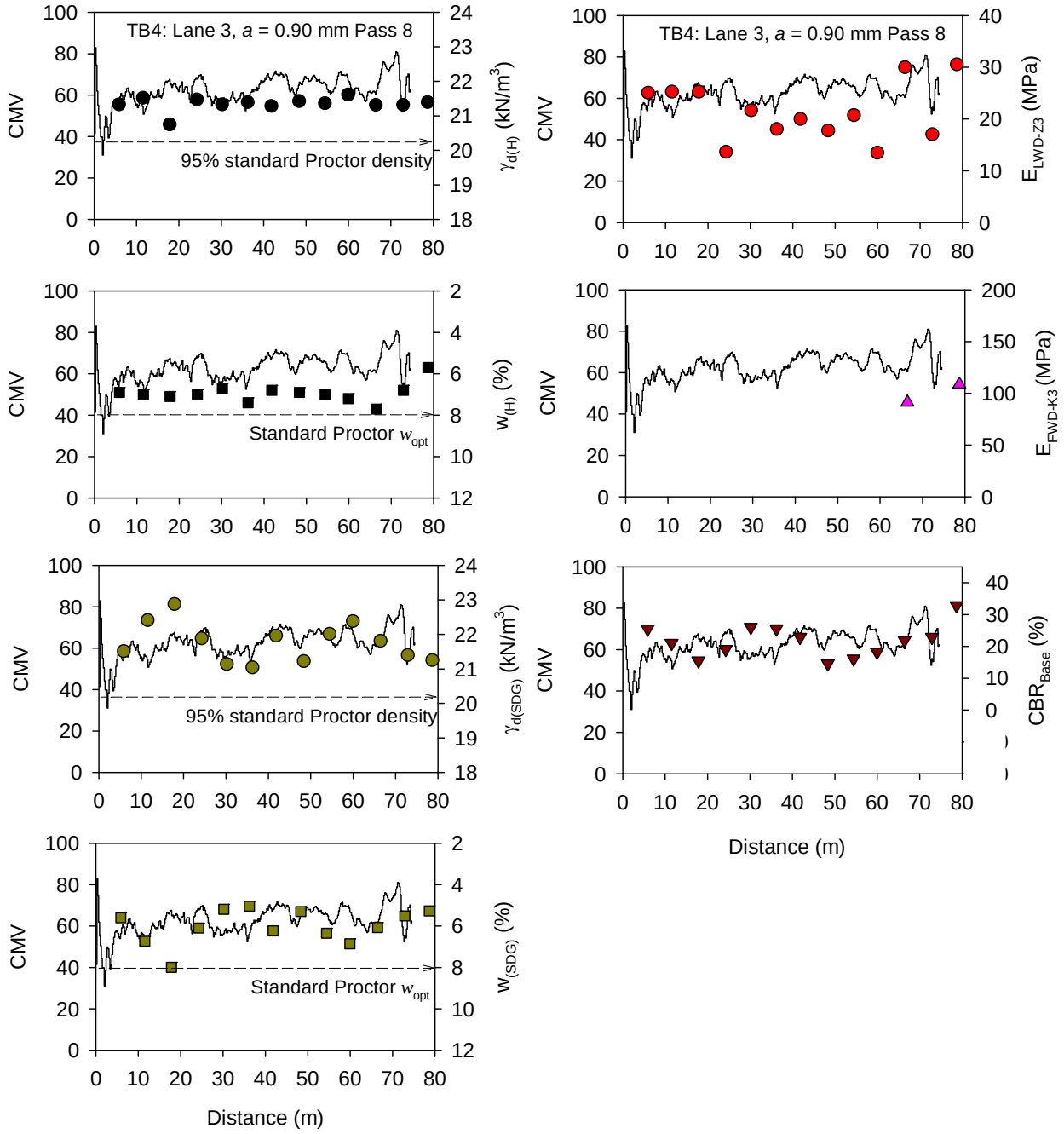

Figure 38. Comparison between CMV and Point-MVs on lane 3 (*a* = 0.90 mm pass 8) – TB4 gravel subbase material

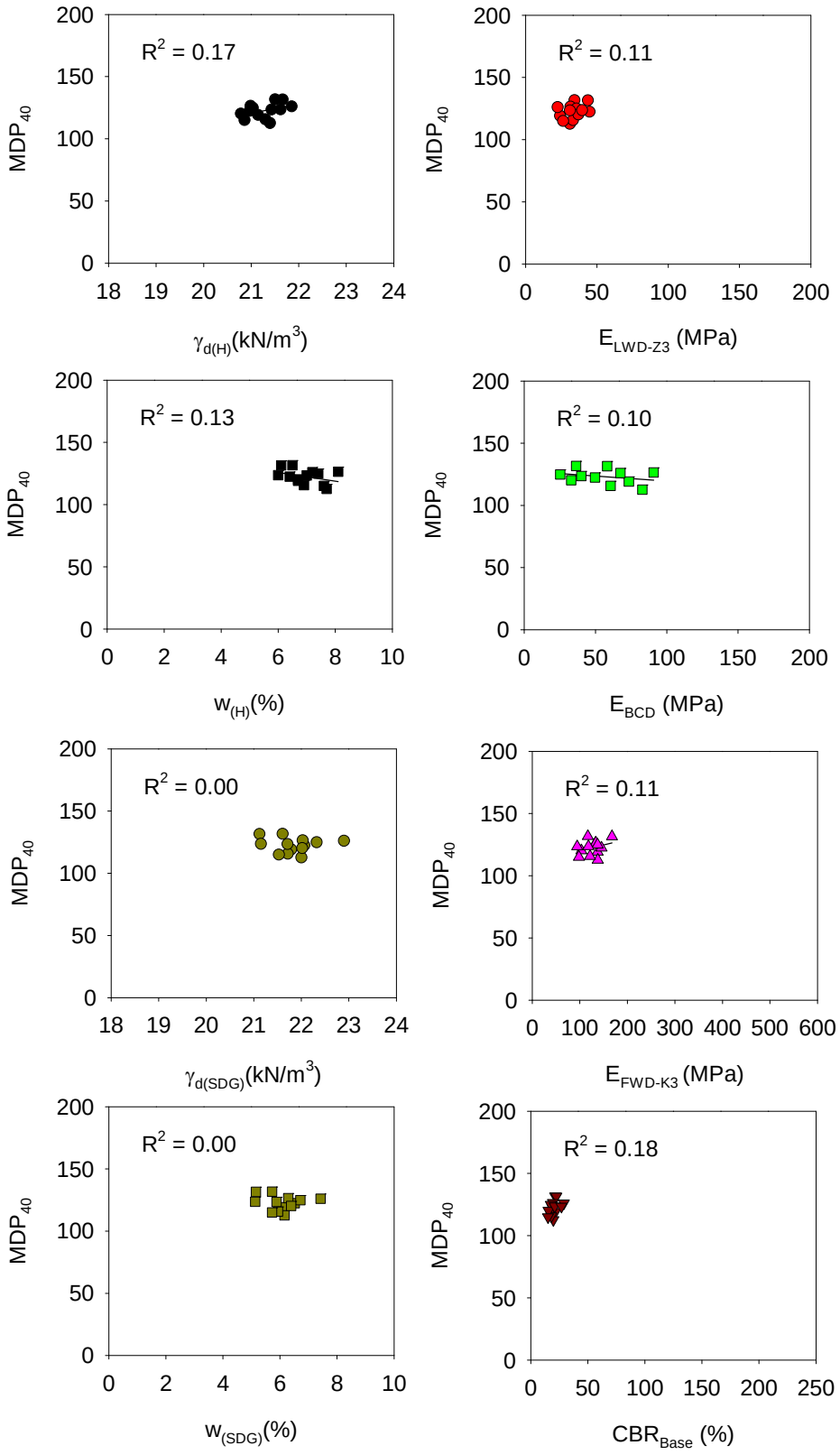

Figure 39. Regression relationships between MDP_{40} and Point-MVs (lane 2 pass 8 static) – TB4 gravel subbase material

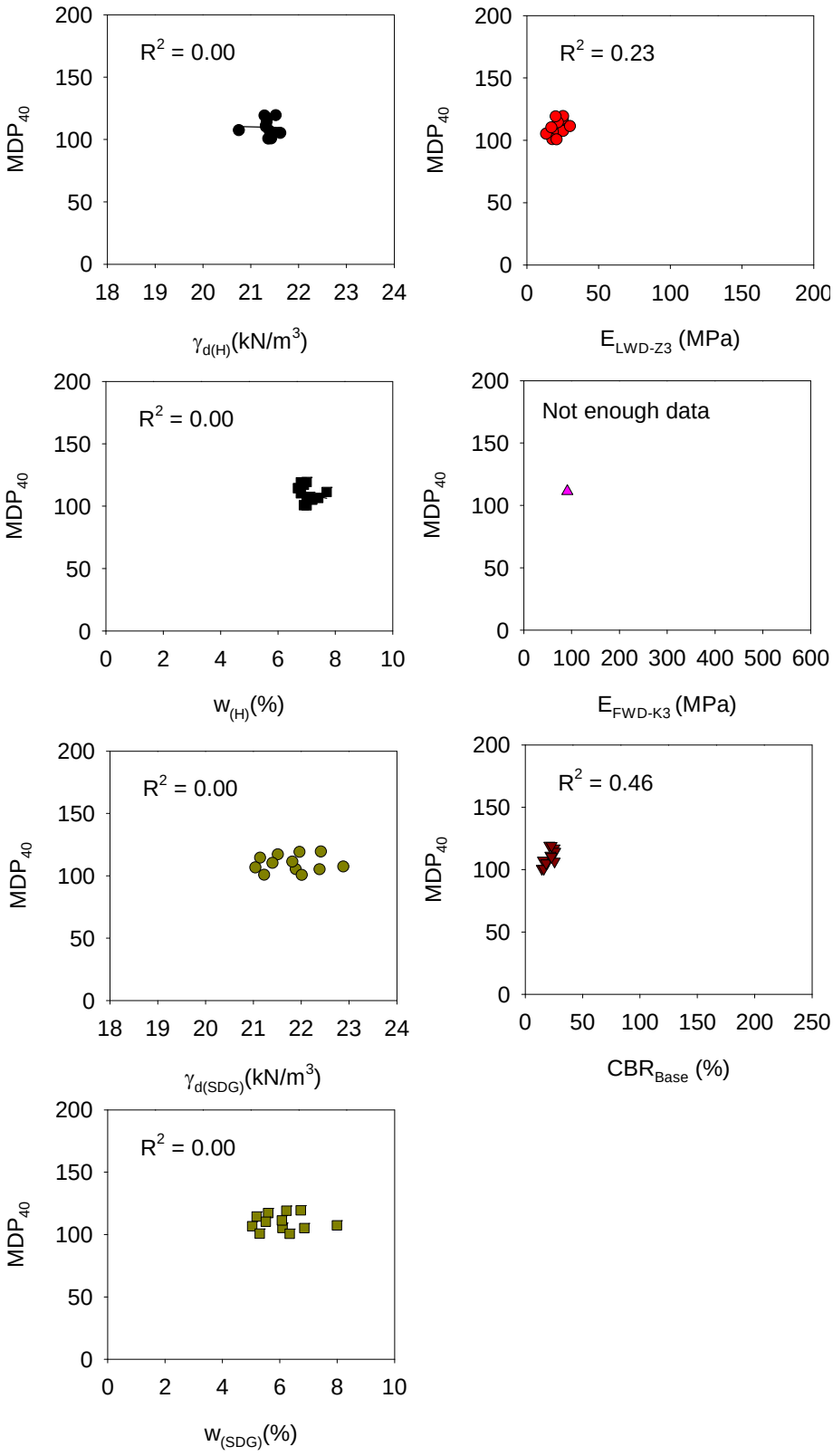

Figure 40. Regression relationships between MDP_{40} and Point-MVs (lane 3 pass 8 *a* = 0.90 mm) – TB4 gravel subbase material

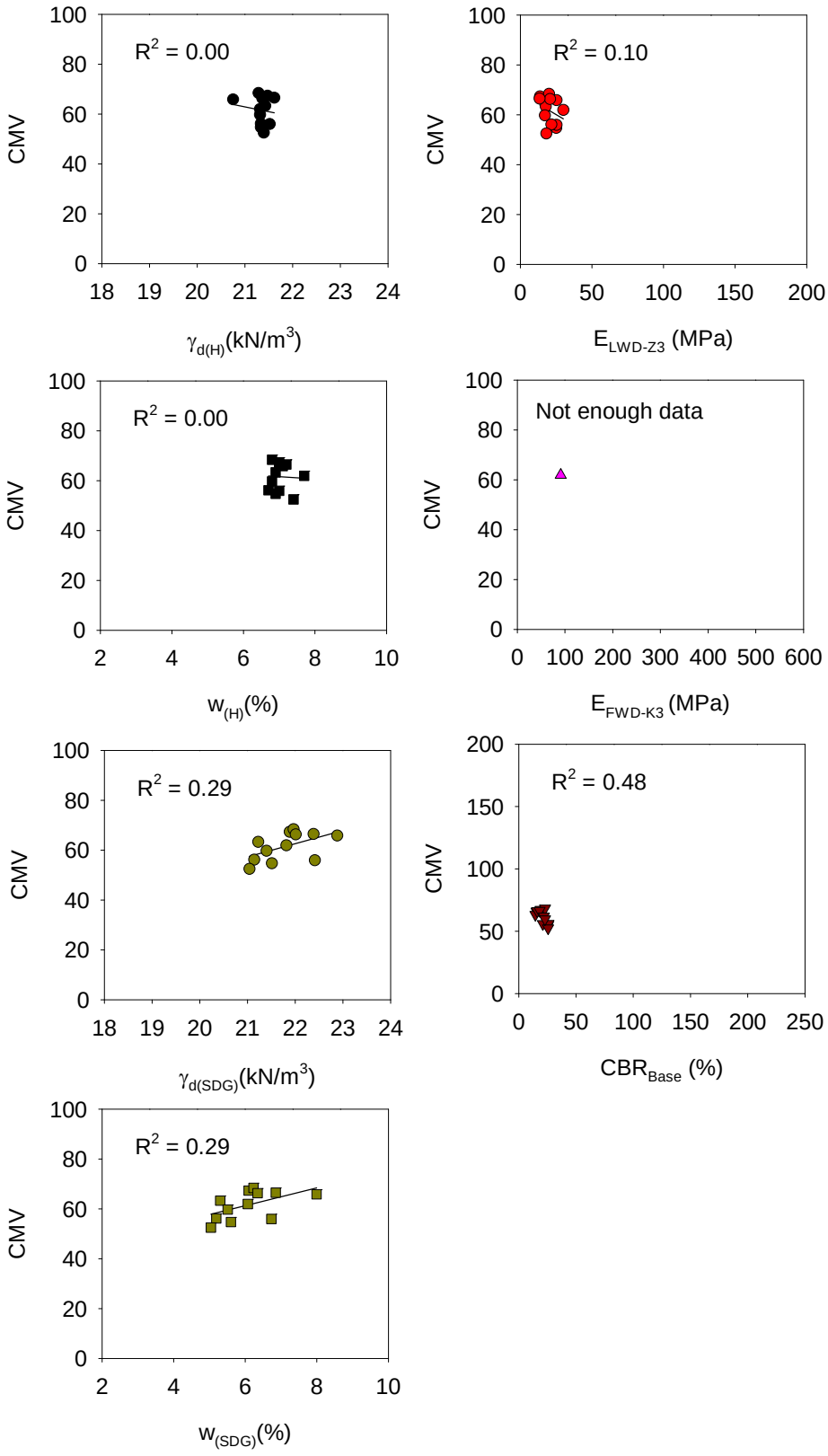

Figure 41. Regression relationships between CMV and Point-MVs (lane 3 pass 8 *a* = 0.90 mm) – TB4 gravel subbase material

Table 10. Summary of regression analysis – TB4 (lanes 2 and 3) gravel subbase material

Relationship	a (mm)	n	R^2
Lane 2			
MDP_{40} = -30.9 + 0.72 ($\gamma_{d(H)}$)	Static	13	0.17
MDP_{40} = 146.4 – 3.44 ($w_{(H)}$)	Static	13	0.13
MDP_{40} = 112.8 + 0.29 ($E_{LWD\text{-}Z3}$)	Static	13	0.11
MDP_{40} = 127.7 – 0.08 (E_{BCD})	Static	13	0.10
MDP_{40} = 110.7 + 0.09 ($E_{FWD\text{-}K3}$)	Static	13	0.11
MDP_{40} = 109.5 + 0.63 (CBR_{Base})	Static	13	0.18
Note: No statistically significant relationship between $\gamma_{d(SDH)}$ and $w_{(SDH)}$ Point-MVs and MDP_{40}			
Lane 3			
MDP_{40} = 96.8 + 0.63 ($E_{LWD\text{-}Z3}$)	0.90	12	0.23
MDP_{40} = 86.8 + 1.11 (CBR_{Base})	0.90	12	0.46
Note: No statistically significant relationship between $\gamma_{d(H)}$, $w_{(H)}$, $\gamma_{d(SDH)}$ and $w_{(SDH)}$ Point-MVs and MDP_{40}			
CMV = -54.3 + 5.31 ($\gamma_{d(SDH)}$)	0.90	12	0.29
CMV = 39.8 + 3.57 ($w_{(SDH)}$)	0.90	12	0.29
MDP_{40} = 68.5 – 0.34 ($E_{LWD\text{-}Z3}$)	0.90	12	0.10
MDP_{40} = 81.3 – 0.95 (CBR_{Base})	0.90	12	0.48

Test bed construction and in-situ testing – TB5 (Lanes 4 and 5)

TB5 was located adjacent to TB4 with the same profile (Figure 29). Two side-by-side lanes (lanes 4 and 5) were selected for this test bed and were subjected to eight roller passes using the Bomag IC roller. Lane 4 was compacted in AFC mode (a_{max} = 1.10, target E_{VIB} = 150 MPa, f = 30 Hz) while lane 5 was compacted in manual low amplitude mode (a = 0.70 mm and f = 30 Hz). DCP-CBR, $w_{(H)}$, $w_{(SDG)}$, $\gamma_{d(H)}$, and $\gamma_{d(SDG)}$ Point-MVs were obtained at 13 test locations within each lane prior to compaction and after pass 8. $E_{LWD\text{-}Z3}$, E_{BCD} and $E_{FWD\text{-}K3}$ Point-MVs were obtained at13 test locations along each lane after pass 8. $E_{FWD\text{-}K3}$ tests performed at one location in lane 4 and two locations in lane 5 produced deflections that are greater than the upper measurement range of the deflection sensors and were not reported in the output file. The moisture content of the subbase material was relatively uniform (6 to 7%).

IC-MVs and Point-MVs – TB5 (Lanes 4 and 5)

Spatial IC-MV (E_{VIB}) maps for each pass on lanes 4 and 5 are provided in Figure 42 and Figure 43, respectively. Line plots with E_{VIB}, vibration amplitude, and *jump* measurements along lanes 4 and 5 for passes 1, 2, 4, 6, and 8 are provided in Figure 44. E_{VIB} plots in Figure 44 indicate that the MVs are repeatable and there is an increase in the MVs with increasing roller passes indicating compaction. No roller jumping (*Jump* = 0) was observed during manual or AFC mode compaction. Vibration amplitude averaged about 1.0 mm but varied between 0.6 to 1.1 mm during AFC mode compaction.

Average E_{VIB}, vibration amplitude, and Point-MV compaction curves for lanes 4 and 5 are presented in Figure 45. The average E_{VIB}, CBR, and γ_d measurements generally increased with increasing roller passes indicating compaction. DCP-CBR depth profiles obtained at pass 0 and 8 from each point location on lanes 4 and 5 are provided in Figure 46 and Figure 47, respectively. Average E_{VIB} values on lane 4 compacted in AFC mode are on-average higher than the average E_{VIB} values on lane 5 compacted in manual mode (presumably due to the lower vibration amplitude used for lane 5). The average amplitude decreased slightly with increasing E_{VIB} values obtained in AFC mode. After pass 8, the average $E_{LWD\text{-}Z3}$ on lane 4 was about 1.6 times higher than on lane 5. However, after pass 8 the average relative compaction values are similar for lanes 4 and 5 (about 101 using $\gamma_{d(H)}$ and about 104% using $\gamma_{d(SDG)}$ measurements).

To assess the differences in compaction uniformity between AFC and manual mode operations, coefficient of variation (COV) of E_{VIB} and Point-MVs after pass 8 are summarized in Table 11. Although the E_{VIB} COV for lane 4 was lower than lane 5, Point-MVs did not show considerable difference in COV. Nevertheless, significant amplitude variations were not observed along the test strip compacted in AFC mode, likely because of the relatively low a_{max} setting (a_{max} = 1.10 mm). This aspect should be further investigated in future projects with different a_{max} and target E_{VIB} settings.

IC-MV plots in comparison with Point-MVs for lanes 4 and 5 after pass 8 are provided in Figure 48 and Figure 49, respectively. Regression analysis between E_{VIB} and Point-MVs by spatially pairing the nearest point data is presented in Figure 50 and Figure 51, and the relationships are summarized in Table 12. With the exception of the E_{VIB} vs. $\gamma_{d(SDG)}$ relationship with R^2 = 0.49, all other relationships produced low R^2 values and sometimes incorrect trends (e.g., E_{VIB} vs. $E_{LWD\text{-}Z3}$). The narrow range of measurements over which the measurements were obtained contributed to these findings.

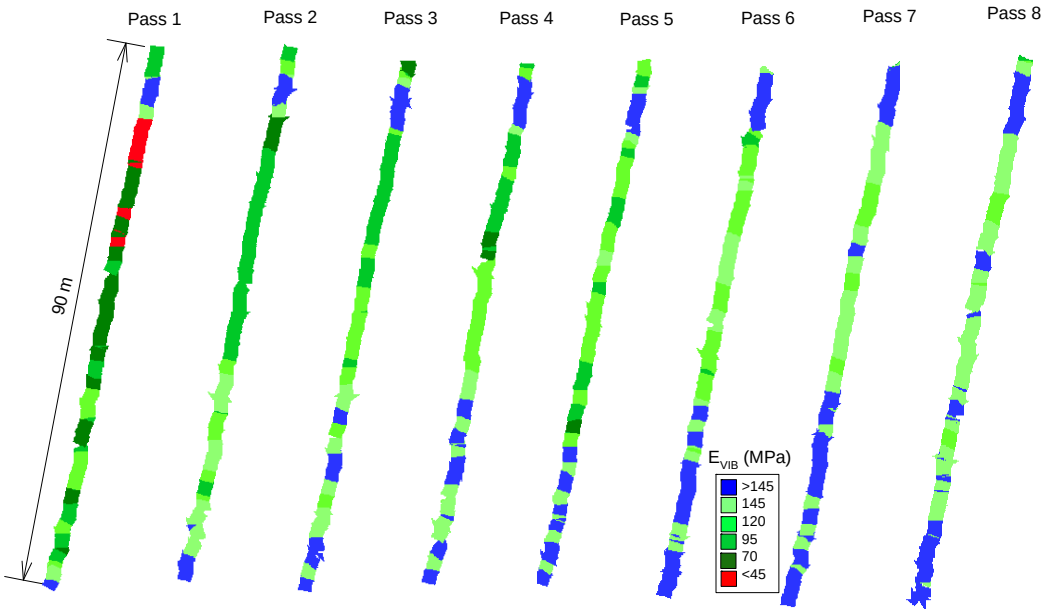

Figure 42. E_{VIB} maps on lane 4 for passes 1 to 8 made using AFC setting a_{max} = 1.10 mm and target E_{VIB} = 150 MPa – TB5 gravel subbase material

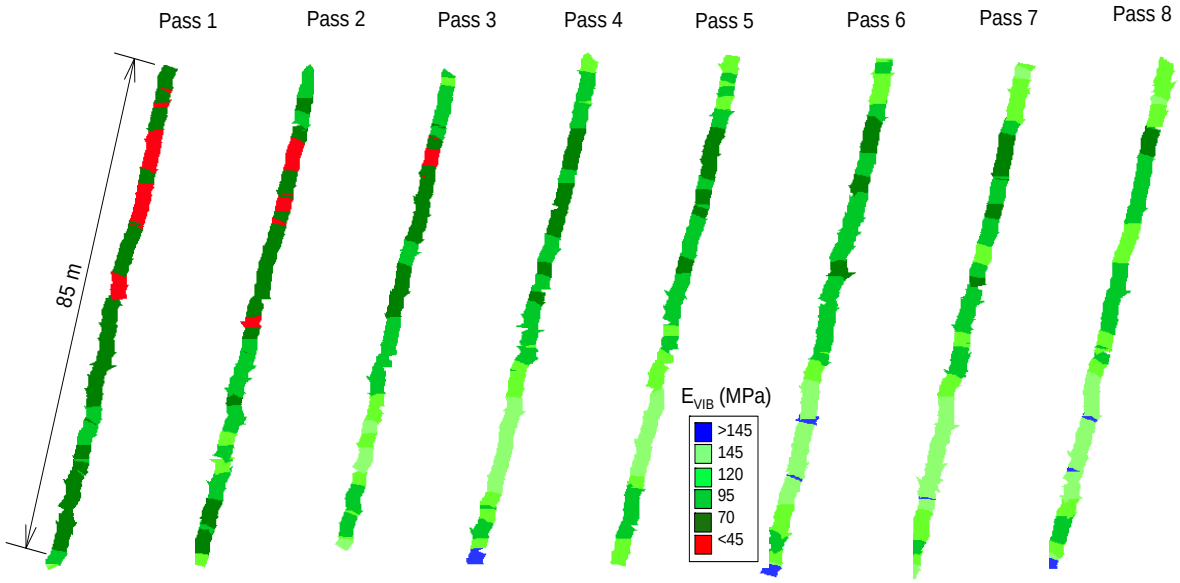

Figure 43. E_{VIB} maps on lane 5 for passes 1 to 8 made using a = 0.70 mm setting – TB5 gravel subbase material

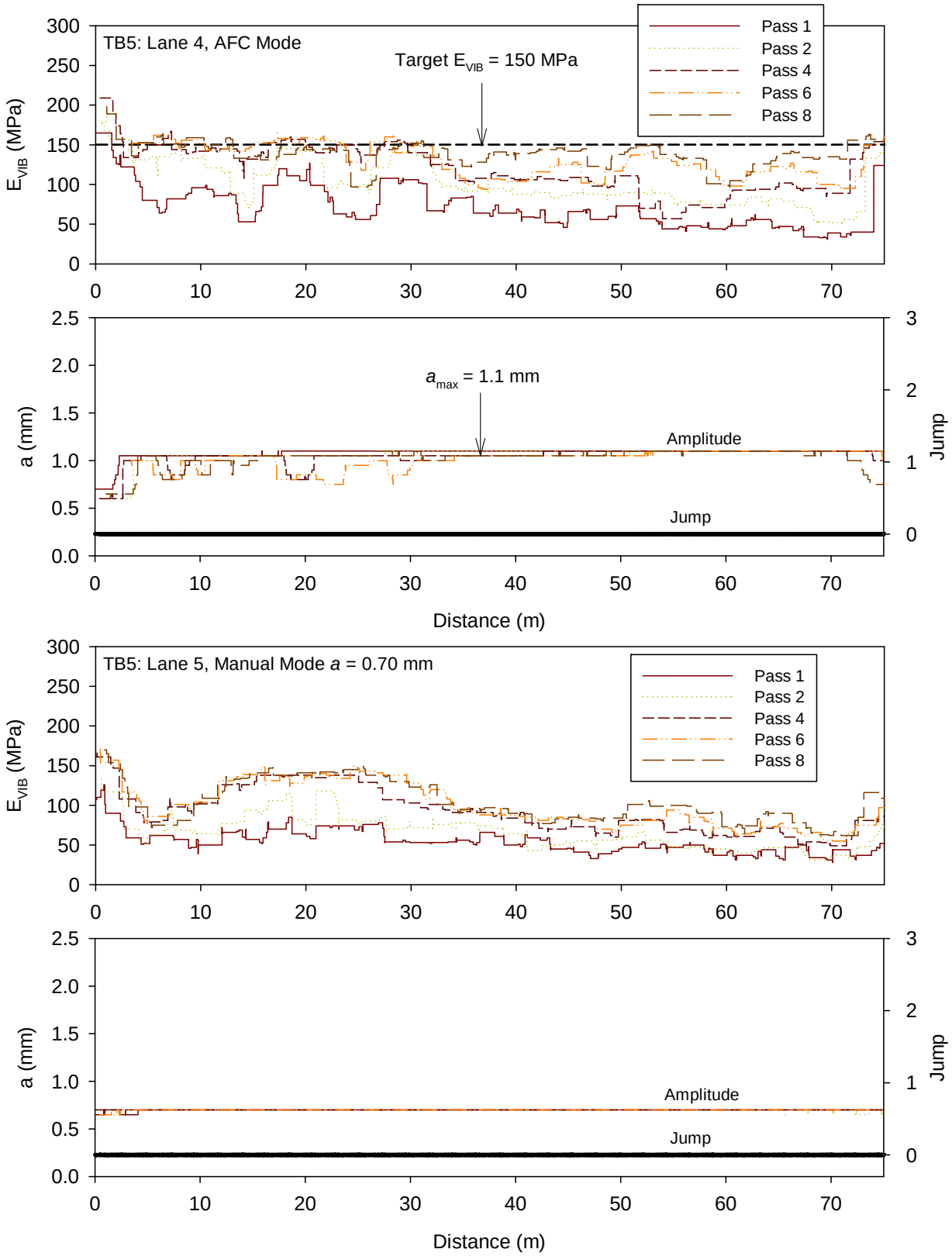

Figure 44. E_{VIB} plots on lanes 3 and 4 for different roller passes – TB5 gravel subbase material

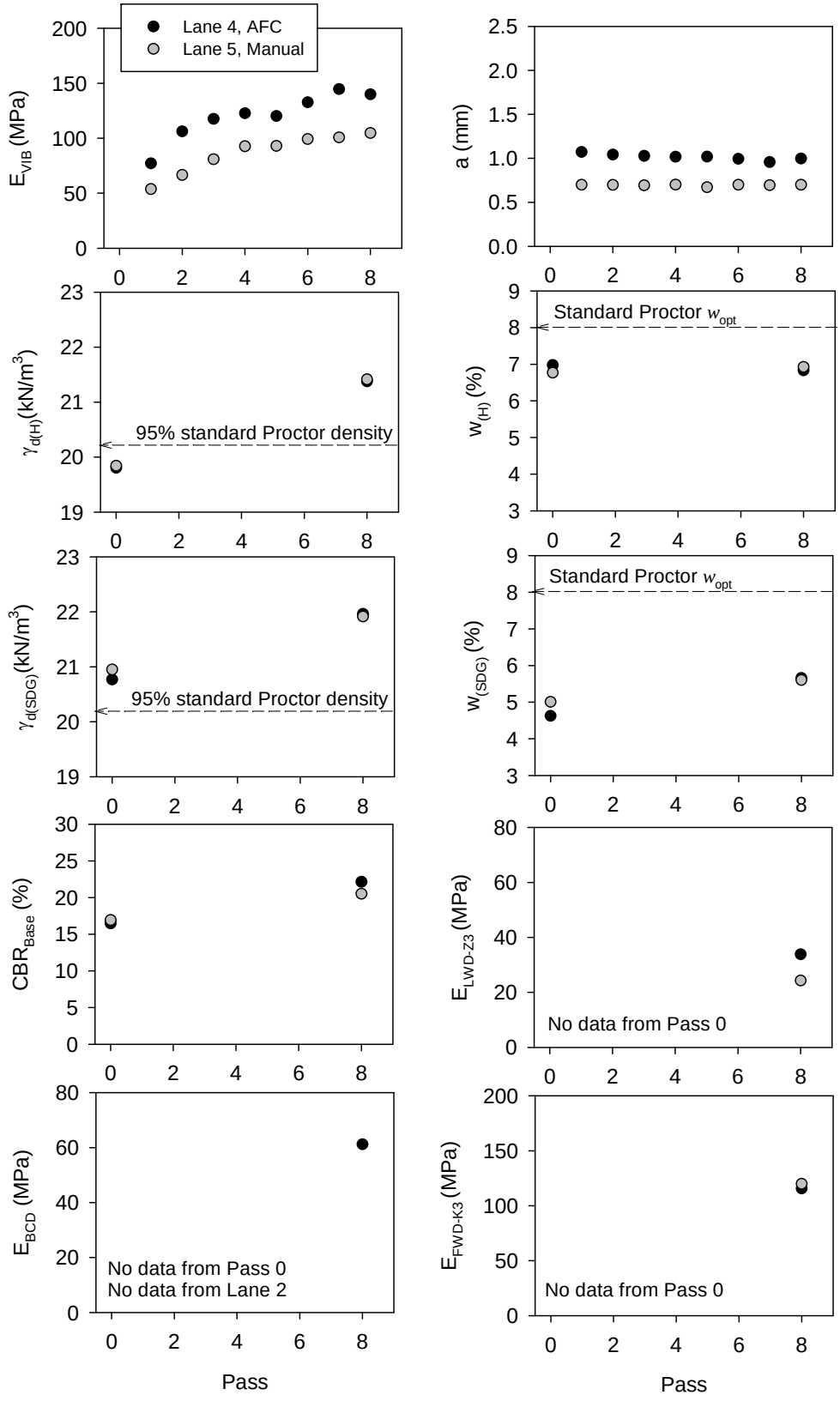

Figure 45. Average E_{VIB} and Point-MV compaction curves on lanes 4 and 5 – TB5 gravel subbase material

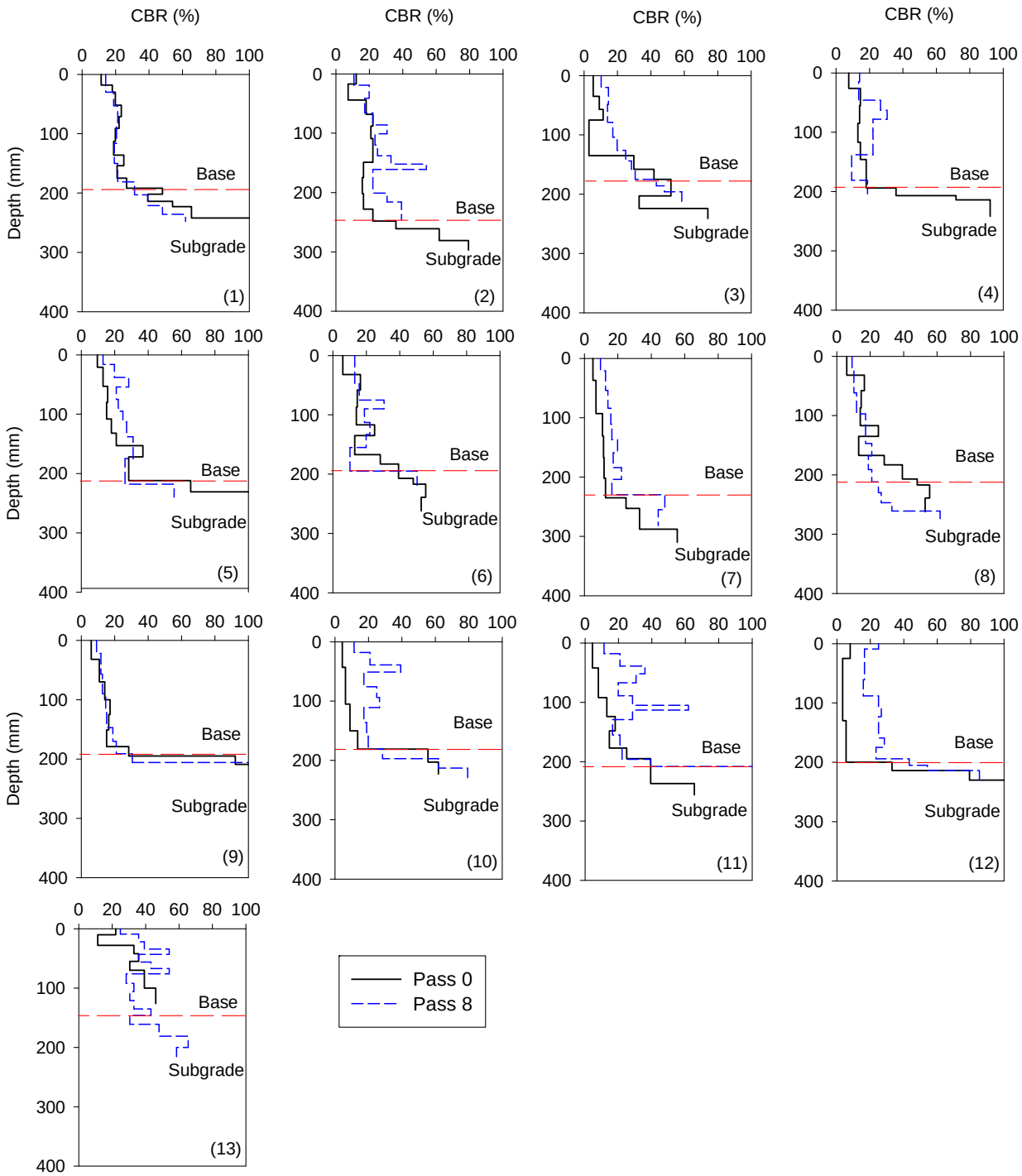

Figure 46. DCP-CBR depth profiles before compaction and after eight roller passes on lane 4 – TB5 gravel subbase material

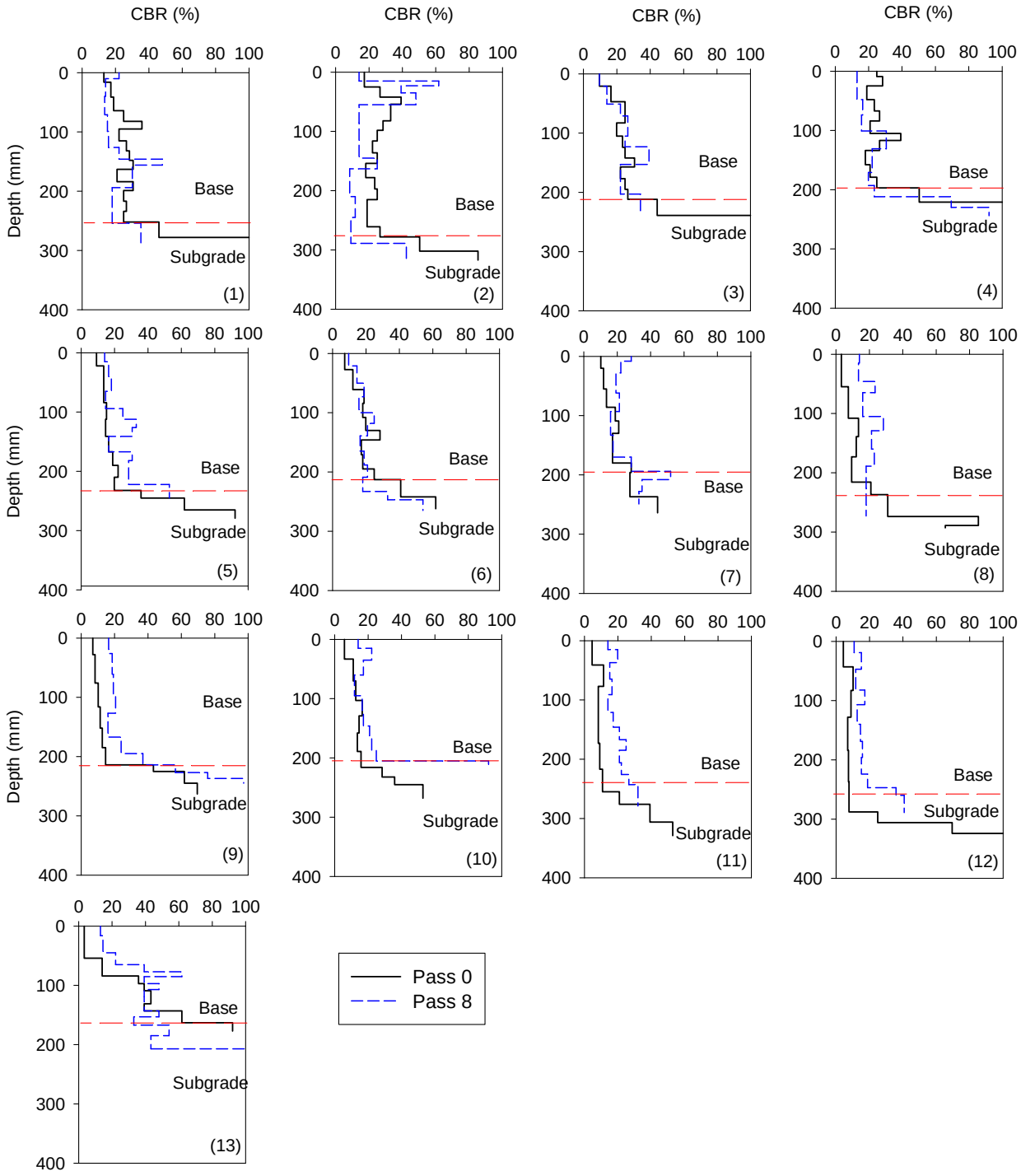

Figure 47. DCP-CBR depth profiles before compaction and after eight roller passes on lane 5 – TB5 gravel subbase material

Table 11. Comparison of COV of IC-MV and Point-MVs for lanes 4 and 5

MV (Pass 8)	Lane 4 AFC COV(%)	Lane 5 Manual COV(%)
E_{VIB}	12	24
$\gamma_{d(H)}$	2	2
$\gamma_{d(SDG)}$	2	2
$w_{(H)}$	10	10
$w_{(SDG)}$	7	8
CBR_{Base}	26	23
$E_{LWD\text{-}Z3}$	31	26
E_{BCD}	27	No measurements
$E_{FWD\text{-}K3}$	12	13

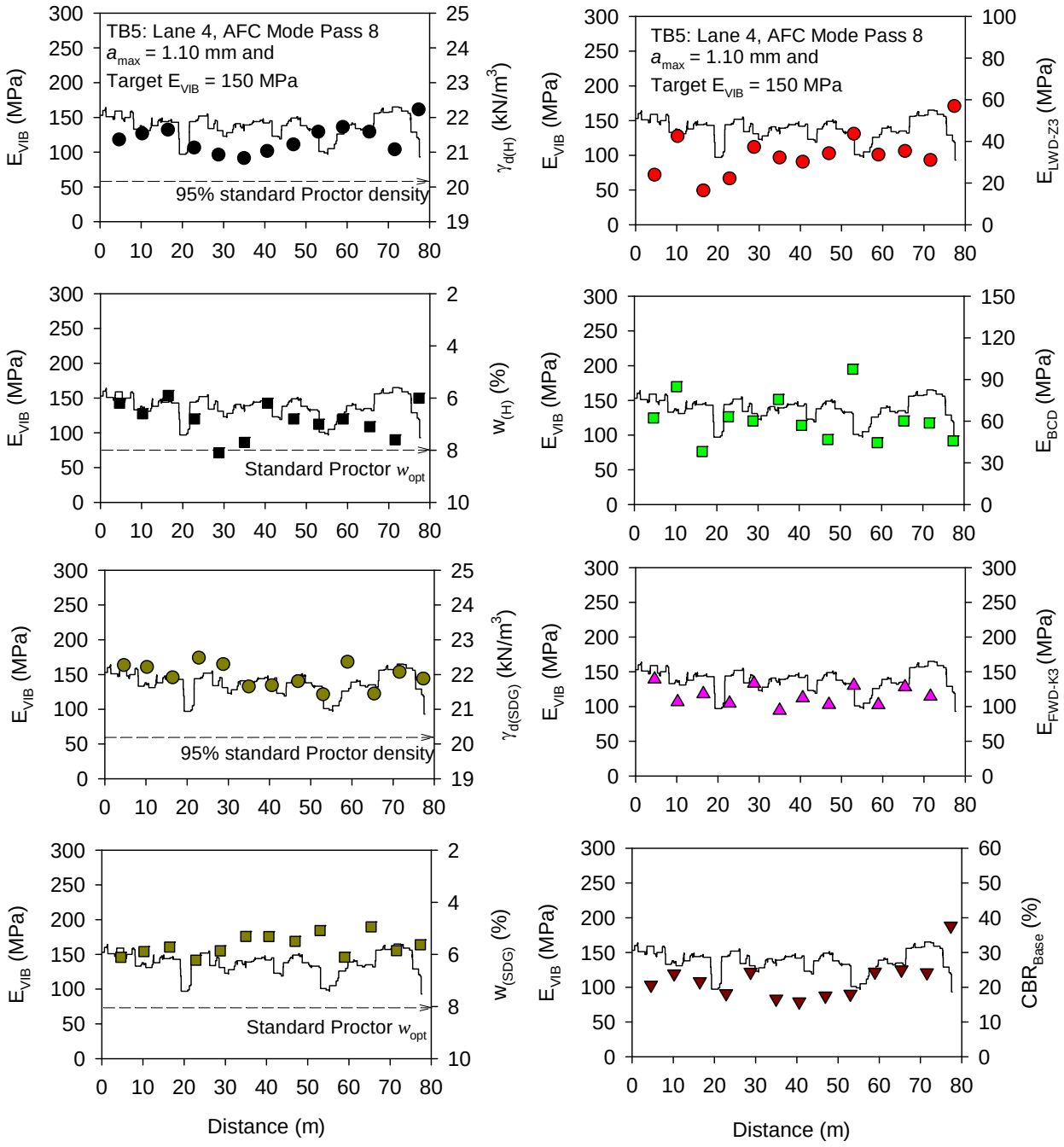

Figure 48. Comparison between E_{VIB} and Point-MVs on lane 4 (AFC mode compaction a_{max} = 1.10 mm and target EVIB = 150 MPa, pass 8) – TB5 gravel subbase material

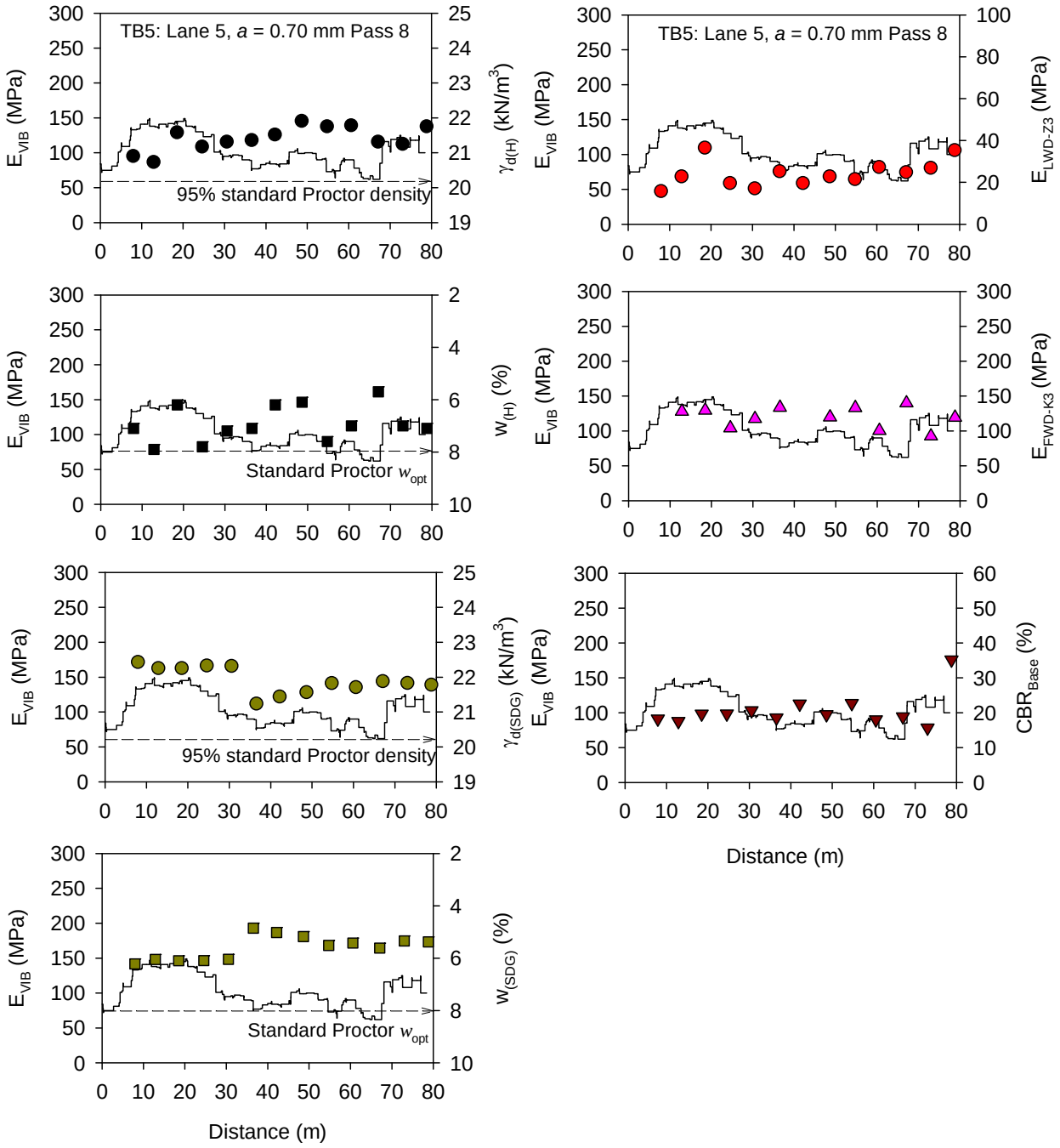

Figure 49. Comparison between E_{VIB} and Point-MVs on lane 5 (manual mode compaction *a* = 0.70 mm pass 8) – TB5 gravel subbase material

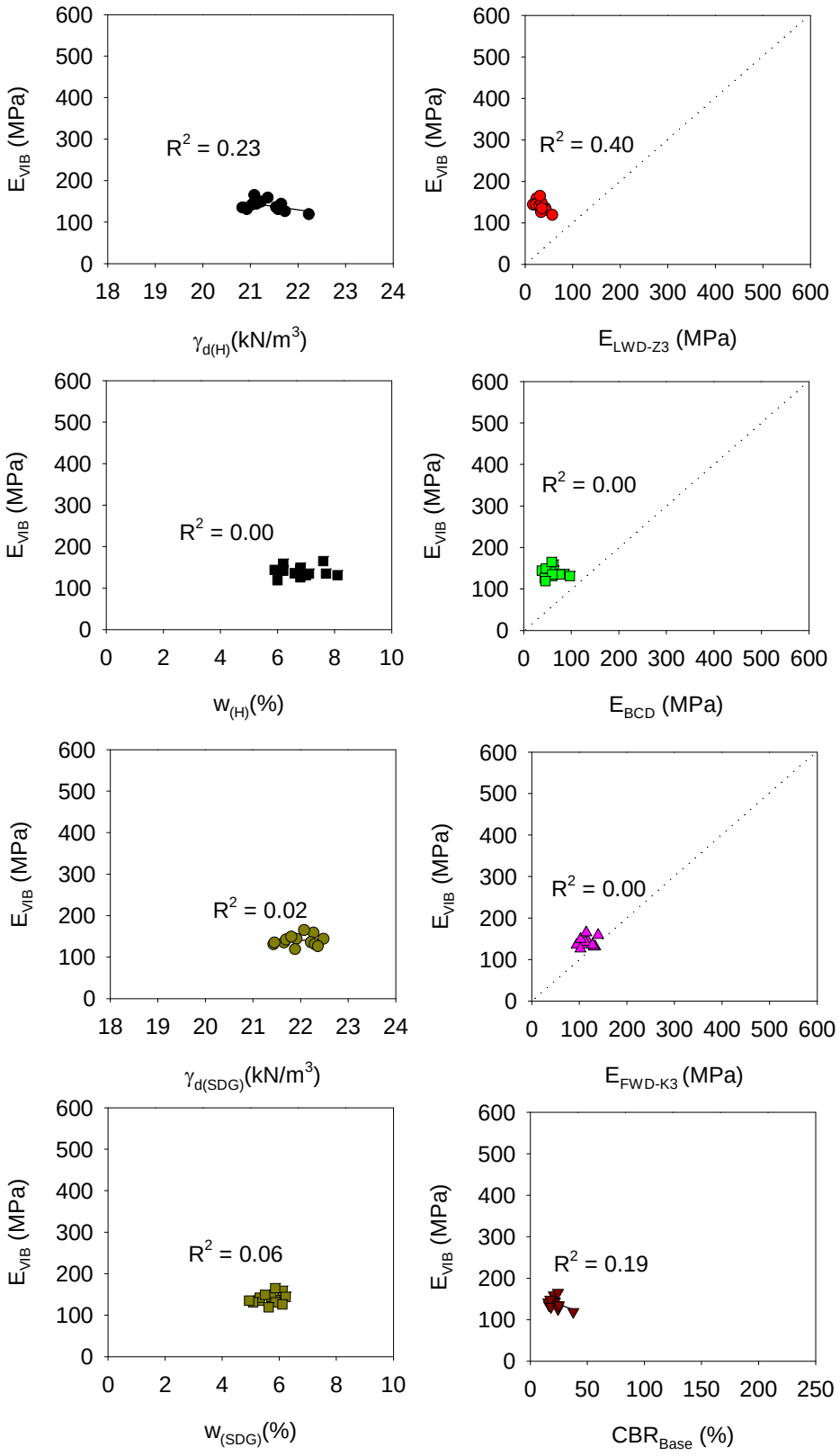

Figure 50. Regression relationships between E_{VIB} and Point-MVs (lane 4 AFC mode compaction) – TB5 gravel subbase material

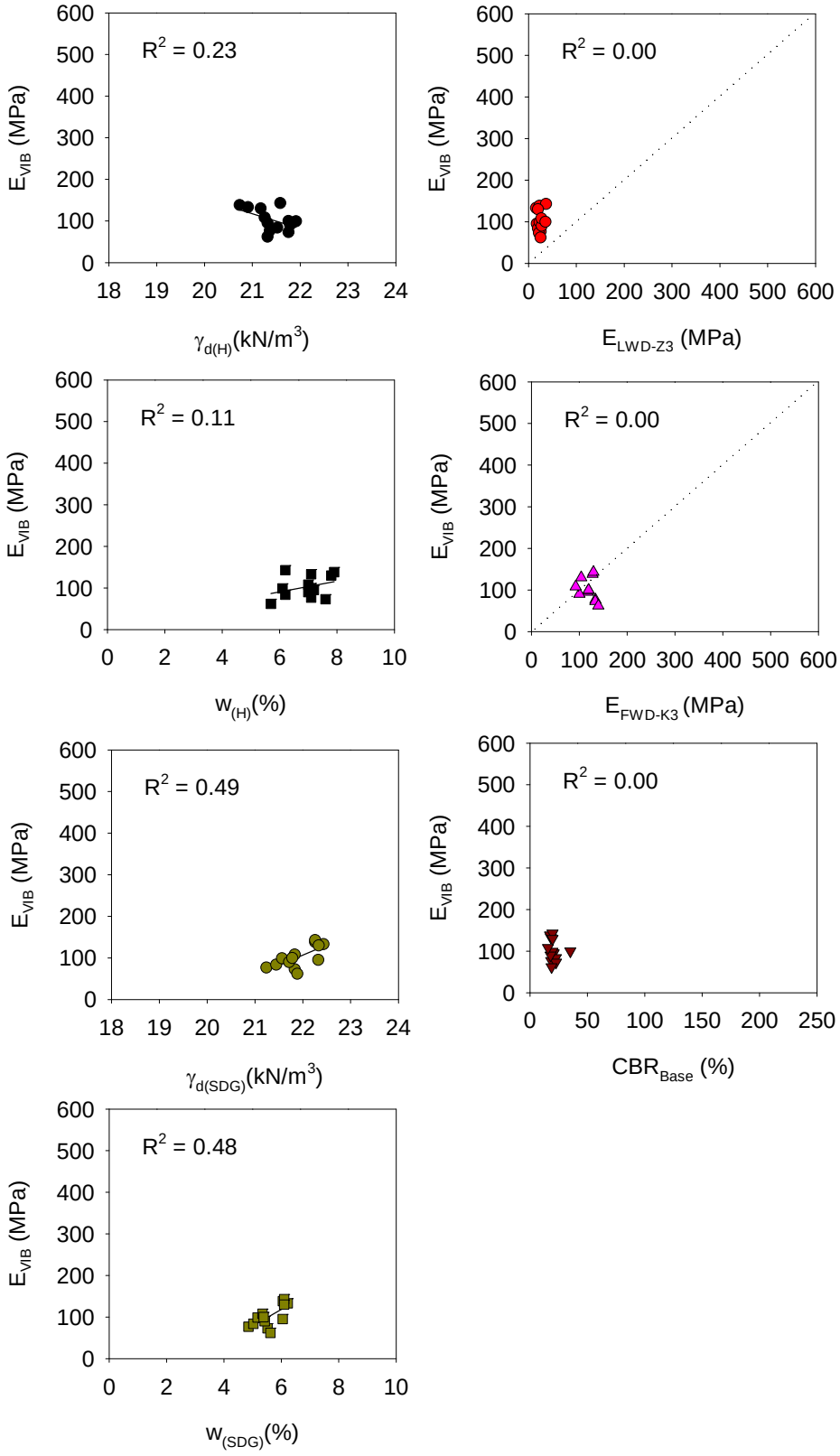

Figure 51. Regression relationships between E_{VIB} and Point-MVs (lane 5 manual mode compaction, a = 0.70 mm) – TB5 gravel subbase material

Table 12. Summary of regression analysis – TB5 (lanes 4 and 5) gravel subbase material

Relationship	a (mm)	n	R^2
Lane 4			
$E_{VIB} = 480.7 – 15.95 (\gamma_{d(H)})$	AFC	13	0.24
$E_{VIB} = 166.5 – 0.79 (E_{LWD-Z3})$	AFC	13	0.40
$E_{VIB} = 161.4 – 0.98 (CBR_{Base})$	AFC	13	0.19
Note: No statistically significant relationship between $w_{(H)}$, $\gamma_{d(SDH)}$, $w_{(SDH)}$, E_{BCD}, and E_{FWD-K3} Point-MVs and E_{VIB}			
Lane 5			
$E_{VIB} = 874.1– 36.03 (\gamma_{d(H)})$	0.70	13	0.23
$E_{VIB} = 11.7 + 13.10 (w_{(H)})$	0.70	13	0.11
$E_{VIB} = -964.1 + 48.67 (\gamma_{d(SDH)})$	0.70	13	0.49
$E_{VIB} = -120.6 + 39.8 (w_{(SDH)})$	0.70	13	0.48
Note: No statistically significant relationship between E_{FWD-Z3}, E_{FWD-K3}, and CBR_{Base} Point-MVs and E_{VIB}			

Summary of Key Findings

Measurements from TB4 involved obtaining MDP_{40} and CMV IC-MVs and Point-MVs along two side-by-side lanes compacted in static mode and in low amplitude vibration mode. Results were analyzed using average IC-MV and Point-MV compaction curves, and by spatially pairing the point data with IC data for correlations. Following are some key findings from this test bed:

- The average MDP_{40}, CMV, CBR, and γ_d measurements on both lanes generally increased with increasing roller pass indicating compaction.
- The average MDP_{40} values obtained in static mode operation are on average about 1.1 times higher than the MDP_{40} values obtained in low amplitude mode operation. The average E_{LWD-Z3} values obtained after pass 8 in the lane compacted in static mode is about 1.6 times higher than in the lane compacted in low amplitude mode. However, the average relative compaction (100 to 101% using $\gamma_{d(H)}$ and about 103% using $\gamma_{d(SDG)}$ measurements), and CBR values (about 21 to 22) are similar for the two lanes after pass 8.
- Regression relationships between MDP_{40} and CMV IC-MVs and Point-MVs showed weak correlations with R^2 values ranging from 0.0 to 0.48. The narrow range of measurements over which the measurements were obtained is a key factor contributing to low R^2 values.

Measurements from TB5 involved obtaining E_{VIB} IC-MVs and Point-MVs along two side-by-side lanes compacted in AFC mode and in manual low amplitude mode. Results were analyzed using average IC-MV and Point-MV compaction curves, and by spatially pairing the point data with IC data for correlations. Following are some key findings from this test bed:

- The average E_{VIB}, CBR, and γ_d measurements on both lanes generally increased with increasing roller pass indicating compaction.
- The average E_{VIB} values obtained in AFC operation (a = 1.0 mm on average) are on-average about 1.3 times higher than the average E_{VIB} values obtained in manual mode operation (a = 0.6 mm). Average $E_{LWD\text{-}Z3}$ values in the lane compacted in AFC mode were about 1.6 times higher than in the lane compacted in manual mode. However, the average relative compaction values (100 to 101% using $\gamma_{d(H)}$ about 103% using $\gamma_{d(SDG)}$ measurements), average $E_{FWD\text{-}K3}$ values (about 116 MPa), and CBR values (about 20 to 22) are similar for the two lanes after pass 8.
- Although the E_{VIB} values showed low COV with AFC operations compared to COV with manual mode operations, Point-MVs did not show considerable difference in the COV values.
- For this test bed, the AFC operations (with settings a_{max} = 1.10 mm and target E_{VIB} = 150 MPa) did not produce increased compaction or improved uniformity compared to manual mode a = 0.70 mm operations. Significant amplitude variations were not observed along the test strip compacted in AFC mode, likely because of the relatively low a_{max} setting. This aspect should be further investigated in future projects with different a_{max} and target E_{VIB} settings.
- With the exception of E_{VIB} vs. $\gamma_{d(SDG)}$ relationship with R^2 = 0.49, all other relationships yielded weak correlations with low R^2 values. The narrow range of measurements over which the measurements were obtained is considered a limiting factor in the correlations.

TBs 6 and 7 Gravel Subbase Production Area Compaction – Bomag & Caterpillar

Test bed construction and in-situ testing

This test bed consisted of a production area with aggregate subbase material placed over the TB1 embankment material. A geosynthetic separation layer was placed over the TB 1 materials prior to fill placement for TB 6 and 7. Plan dimensions of the test bed are about 17 m x 200 m. The area was compacted with two roller passes using the Caterpillar IC roller in the low amplitude settings (a = 0.90 mm) for, followed by four roller passes with the Bomag IC roller in the low amplitude setting (a = 0.70 mm). Nominal machine settings during compaction are summarized in Table 2. After pass 6, some test locations were selected for Point-MVs ($E_{LWD\text{-}Z3}$, E_{BCD}, $w_{(H)}$, and $\gamma_{d(H)}$) by NYDOT personnel using the IC map on the on-board display unit and were tested by the ISU research team. The test location selection process and review of on-board display IC maps provided hands-on experience to the NYDOT personnel and simulated a production operation.

CMV and MDP_{40} IC-MV maps and histograms for passes 1 and 2 are shown in Figure 52 and Figure 53, respectively. The average CMV and MDP_{40} values increased from pass 1 to 2 (CMV – 53.9 to 67.6 and MDP – 106.7 to 110.9), indicating increasing compaction. E_{VIB} IC-MV maps and histograms for passes 3 to 6 are shown in Figure 54 and Figure 55, respectively. The average E_{VIB} values increased with increasing passes (E_{VIB} – 64.7 to 80.2 from passes 3 to 6).

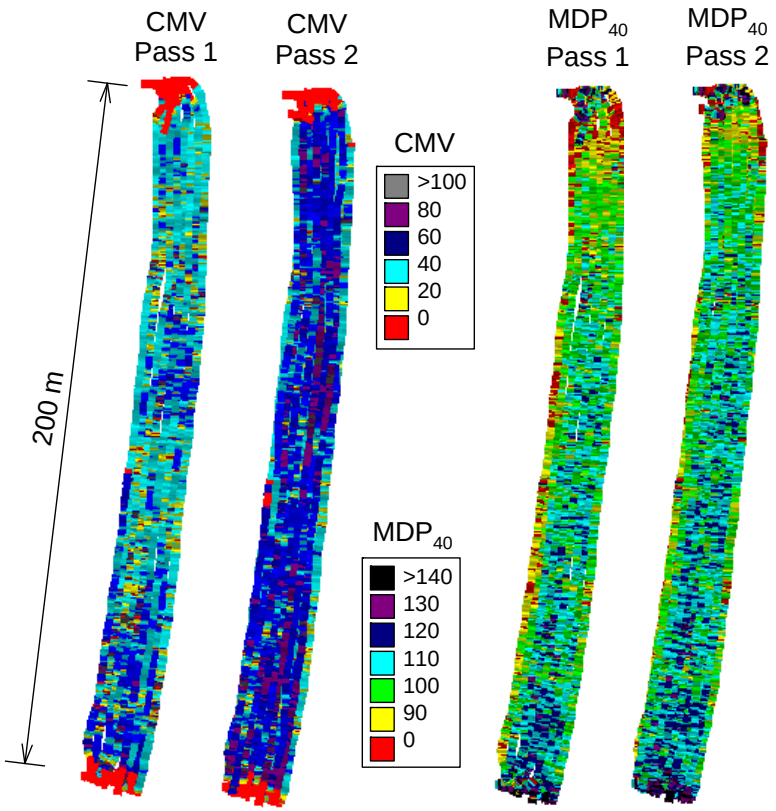

Figure 52. CMV and MDP_{40} spatial maps for passes 1 and 2 – TB6 gravel base material production compaction

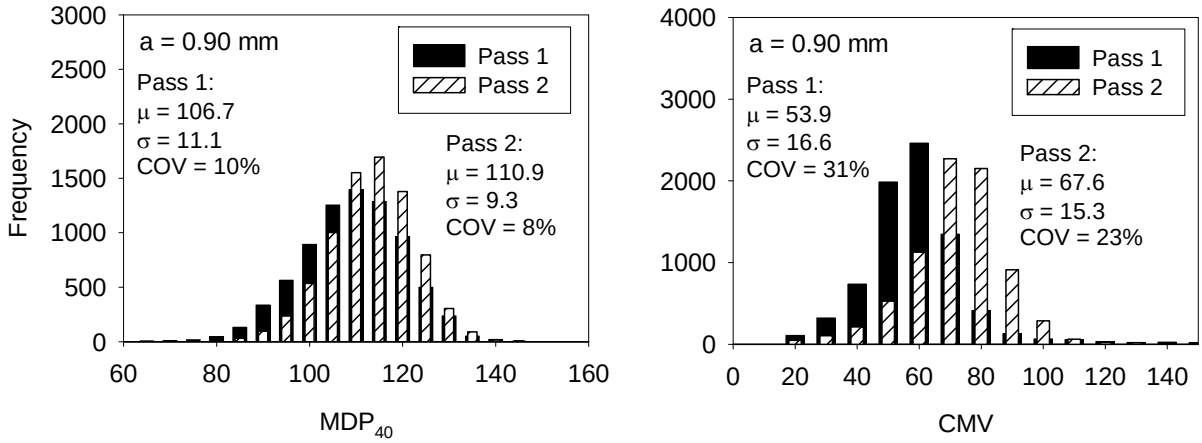

Figure 53. Histograms of CMV and MDP_{40} values for passes 1 and 2 – TB6 gravel base material production compaction

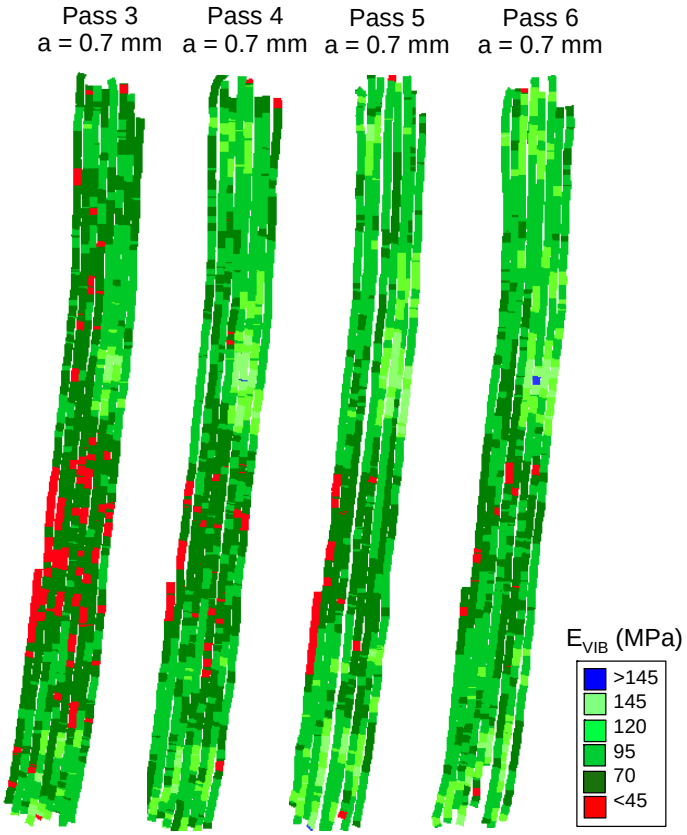

Figure 54. E_{VIB} spatial maps for passes 3 to 6 – TB6 gravel base material production compaction

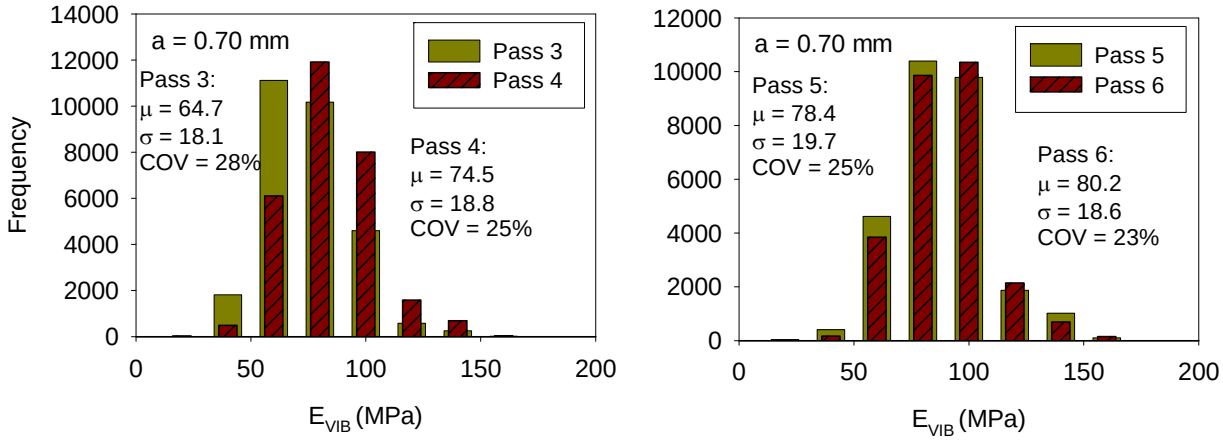

Figure 55. Histograms of E_{VIB} values for passes 1 and 2 – TB6 gravel base material production compaction

Geostatistical Analysis of IC-MVs

Semivariograms of MDP_{40}, CMV, and E_{VIB} IC-MVs for all compaction passes are presented in Figure 56 and a summary of the spatial statistics (i.e., nugget, sill, and range) in comparison with the univariate statistics are provided in Table 13. Similar to semivariograms for TB1, the experimental semivariograms of the IC-MVs in this test bed also showed nested spatial structures (except for one case) with short-range and long-range components. The pass 2 CMV experimental semivariogram did not exhibit a nested structure. A nested spherical variogram was fit to the experimental data. Similar to findings in TB1, it is possible that the long-range spatial structure is a result of spatial variation in underlying support conditions while the short-range spatial structure is a result of soil properties close to the surface.

The MDP_{40} and CMV semivariograms showed increased uniformity (with decreasing sill values) from pass 1 to 2 (see Table 13). This is also reflected in decreasing COV and standard deviation (σ) values of MDP_{40} and CMV from pass 1 to 2 (see Table 13). The E_{VIB} semivariograms showed increased non-uniformity (with increasing sill values) from passes 3 to 5 and then increased uniformity (with decreasing sill values) from passes 5 to 6. This behavior is also reflected in the standard deviation values of E_{VIB} as summarized in Table 13.

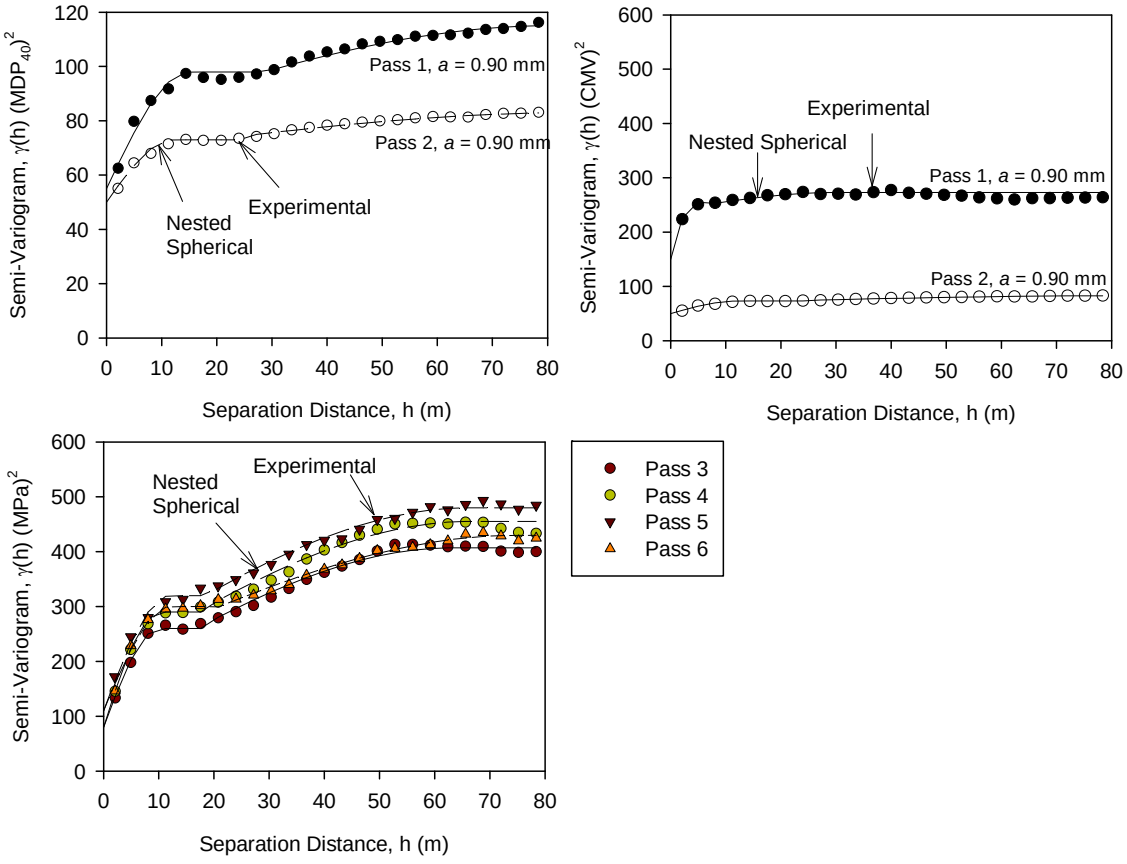

Figure 56. Semivariogram plots of IC-MVs for passes 1 to 6 – TBs6/7 gravel base material production compaction

Table 13. Summary of univariate and spatial statistics – TBs 6/7 embankment material

				Univariate Statistics			Spatial Statistics				
Pass	MV	n	*a* (mm)	μ	σ	COV (%)	Nugget	$Sill_1$	$Range_1$	$Sill_2$	$Range_2$
1	MDP_{40}	7735	0.90	106.7	11.1	10	55	98	15	115	80
1	CMV	7735	0.90	53.9	16.6	31	150	255	4	273	30
2	MDP	7754	0.90	110.9	9.3	8	50	73	12	83	85
2	CMV	7754	0.90	67.6	15.3	23	170	235	12	—	—
3	E_{VIB}	28574	0.70	64.7	18.1	28	80	260	10	407	63
4	E_{VIB}	28866	0.70	74.7	18.8	25	80	290	10	455	66
5	E_{VIB}	28228	0.70	78.4	19.7	25	110	320	12	480	66
6	E_{VIB}	27198	0.70	80.2	18.6	23	110	300	12	430	75

Regression Analysis between IC-MVs and Point-MVs

Regression analysis results between E_{VIB} and Point-MVs obtained after pass 6 are presented in Figure 57 and the relationships are summarized in Table 14. Simple linear relationships showed the best fit for all Point-MVs. Relationships with $E_{LWD\text{-}Z3}$ an E_{BCD} showed good correlations with R^2 values of about 0.50 and 0.44, respectively. E_{VIB} relationship with $\gamma_{d(H)}$ showed the opposite trend, i.e., decreasing E_{VIB} value with increasing $\gamma_{d(H)}$. E_{VIB} relationship with $w_{(H)}$ yielded a weak correlation ($R^2 = 0.27$), but a trend of increasing E_{VIB} with increasing moisture content. Here again many of the data sets are captured over a narrow range of measurements.

Table 14. Summary of regression analysis – TB7 gravel subbase material

Relationship	a (mm)	n	R^2
$E_{VIB} = 927.3 – 39.37\ (\gamma_{d(H)})$	0.70	9	0.32
$E_{VIB} = -40.2 – 18.98\ (w_{(H)})$	0.70	9	0.27
$E_{VIB} = 30.6 + 1.49\ (E_{LWD\text{-}Z3})$	0.70	9	0.49
$E_{VIB} = -0.84 + 1.87\ (E_{BCD})$	0.70	9	0.49

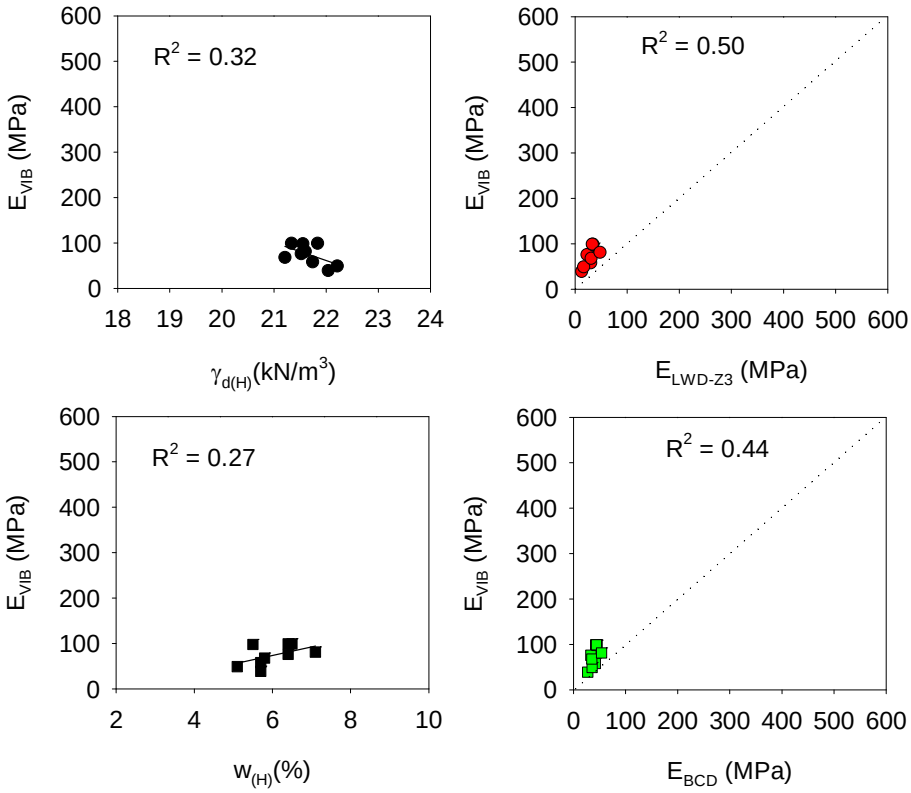

Figure 57. Regression relationships between E_{VIB} and Point-MVs (after pass 6) – TB7 gravel subbase material

Summary of Key Findings

Measurements from TBs 6 and 7 involved IC-MV (MDP_{40}, CMV, E_{VIB}) maps for each compaction pass over a production area compacting gravel subbase material. After pass 6, Point-MVs (E_{LWD-Z3}, E_{BCD}, $w_{(H)}$, and $\gamma_{d(H)}$) were obtained from 10 selected test locations using the IC-MV map. Regression analysis was performed between IC-MVs and Point-MVs by spatially pairing the data and geostatistical analysis is performed on the spatial IC-MV data obtained from each pass. Following is a summary of key findings from these analyses:

- Regression analysis results between IC-MVs and Point-MVs produced simple linear relationships. Relationships with E_{LWD-Z3} an E_{BCD} yielded R^2 values of about 0.50 and 0.44, respectively. E_{VIB} relationship with $\gamma_{d(H)}$ yielded a weak relationship. E_{VIB} vs. $w_{(H)}$ indicate some influence of moisture content on E_{VIB} values R^2 value = 0.27.
- With the exception of CMV semivariogram for pass 2, all other semivariograms exhibited a nested spatial structure with short-range and long-range components. Similar to findings from TB1, a possible explanation for the long-range and short-range structures is attributed to spatial variation in underlying support conditions and spatial variation in soil properties close to the surface, respectively.
- The MDP_{40} and CMV values showed increased uniformity (with decreasing sill, COV, and σ values) from pass 1 to 2. The E_{VIB} values showed increased non-uniformity (with

increasing sill and σ values) from passes 3 to 5 and then increased uniformity (with decreasing sill and σ values) from passes 5 to 6.

TB9 Gravel Subbase Production Area Compaction – Caterpillar

Test bed construction and in-situ testing

The test bed consisted of aggregate subbase material placed over the geosynthetic separation layer and compacted embankment layer. The area was compacted with the Caterpillar IC roller using the low amplitude settings (a = 0.90 mm, f = 30 Hz). Compaction operations on the test bed were performed by the contractor. The area was compacted in two different sections (TBs 9A and 9B). The TB9B area was located just south of TB9A. The roller operator was trained on-site to make use of the on-board display unit and was reportedly instructed to perform two passes (one pass in forward direction and one pass in reverse direction) using the low amplitude setting. Following the final pass, test locations were selected to obtain $E_{LWD\text{-}Z3}$, E_{BCD}, $w_{(H)}$, and $\gamma_{d(H)}$ Point-MVs using the IC-MV map.

MDP_{40}, CMV, and pass coverage maps after the final pass are shown in Figure 58 and Figure 59 for TBs 9A and 9B, respectively. The pass coverage maps in Figure 58 and Figure 59 indicate that the operator made a minimum of two roller passes as instructed over the test areas and the resulting roller coverage was very uniform. Field observations on TB9B indicated that the dump trucks placing the fill followed a process of backing up in to the test bed area, dumping the fill, and returning back. A dozer was used to spread the material and then was compacted using the roller. The area that was used to dump the subbase fill material is highlighted on Figure 59 produced somewhat higher CMV measurement values.

Regression Analysis between IC-MVs and Point-MVs

Regression analysis results between IC-MVs and Point-MVs obtained after the final pass are presented in Figure 60 and Figure 61, and the relationships are summarized in Table 15. Simple linear relationships showed the best fit for all Point-MVs. IC-MVs relationships with $E_{LWD\text{-}Z3}$ an E_{BCD} yielded R^2 values ranging from 0.47 to 0.70. IC-MVs relationships with $\gamma_{d(H)}$ produced weak correlations with an opposite trend, i.e., decreasing IC-MV with increasing $\gamma_{d(H)}$. IC-MVs relationships with $w_{(H)}$ yielded $R^2 = 0.59$.

Summary of Key Findings

Measurements from TB9 involved obtaining IC-MV (MDP_{40} and CMV) maps during compaction over a production area compacting gravel subbase and obtaining. Point-MVs ($E_{LWD\text{-}Z3}$, E_{BCD}, $w_{(H)}$, and $\gamma_{d(H)}$) after the final pass using the IC-MV maps. The contractor operated the roller for this test bed. Regression analysis was performed between IC-MVs and Point-MVs by spatially pairing the data. Following is a summary of field observations and key findings from this test bed:

- The pass coverage maps on the on-board display unit were successfully used by the roller operator (contractor representative) to make a minimum of two roller passes as instructed over the test areas. The resulting roller coverage was very uniform.

- A portion of the test bed area that was used to place the subbase fill material by the dump trucks produced somewhat higher CMV measurement values, suggesting additional compaction contributed by the construction traffic.
- Regression analysis results between IC-MVs and Point-MVs showed simple linear relationships. IC-MVs relationships with $E_{LWD\text{-}Z3}$ an E_{BCD} yielded R^2 values ranging from 0.47 to 0.70. IC-MVs relationships with $\gamma_{d(H)}$ were weak. IC-MVs vs. $w_{(H)}$ relationships were stronger with $R^2 = 0.59$.

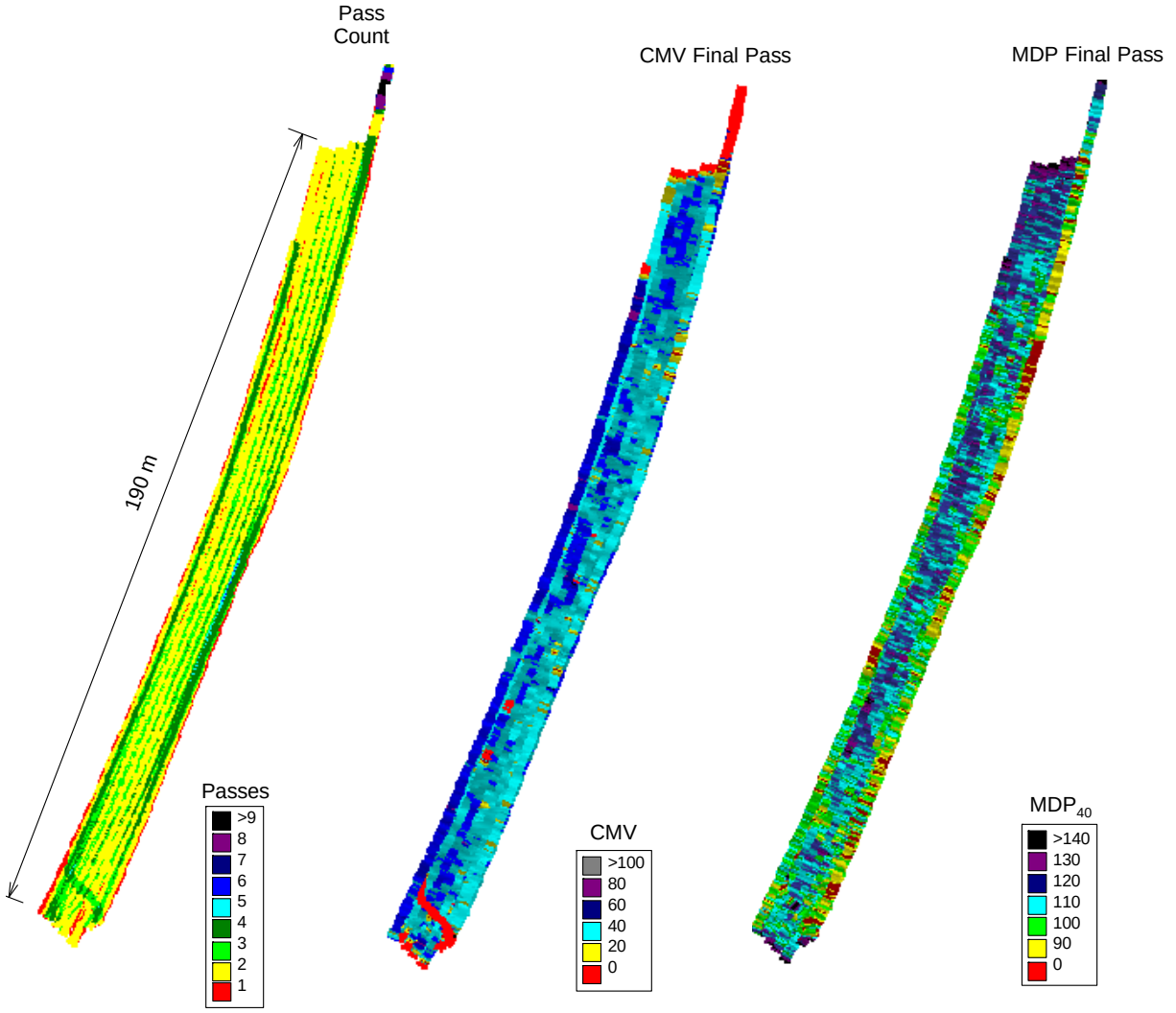

Figure 58. CMV and MDP_{40} spatial maps after final pass – TB9a gravel subbase material production compaction

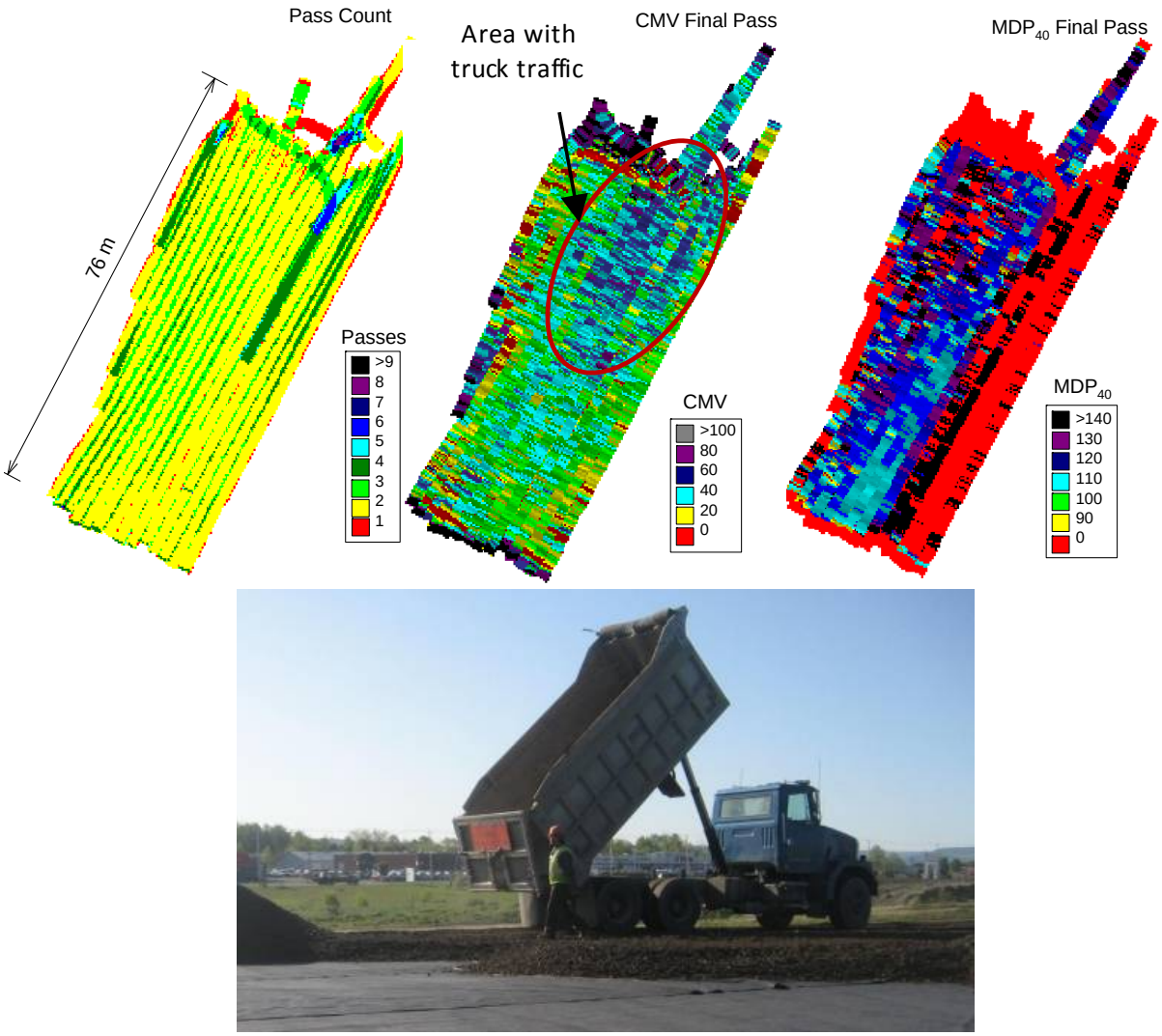

Figure 59. CMV and MDP_{40} spatial maps after final pass – TB9b gravel subbase material production compaction (highlighted area subjected to truck traffic carrying/dumping the base material)

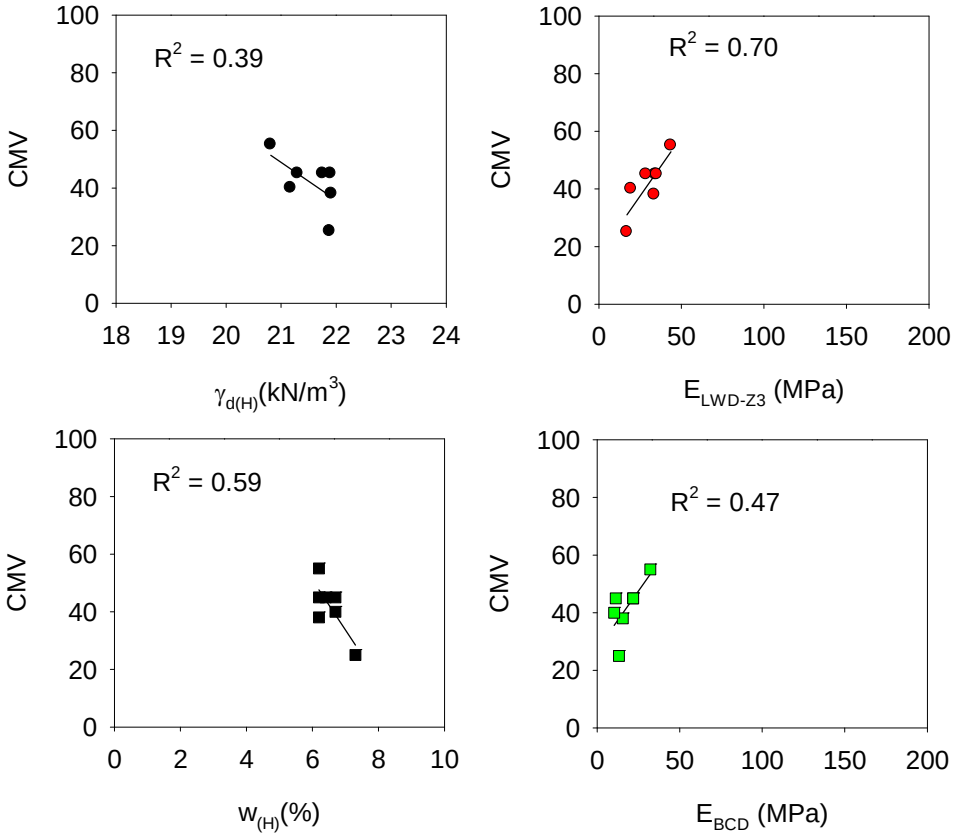

Figure 60. Regression relationships between CMV and Point-MVs (after final pass) – TB9A gravel subbase material

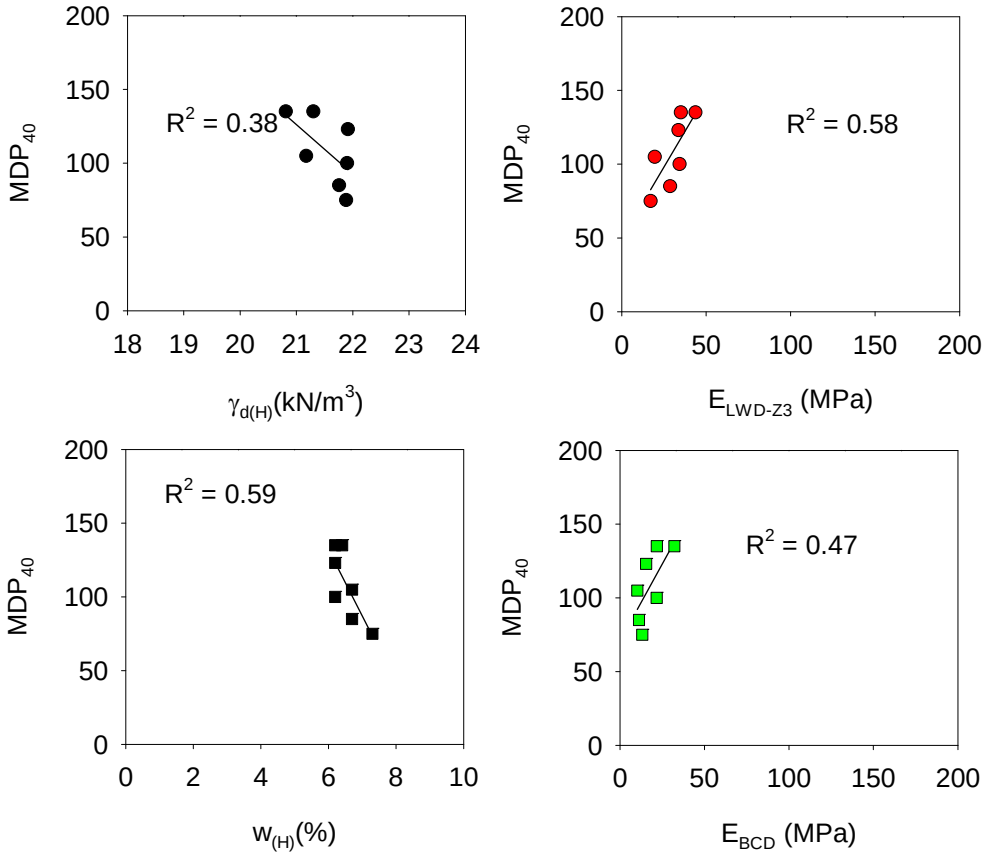

Figure 61. Regression relationships between MDP_{40} and Point-MVs (after final pass) – TB9A gravel subbase material

Table 15. Summary of regression analysis – TB9 gravel subbase material

Relationship	a (mm)	n	R^2
$CMV = 22.8 - 0.03\ (\gamma_{d(H)})$	0.90	7	0.39
$CMV = 8.0 - 0.03\ (w_{(H)})$	0.90	7	0.59
$CMV = -5.2 + 0.85\ (E_{LWD\text{-}Z3})$	0.90	7	0.70
$CMV = -6.3 + 0.58\ (E_{BCD})$	0.90	7	0.47
$MDP_{40} = 22.8 - 0.01\ (\gamma_{d(H)})$	0.90	7	0.38
$MDP_{40} = 8.0 - 0.01\ (w_{(H)})$	0.90	7	0.59
$MDP_{40} = -2.2 + 0.30\ (E_{LWD\text{-}Z3})$	0.90	7	0.58
$MDP_{40} = -6.3 + 0.22\ (E_{BCD})$	0.90	7	0.47

TB10 Embankment Material – Caterpillar and Bomag

Test bed construction and in-situ testing

This test bed consisted of embankment granular subgrade material with three adjacent roller lanes as indicated in Figure 62. 1.0 m wide x 0.3 m deep and 2.0 m wide x 1.0 m deep trenches at locations indicated in Figure 62 were scarified using a backhoe to create a loose uncompacted layer of embankment fill material. Lane 1 was compacted using the Caterpillar IC roller in manual low amplitude mode (a = 0.90mm and f = 30 Hz), lane 2 was compacted using the Bomag IC roller in AFC mode (a_{max} = 1.10 mm and a_{max} = 2.5 mm, target E_{VIB} = 150 MPa, and f = 28 Hz), and lane 3 was compacted using the Bomag IC roller in manual low amplitude mode (a= 0.70mm and f = 30 Hz). Passes 1 to 8 were made at 4 km/h nominal speed and passes 9 and 10 were made at 2 km/h nominal speed. Point-MVs (DCP-CBR, $E_{LWD\text{-}Z3}$, E_{BCD}, $\gamma_{d(H)}$, $\gamma_{d(SDG)}$, $w_{(H)}$, and $w_{(SDG)}$) were obtained after 0, 1, 2, 8, and 10 roller passes on each lane. 2-m deep DCP tests were conducted in the 2-m deep trench area. $E_{FWD\text{-}K3}$ measurements were obtained after pass 8 along three lanes. $E_{FWD\text{-}K3}$ measurements in the trench areas produced deflection values that are greater than the upper measurement range of the sensors and therefore are not reported.

IC-MVs and Point MVs – Lane 1

MDP_{40} measurements in lane 1 for multiple passes are provided in Figure 63. Due to very stiff conditions for most of the lane (except for locations of the trenches), drum jumping was observed. RMV measurements were not available in the output files and the CMV measurements could not be interpreted. Therefore, CMV results are not presented for this test bed. MDP_{40} plots in comparison with Point-MVs for passes 1, 2, and 8 are presented in Figure 64 and Figure 65. DCP-CBR depth profiles at three test locations each in the 1 m wide trench and the 2 m wide trench for passes 0, 1, 2, and 8 are presented in Figure 66. CBR depth profiles in the 2 m wide trench indicate increasing compaction up to a depth of about 1 m below the surface after 8 passes.

Results showed relatively low MDP_{40} values in the trench areas compared to areas outside the trench. The $E_{LWD\text{-}Z3}$, E_{BCD}, CBR_{300}, and $\gamma_{d(H)}$ measurements also indicated low values in the trench areas compared to areas that are compacted. Regression analysis results between MDP_{40} and Point-MVs is presented in Figure 67. Correlation between MDP_{40} and $E_{LWD\text{-}Z3}$, CBR_{Base}, and $E_{FWD\text{-}K3}$ Point-MVs yielded non-linear logarithmic relationships with R^2 = 0.59 to 0.72. Relationships with $\gamma_{d(H)}$ and E_{BCD} were weak. Moisture variation was minimal (5 to 7%) and therefore was not statistically significant in the analysis.

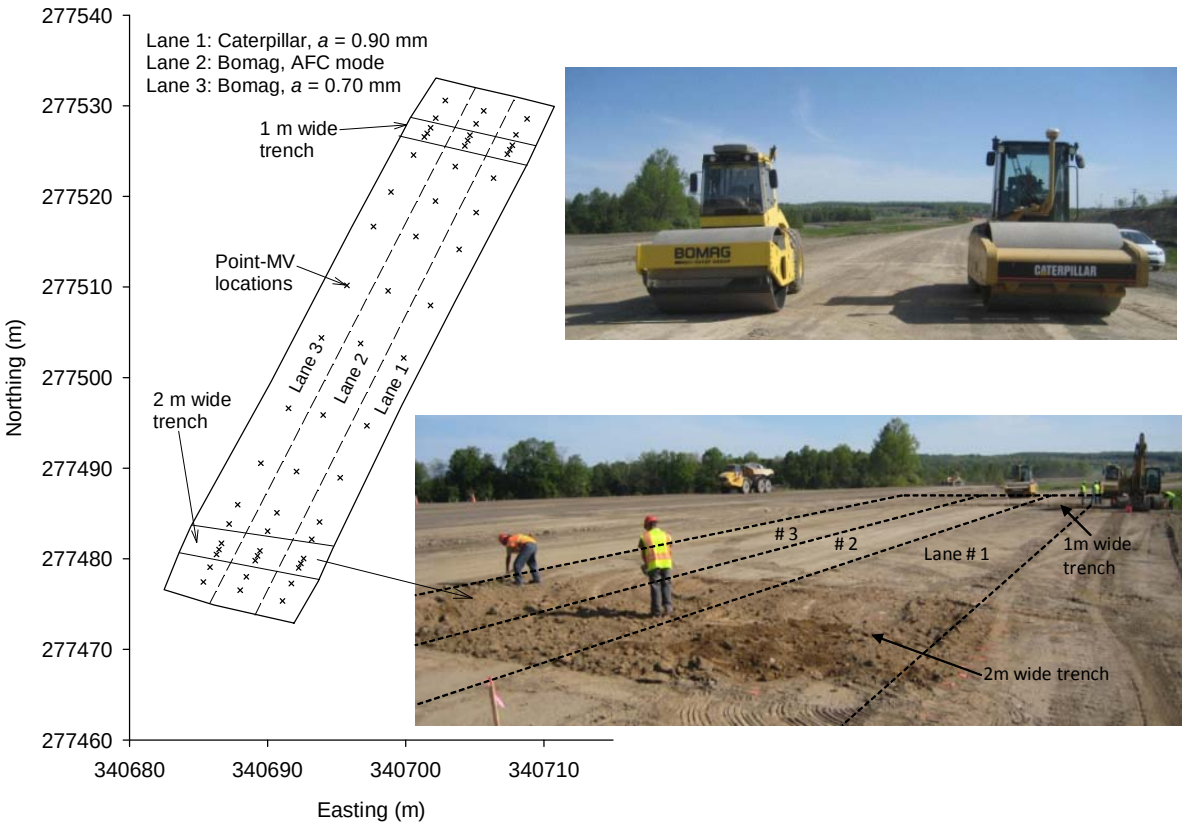

Figure 62. TB10 area with three lanes compacted using the IC rollers – 1 m and 2 m wide trenches excavation on either ends of the test bed

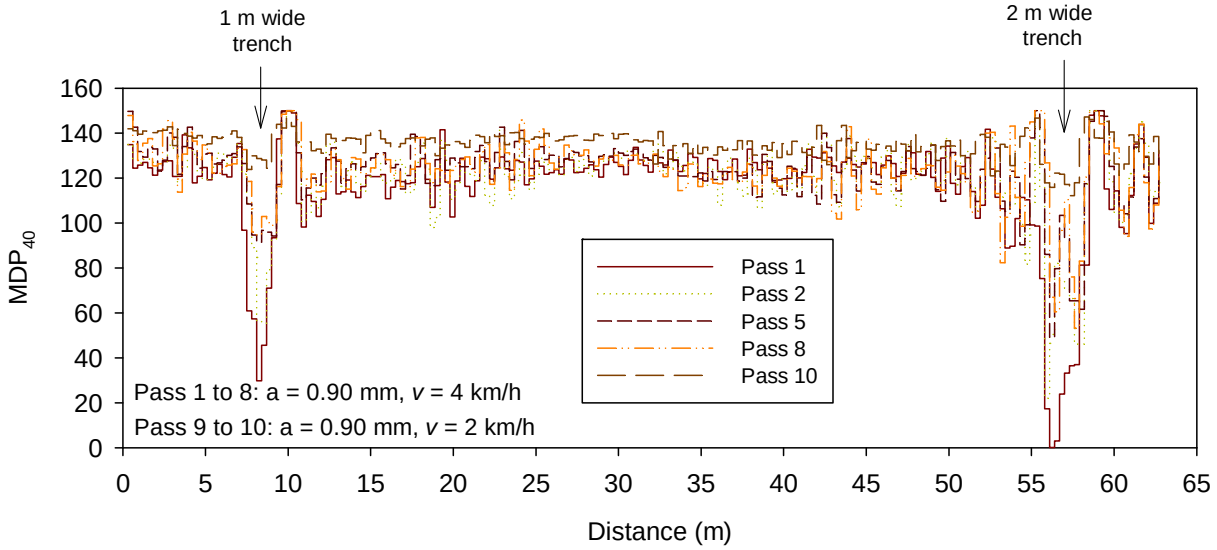

Figure 63. MDP_{40} plots for passes 1, 2, 5, 8, and 10 on TB10 along lane 1

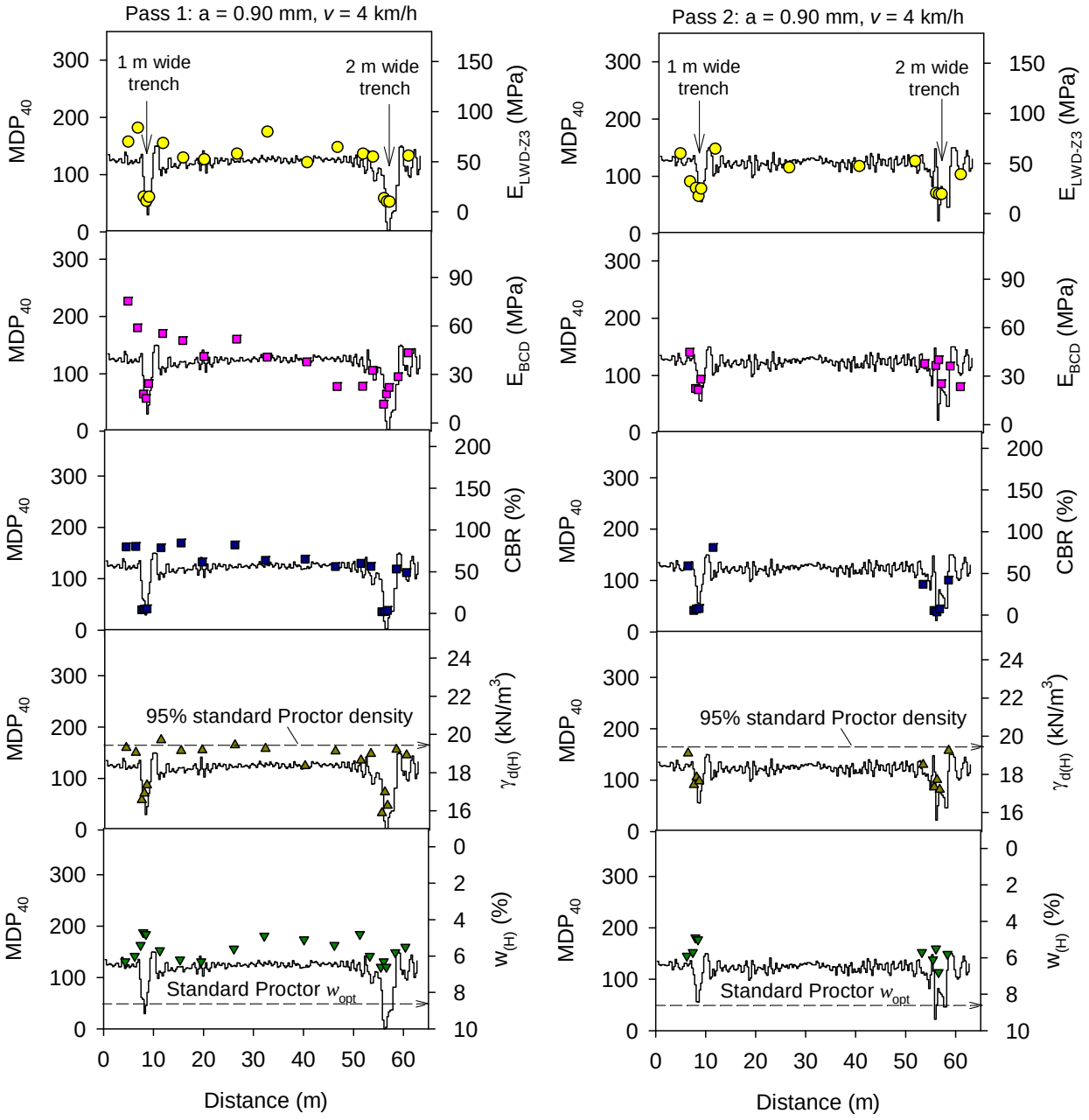

Figure 64. Comparison between MDP_{40} and Point MVs after passes 1 and 2 on TB10 along lane 1

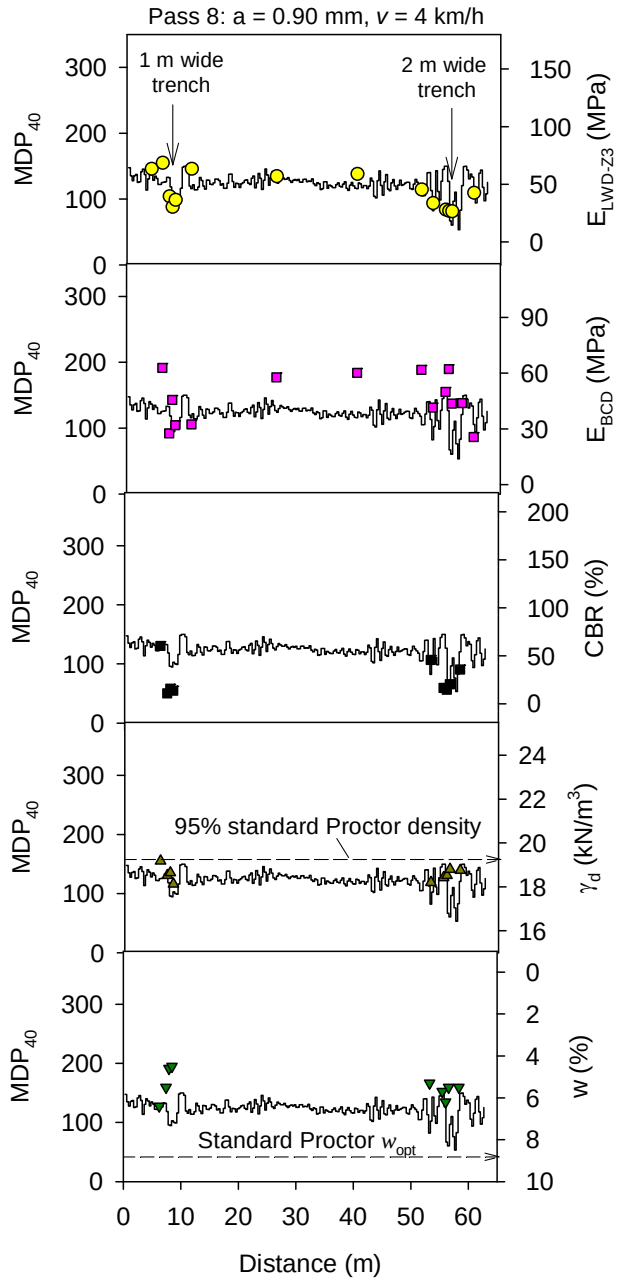

Figure 65. Comparison between MDP_{40} and Point MVs after pass 8 on TB10 along lane 1

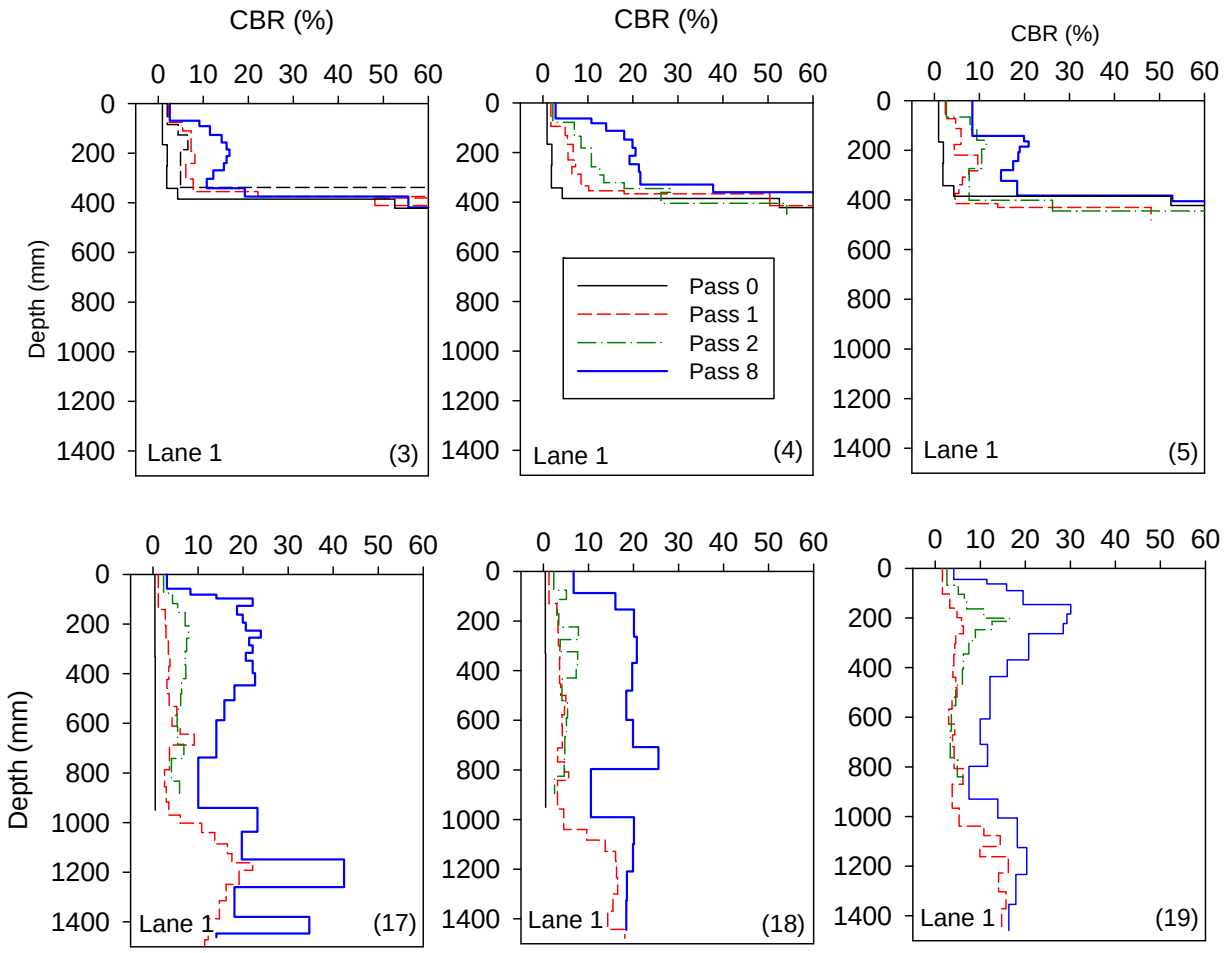

Figure 66. DCP-CBR profiles after 0, 1, 2, and 8 roller passes on TB10 lane 1 (note test location numbers in parenthesis – (3), (4), and (5) in 1 m wide trench and (17), (18), and (19) in 2 m wide trench)

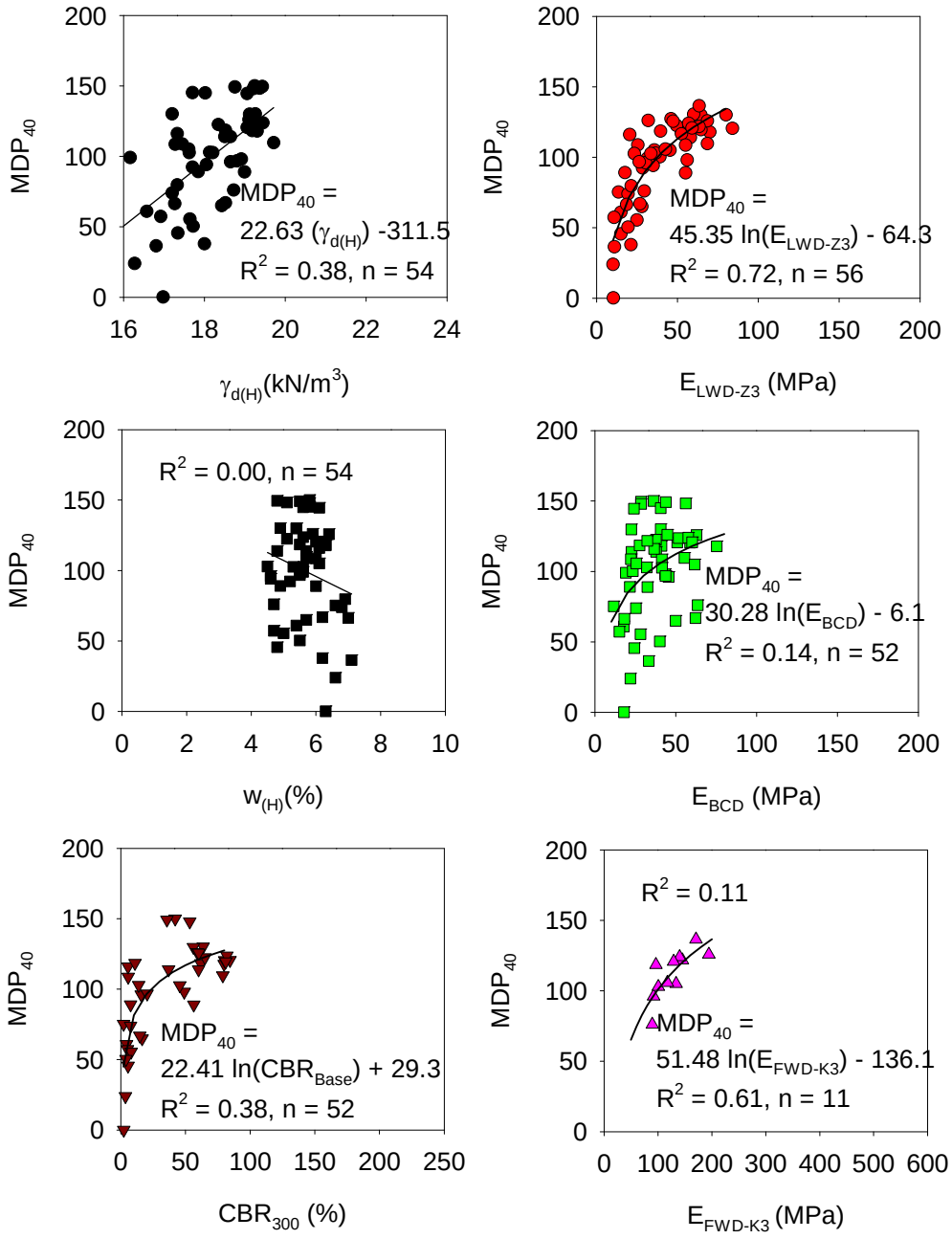

Figure 67. Regression relationships between MDP_{40} and Point-MVs – TB10 lane 1 embankment material

IC-MVs and Point MVs – Lanes 2 and 3

E_{VIB} measurements in lanes 2 and 3 for multiple passes are provided in Figure 68 and Figure 69, respectively. Vibration amplitude measurements on lane 2 compacted in AFC mode are also presented in Figure 68. Results from lane 2 indicate that when $E_{VIB} < 150$ MPa, the amplitude is at $a_{max} = 1.10$ mm for passes 1 to 8 and 2.50 mm for passes 9 to 10, and the amplitude is effectively reduced up to 0.60mm when $E_{VIB} > 150$ MPa. E_{VIB} plots in comparison with Point-MVs for passes 1, 2, 8, and 10 are presented in Figure 70 and Figure 71 for lane 2, and Figure 72

and Figure 73 for lane 3. DCP-CBR depth profiles at three test locations each in the 1 m wide trench and the 2 m wide trench for passes 0, 1, 2, 8, 10 are presented in Figure 74 for lane 2 and Figure 75 for lane 3. CBR profiles in the 2 m wide trench along lanes 2 and 3 indicate increasing compaction up to a depth of about 1 to 1.4 m below the surface after 8 passes. Results showed relatively low E_{VIB} values in the trench areas compared to areas outside the trench. The $E_{LWD\text{-}Z3}$, E_{BCD}, CBR_{300}, and $\gamma_{d(H)}$ measurements showed a similar trend.

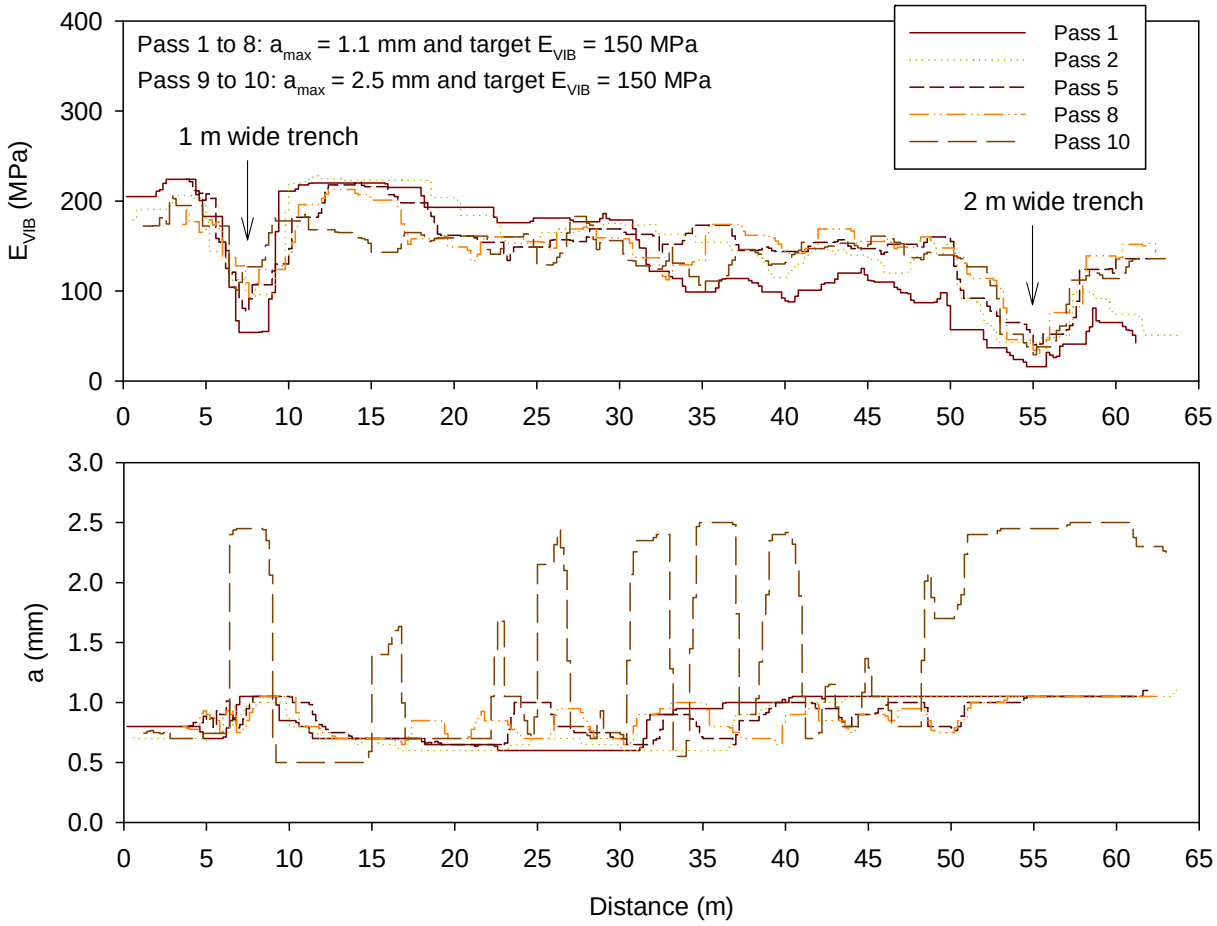

Figure 68. E_{VIB} and amplitude plots for passes 1, 2, 5, 8, and 10 on TB10 along lane 2 compacted using AFC mode

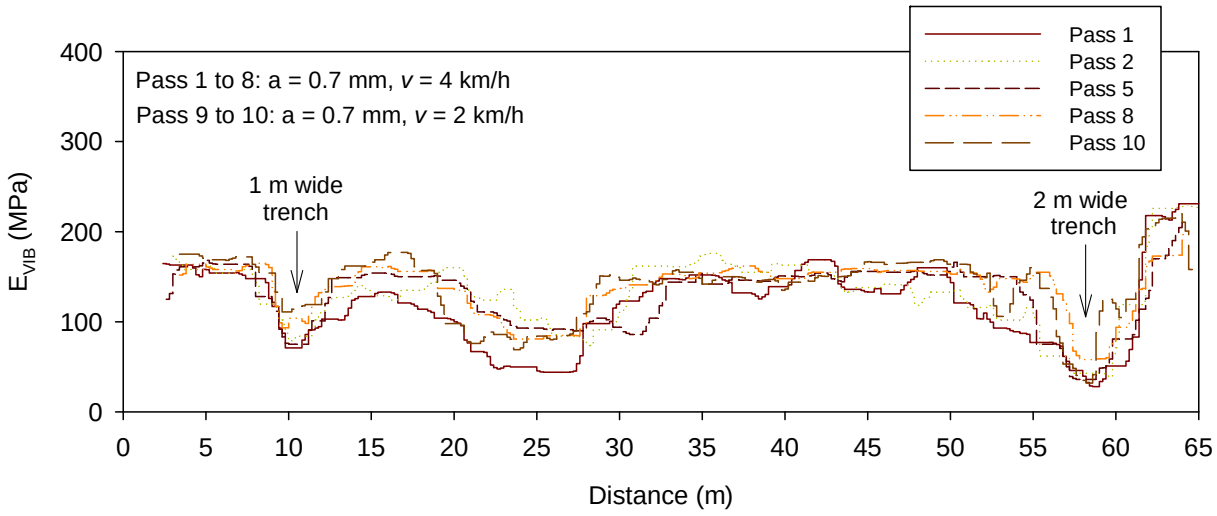

Figure 69. E_{VIB} and amplitude plots for passes 1, 2, 5, 8, and 10 on TB10 along lane 3 compacted using manual mode

Regression analysis results between E_{VIB} and Point-MVs from lanes 2 and 3 are presented in Figure 76 and Figure 77, respectively. For lane 2 where E_{VIB} values were obtained in AFC mode, regression relationships produced weak correlations between E_{VIB} and all Point-MVs ($R^2 < 0.5$) with exception for relationship with $E_{FWD\text{-}K3}$. Also for lane 3 where E_{VIB} values were obtained in manual mode, regression relationships produced weak correlations between E_{VIB} and all Point-MVs ($R^2 < 0.5$). Results from lane 2 are expected to be influenced by amplitude (amplitude varied from 0.60 to 1.10 mm), and therefore are analyzed using multiple regression analysis to quantify the influence of amplitude on E_{VIB} measurements. Results from multiple regression analysis are summarized in Table 16. The statistical significance of amplitude in the relationship is assessed using the *p*- and *t*-values as described earlier in the report. The results presented in Table 16 indicate that amplitude is significant for E_{VIB} relationships with three Point-MVs ($E_{LWD\text{-}Z3}$, E_{BCD}, and $\gamma_{d(H)}$) and also contribute to increased R^2 values. Note that in Table 16, the adjusted R^2 values (for the number of parameters using Eq. 11) are reported to allow for comparison with R^2 values from simple linear regression analysis.

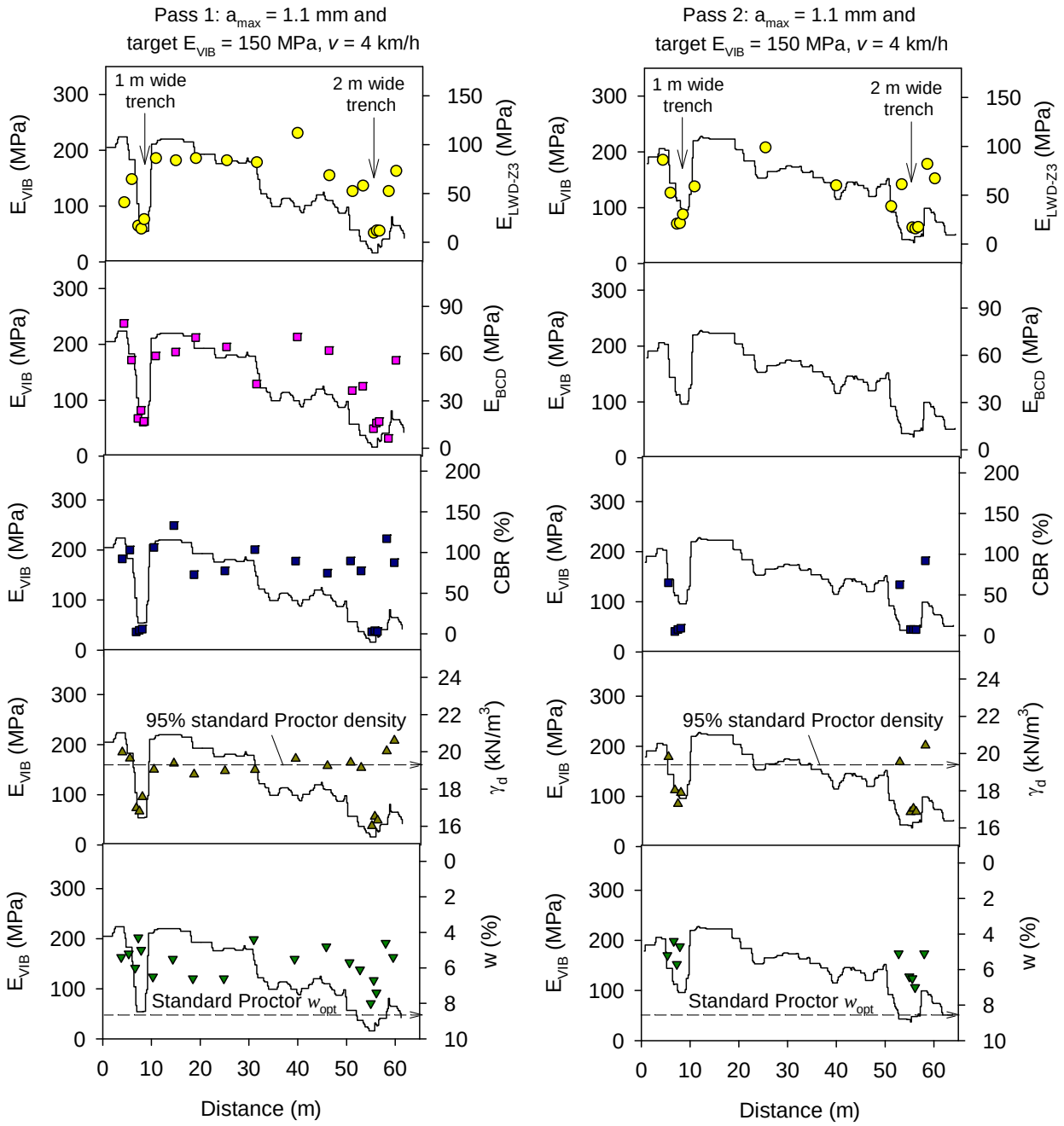

Figure 70. Comparison between E_{VIB} and Point MVs after passes 1 and 2 on TB10 along lane 2

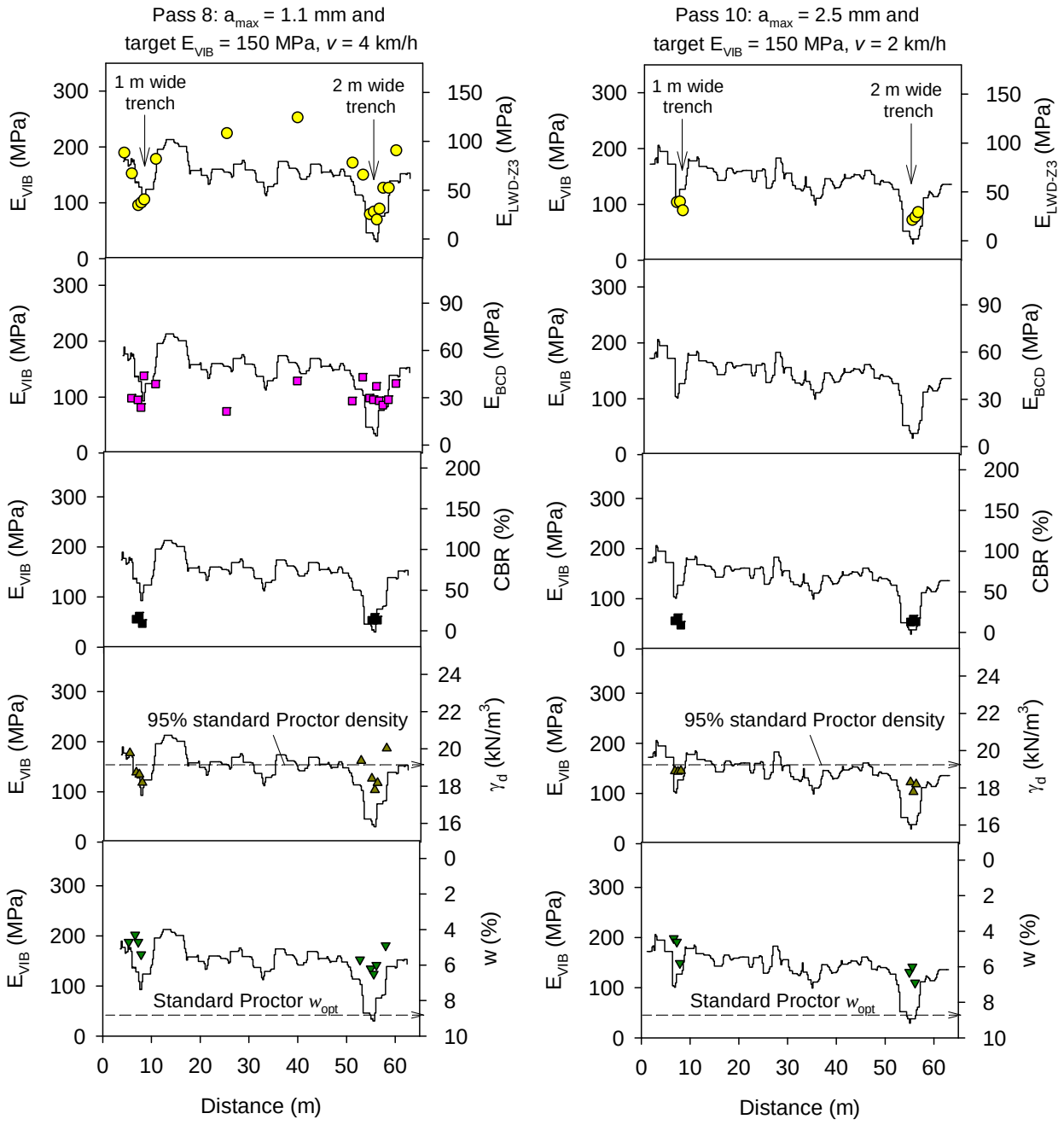

Figure 71. Comparison between E_{VIB} and Point MVs after passes 8 and 10 on TB10 along lane 2

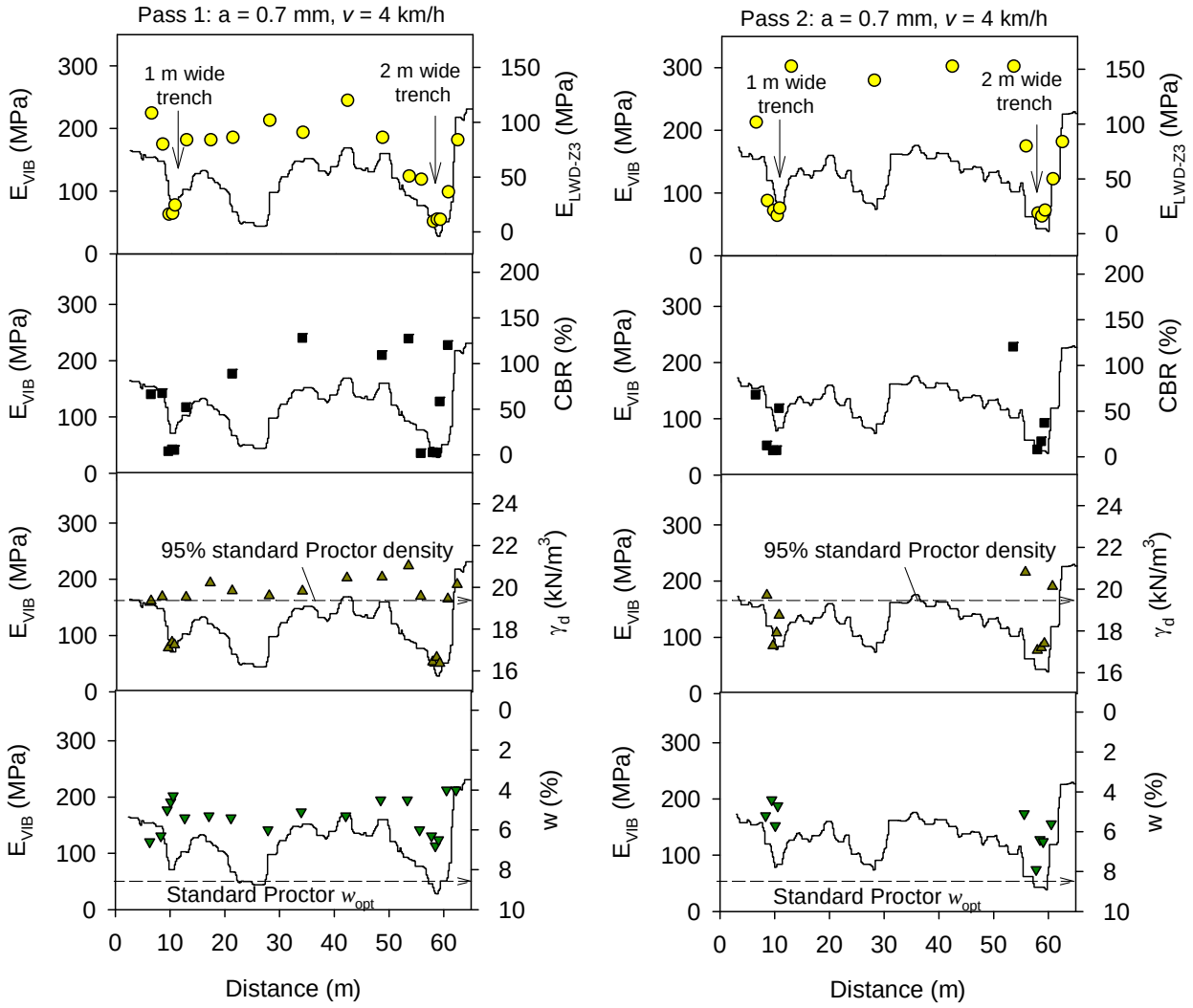

Figure 72. Comparison between E_{VIB} and Point MVs after passes 1 and 2 on TB10 along lane 3

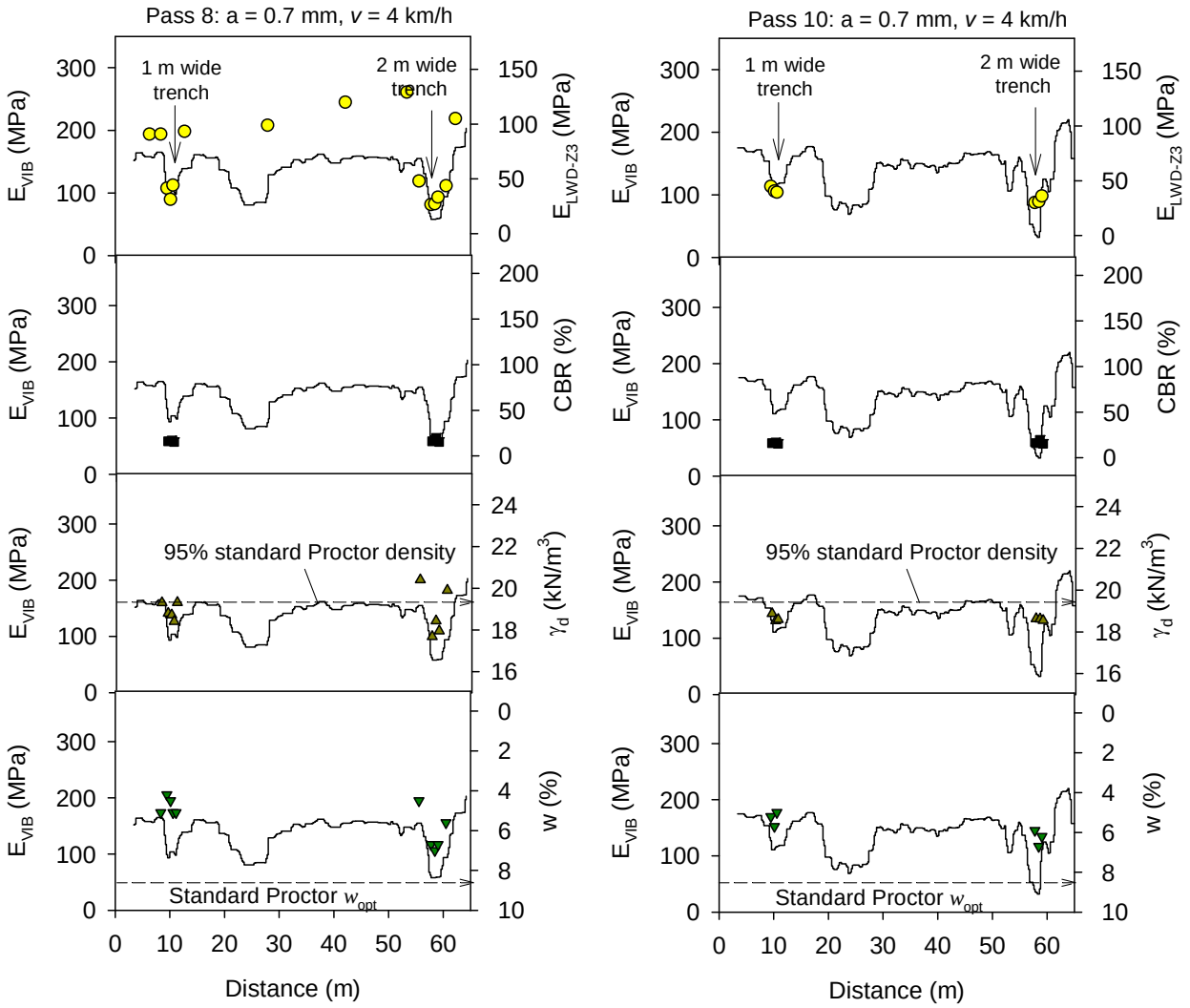

Figure 73. Comparison between E_{VIB} and Point MVs after passes 8 and 10 on TB10 along lane 3

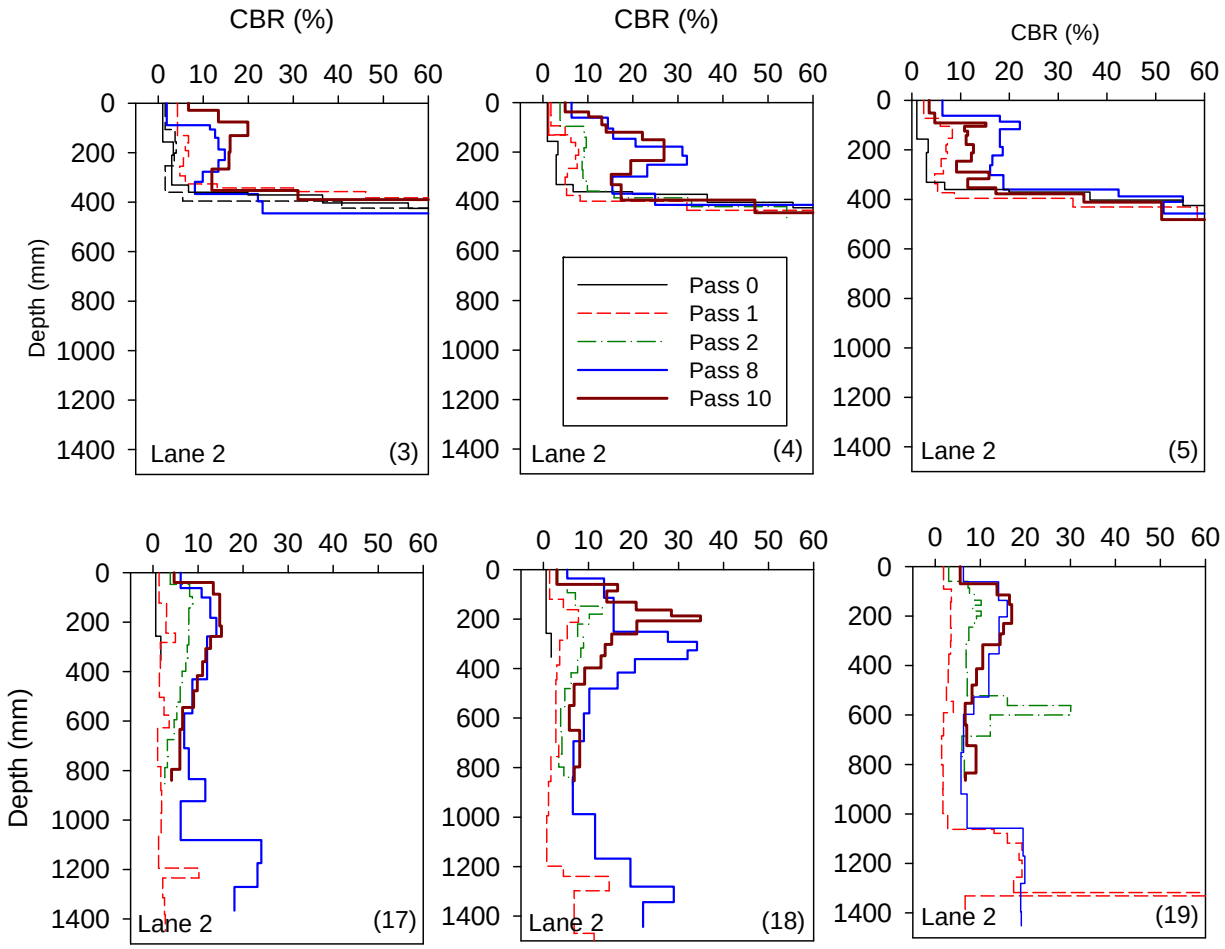

Figure 74. DCP-CBR profiles after 0, 1, 2, and 8 roller passes on TB10 lane 2 (note test location numbers in parenthesis – (3), (4), and (5) in 1 m wide trench and (17), (18), and (19) in 2 m wide trench)

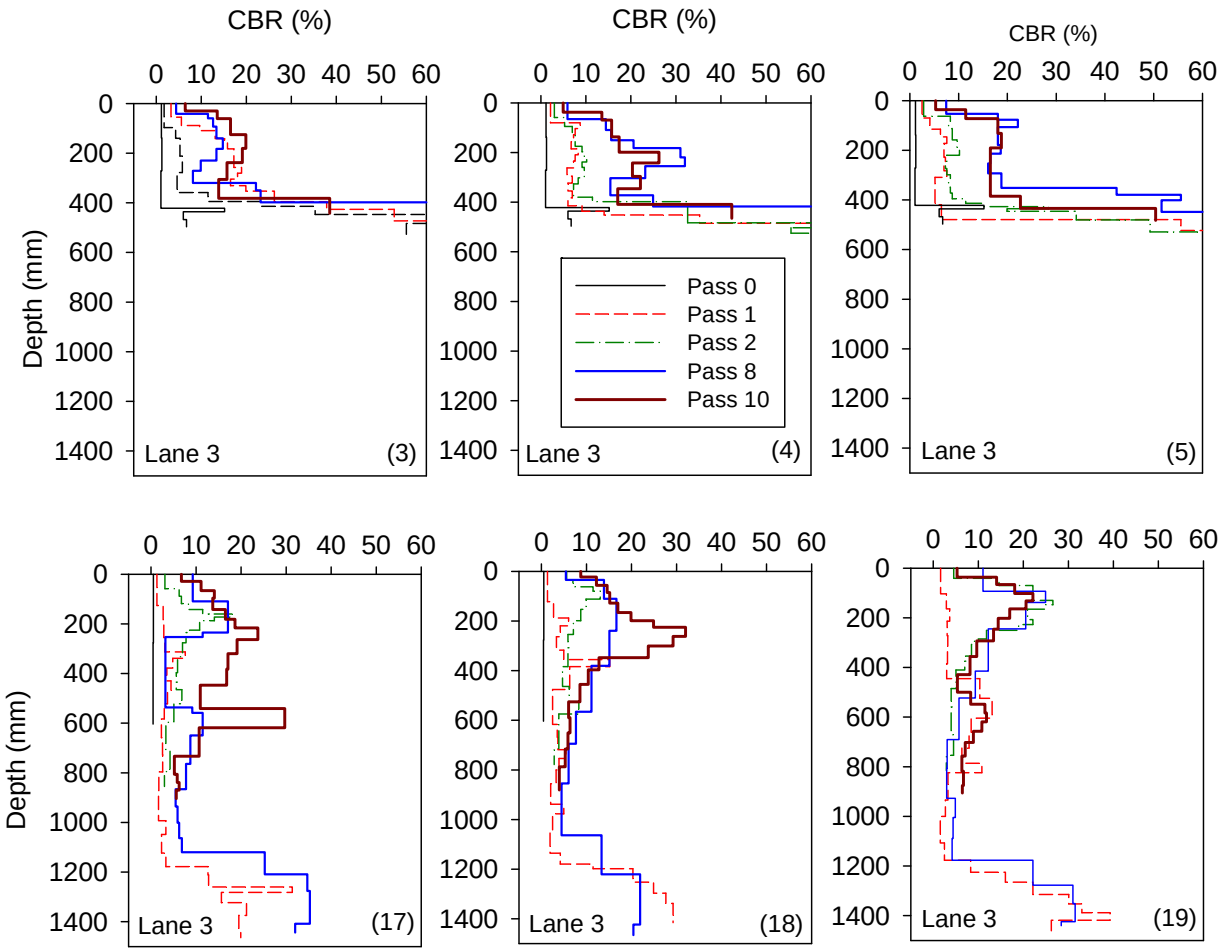

Figure 75. DCP-CBR profiles after 0, 1, 2, and 8 roller passes on TB10 lane 3 (note test location numbers in parenthesis – (3), (4), and (5) in 1 m wide trench and (17), (18), and (19) in 2 m wide trench)

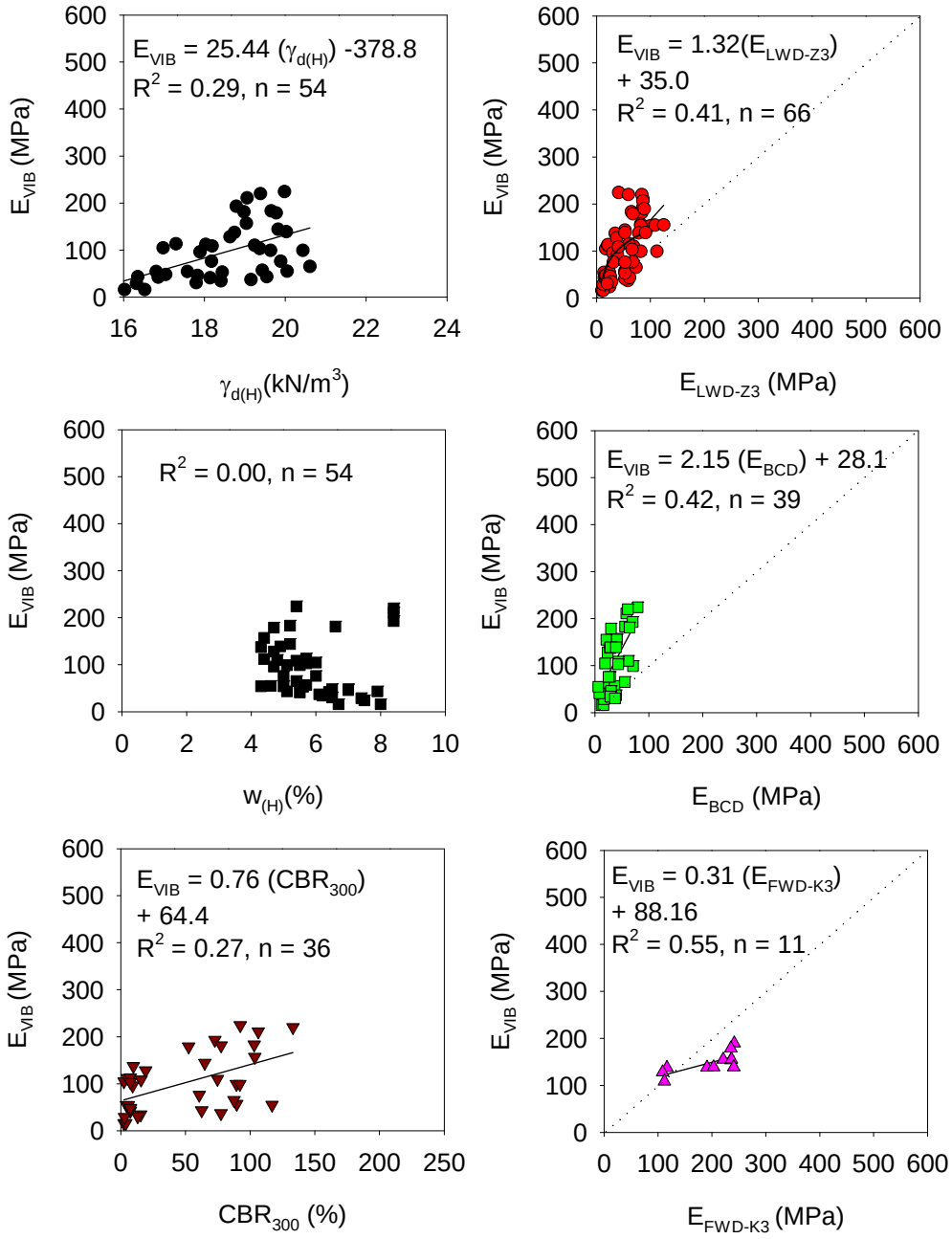

Figure 76. Regression relationships between E_{VIB} and Point-MVs (lane 2 AFC mode compaction *a* = 0.60 to 1.10 mm) – TB10 embankment material

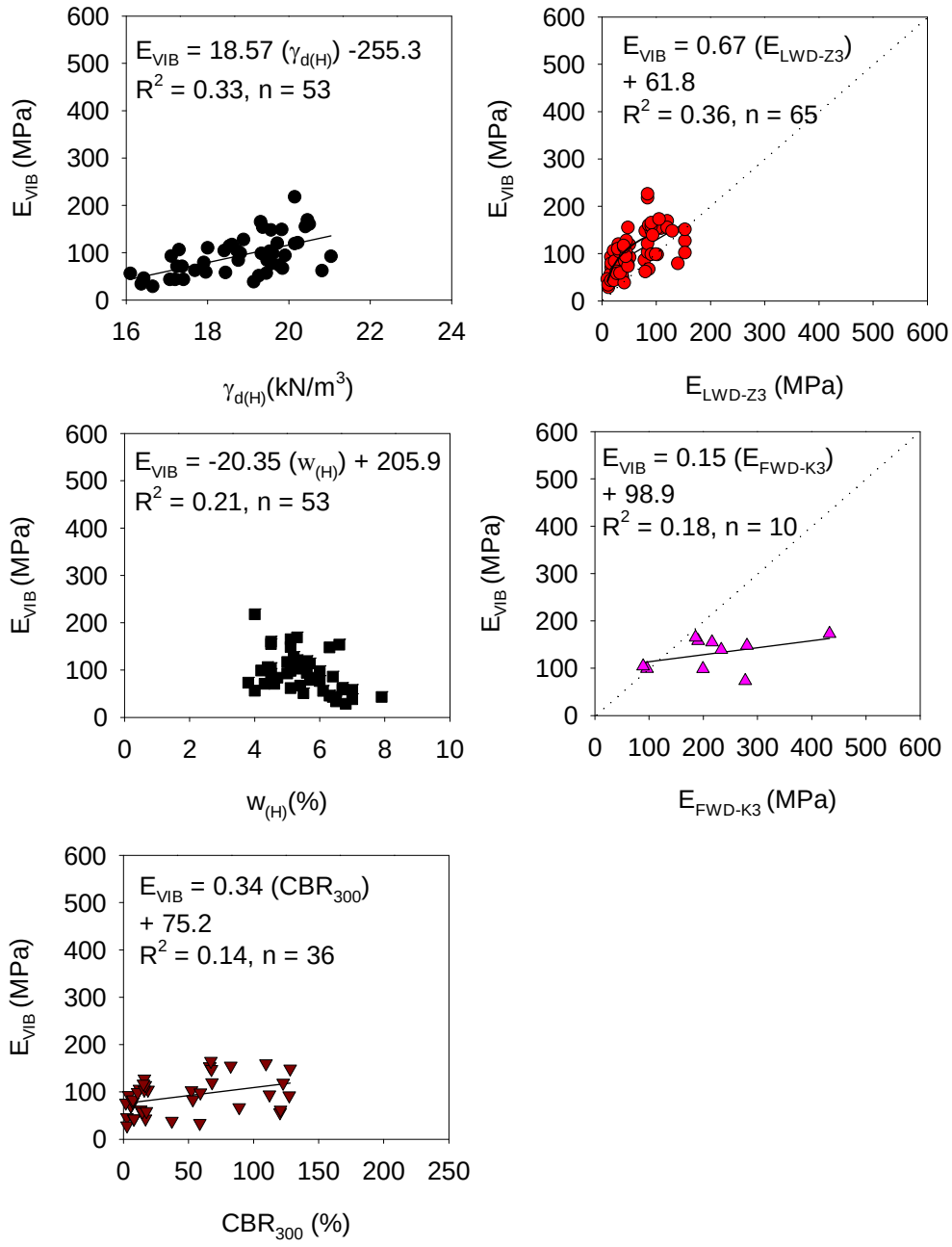

Figure 77. Regression relationships between E_{VIB} and Point-MVs (lane 3 manual mode *a* = 0.70 mm) – TB10 embankment material

Table 16. Summary of multiple regression analysis – TB10 lane 2

Model	Term	Estimate	Std Error	*t* Ratio	Prob>t (*p* value)	R^2 (adjusted)	Amplitude significant?
$E_{VIB} = b_0 + b_1 E_{LWD\text{-}Z3} + b_2 a$	b_0	61.69	21.17	2.91	0.0051	0.44	Yes
	b_1	1.19	0.22	5.51	<0.0001		
	b_2	-17.94	11.92	-3.51	0.0374		
$E_{VIB} = b_0 + b_1 E_{BCD} + b_2 a$	b_0	283.02	46.15	6.13	<0.0001	0.70	Yes
	b_1	1.27	0.35	3.66	0.0008		
	b_2	-238.72	41.55	-5.75	<0.0001		
$E_{VIB} = b_0 + b_1 \gamma_{d(H)} + b_2 a$	b_0	-330.30	101.86	-3.24	0.0022	0.37	Yes
	b_1	24.72	5.42	4.56	<0.0001		
	b_2	-29.64	11.70	-2.53	0.0146		
$E_{VIB} = b_0 + b_1 CBR_{300} + b_2 a$	b_0	87.46	24.42	3.58	0.0009	0.30	No
	b_1	0.68	0.21	3.20	0.0027		
	b_2	-16.86	15.71	-1.07	0.2899		
$E_{VIB} = b_0 + b_1 E_{FWD\text{-}K3} + b_2 a$	b_0	133.55	36.63	3.65	0.0065	0.64	No
	b_1	0.29	0.09	3.25	0.0117		
	b_2	-47.35	33.51	-1.41	0.1954		

Note: a parameter is considered statistically significant if $p < 0.10$ and $t < -2$ or $> +2$.

Analysis of compaction in excavated trenches

Average IC-MV and Point-MV compaction curves for the 0 m, 1 m, and 2 m trench areas on lanes 1, 2, and 3 are presented in Figure 78. The average compaction curves indicate that the average dry density, modulus, and CBR measurements generally increased with increasing roller passes up to pass 8 in the 1 m and 2 m trench areas. For the areas outside the trenches (e.g. 0 m trench) the values varied slightly with pass due to possible decompaction and recompaction. In some cases the number of measurements for each pass also differed in the 0 m trench areas. A summary of average IC-MV and Point-MVs in the three areas after pass 8 are provided in Table 17.

No significant difference is noticed in the density of the material at the surface in the 1 m and 2 m trenches in lane 2 compacted in AFC mode and lane 3 compacted in manual mode (91% relative compaction in the 1 m trench and 88 to 89% relative compaction in the 2 m trench). Similarly, $E_{LWD\text{-}Z3}$ and CBR_{300} measurements did not show considerable differences (see Table 17).

DCP-CBR depth profiles presented in Figure 66, Figure 74, and Figure 75 for lanes 1, 2, and 3, respectively were analyzed to determine the depth of influence for compaction in the 2 m trenches. Average change (per each lane which constitutes three measurements in the 2 m trench) in CBR relative to pass 1 for compaction depths of 0 to 300 mm, 300 to 600 mm, 600 to 900 mm, 900 to 1200 mm, and 1200 to 1500 mm are presented for lanes 1, 2, and 3 in Figure 79. Comparisons between changes in CBR depth profiles (relative to pass 1) are presented in Figure 80. With exception of the CBR depth profile after pass 10 on lane 2, all other CBR profiles indicate that the incremental increase in CBR decreases with depth. No considerable differences are observed in the CBR depth profiles between lane 2 compacted in AFC mode and lane 3 compacted in manual mode.

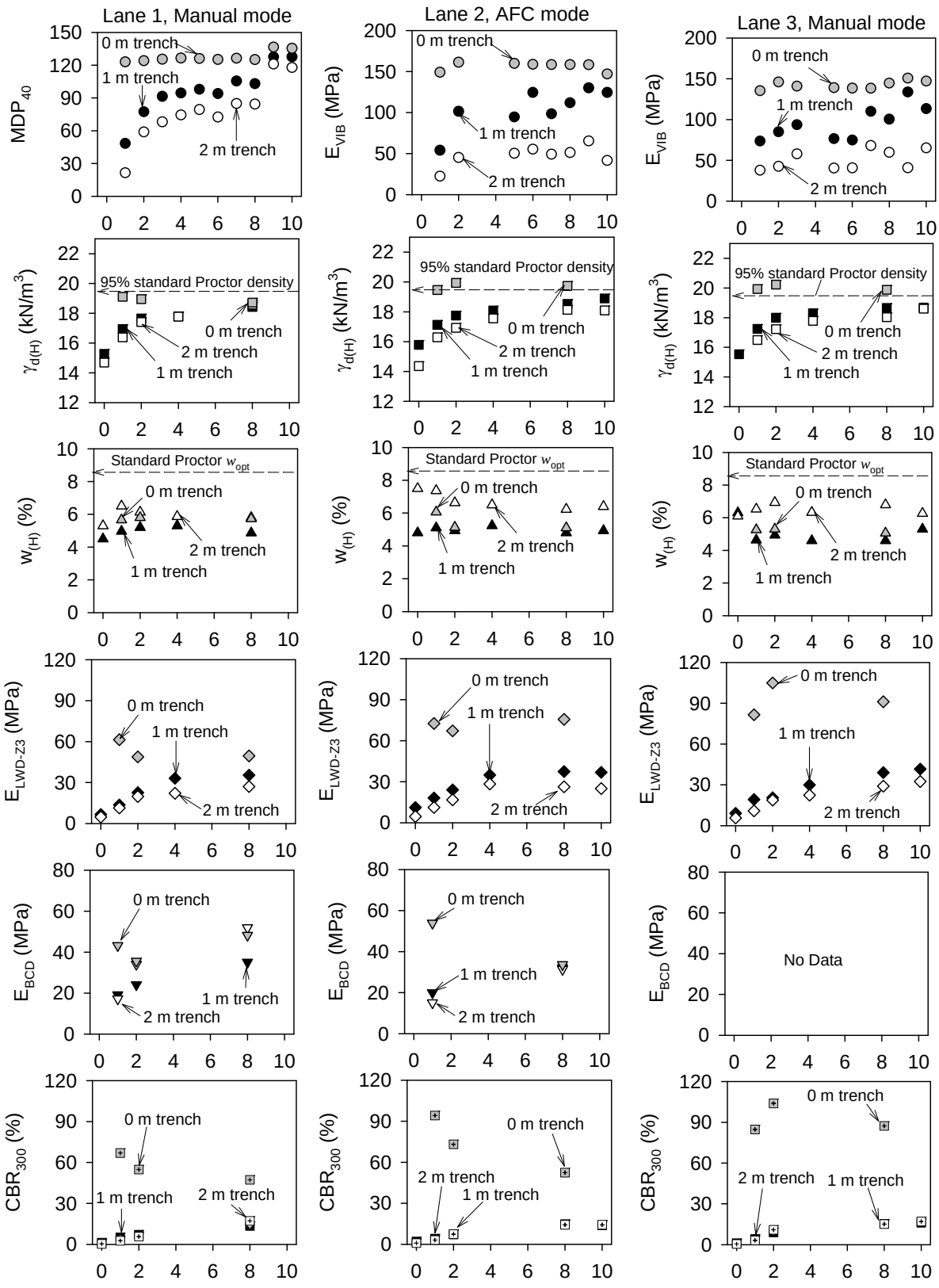

Figure 78. Comparison of average (average over the distance of 1m wide trench, 2 m wide trench, and no trench areas) compaction curves of IC-MVs and Point MVs – TB10

Table 17. Summary of average IC-MVs and Point MVs for the 0 m, 1m, and 2m trench areas – TB10 lanes 1, 2, and 3

MV	0 m trench	1 m trench	2 m trench
Lane 1: a = 0.90 mm, f = 30 Hz			
MDP_{40}	125.1	103.0	84.4
$\gamma_{d(H)}$ (kN/m^3)	18.71	18.43	18.58
Relative compaction (%)	91	90	91
$w_{(H)}$ (%)	5.7	4.9	5.8
$E_{LWD\text{-}Z3}$ (MPa)	49.6	35.4	27.1
E_{BCD} (MPa)	48.2	35.1	51.9
CBR_{300} (%)	47.3	13.5	17.2
Lane 2: AFC mode a_{max} = 1.10 mm, f = 28Hz			
E_{VIB} (MPa)	158.4	111.9	51.2
$\gamma_{d(H)}$ (kN/m^3)	19.73	18.52	18.13
Relative compaction (%)	96	91	89
$w_{(H)}$ (%)	5.1	4.8	6.2
$E_{LWD\text{-}Z3}$ (MPa)	76.7	37.5	26.3
E_{BCD} (MPa)	33.6	32.1	31.4
CBR_{300} (%)	52.5	14.9	14.3
Lane 3: a = 0.70 mm, f = 28Hz			
E_{VIB} (MPa)	144.6	100.4	59.8
$\gamma_{d(H)}$ (kN/m^3)	19.87	18.65	18.03
Relative compaction (%)	97	91	88
$w_{(H)}$ (%)	5.1	4.6	6.8
$E_{LWD\text{-}Z3}$ (MPa)	91.1	39.0	29.0
CBR_{300} (%)	87.3	15.3	15.2

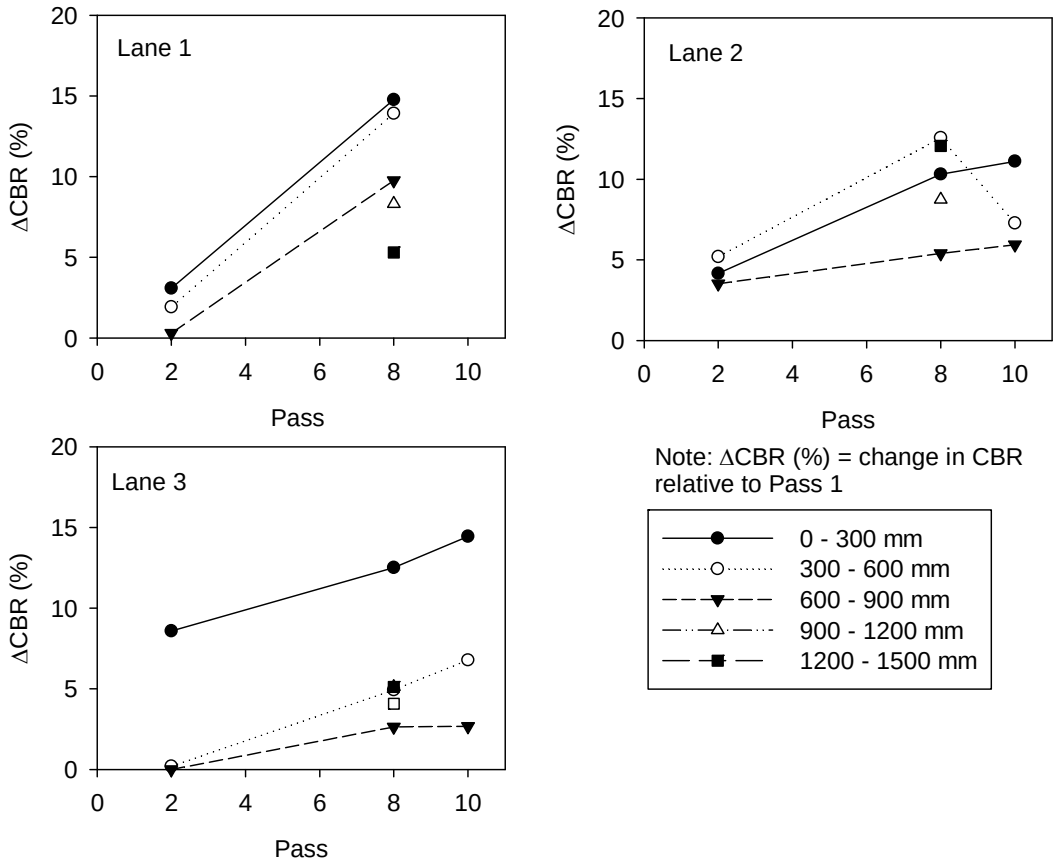

Figure 79. Comparison between change in CBR at different depth increments relative to pass 1 in 2 m wide trench – TB10 lanes 1, 2, and 3

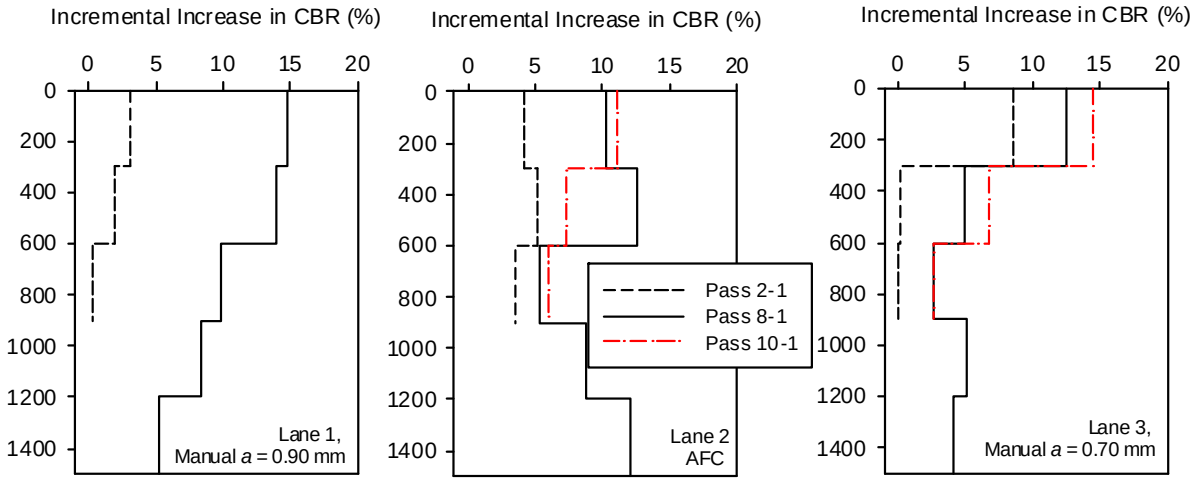

Figure 80. Comparison between incremental increase in CBR with depth relative to pass 1 in the 2 m wide trench – TB10 lanes 1, 2, and 3

Summary of Key Points

Construction of this test bed involved creating 1 m wide x 0.3 m deep and 2.0 m wide x 1.0 m deep loose fill layer trenches in the compacted embankment subgrade. The test bed was divided into three lanes for compaction using the Bomag IC roller using AFC and manual modes, and the Caterpillar IC roller using manual low amplitude mode. Point-MVs were obtained at several intermediate passes to assess compaction of the loose material. Regression analysis was performed between IC-MVs and Point-MVs by spatially pairing the data. DCP-CBR depth profiles were analyzed to assess the compaction influence depth with different roller operation modes. Following is a summary of field observations and key findings from this test bed:

- Results demonstrated that the IC-MVs effectively identified the loose trench areas compared to the areas that were previously compacted. The $E_{LWD\text{-}Z3}$, E_{BCD}, CBR_{300}, and $\gamma_{d(H)}$ measurements also indicated comparatively low values in the trench areas.
- Correlations between MDP_{40} and $E_{LWD\text{-}Z3}$, CBR_{Base}, and $E_{FWD\text{-}K3}$ Point-MVs showed non-linear logarithmic relationships with $R^2 = 0.59$ to 0.72. Relationships with $\gamma_{d(H)}$ and E_{BCD} yielded weaker correlations ($R^2 < 0.4$).
- Amplitude measurements in AFC mode indicate that when $E_{VIB} < 150$ MPa, the amplitude is at the a_{max}, and the amplitude is effectively reduced up to 0.60 mm when $E_{VIB} > 150$ MPa.
- Regression relationships between E_{VIB} values and Point-MVs obtained in AFC mode and in manual mode yielded weak correlations ($R^2 < 0.5$) with exception of the relationship with $E_{FWD\text{-}K3}$ on lane 2. E_{VIB} results obtained in AFC mode were analyzed using multiple regression analysis to quantify the influence of amplitude on the regression relationships. Results indicate that amplitude is significant for E_{VIB} relationships with three Point-MVs ($E_{LWD\text{-}Z3}$, E_{BCD}, and $\gamma_{d(H)}$) and also contribute to improvement in the R^2 values.
- The compaction curves of average dry density, modulus, and CBR measurements generally increased with increasing passes up to pass 8 in the 1 m and 2 m trench areas. No significant difference was measured in terms of density of the material at the surface in the 1 m and 2 m trenches between lanes compacted using AFC mode and manual mode (91% relative compaction in the 1m trench and 88 to 89% relative compaction in the 2m trench). Similarly, $E_{LWD\text{-}Z3}$ and CBR_{300} measurements did not demonstrate considerable differences between AFC mode and manual mode compacted lanes.
- Analysis of incremental increase in CBR relative to pass 1 in the 2 m trench for different compaction depths did not present considerable differences between AFC mode and manual mode compaction.

COMBINED REGRESSION ANALYSIS

Data presented above captured IC-MVs and corresponding Point-MVs over a wide measurement range. The data from multiple test beds are combined in this section to develop site wide correlation results. As discussed above, many of the test bed results only represented a narrow range of measurement values. Combining results should provide a perspective on more general trends and associated variability.

Relationships between MDP_{40} obtained in low amplitude setting (a = 0.90 mm, f = 30 Hz) and various Point-MVs are presented in Figure 81. Non-linear logarithmic relationships showed the best fit for all Point-MVs. Relationships with $E_{LWD\text{-}Z2}$, $E_{LWD\text{-}Z3}$, $E_{FWD\text{-}K3,}$ and CBR showed good correlations with R^2 values > 0.60. Correlation with E_{BCD} showed relatively low R^2 value (0.10). Similar non-linear logarithmic relationships between MDP_{40} obtained in static mode and $E_{LWD\text{-}Z3}$ and $E_{FWD\text{-}K3}$ Point-MVs are presented in Figure 82. These relationships also yielded good correlations with R^2 values > 0.70.

Non-linear power relationships between CMV obtained in low amplitude setting (a = 0.90 mm, f = 30 Hz) and $E_{LWD\text{-}Z2}$ and CBR Point-MVs are presented in Figure 83. Due to limited measurements and the narrow measurement range, these relationships yielded relatively weak correlations with R^2 values < 0.40.

Simple linear relationships between E_{VIB} obtained in the low amplitude setting (a = 0.70 mm, f = 28 Hz) and $E_{LWD\text{-}Z3}$ and $E_{FWD\text{-}K3}$ Point-MVs are presented in Figure 84. These relationships produced correlations with R^2 values > 0.7.

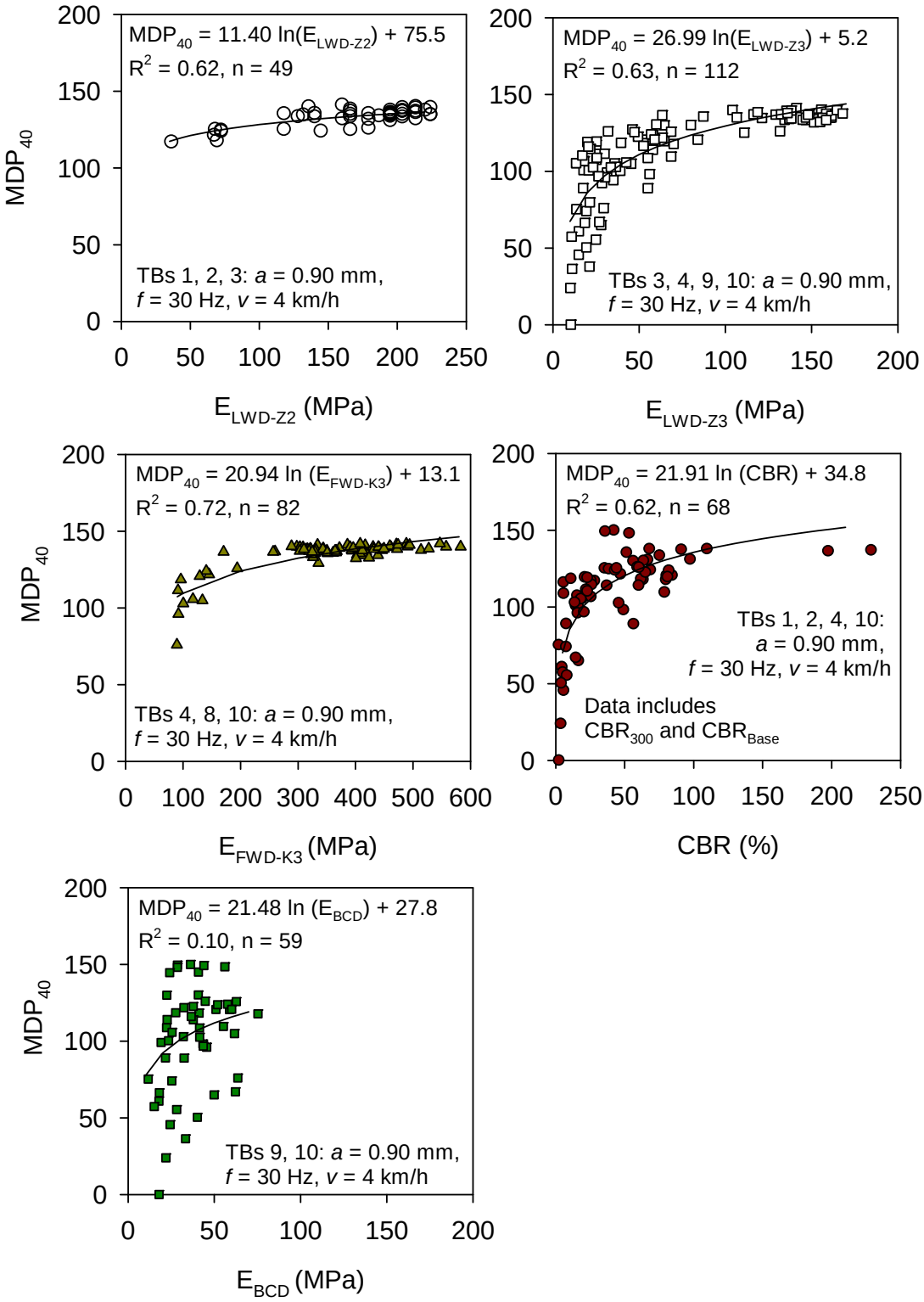

Figure 81. Regression analysis between MDP_{40} (*a* = 0.90 mm, *f* = 30 Hz, and *v* = 4 km/h) and Point-MVs combining data from different test beds

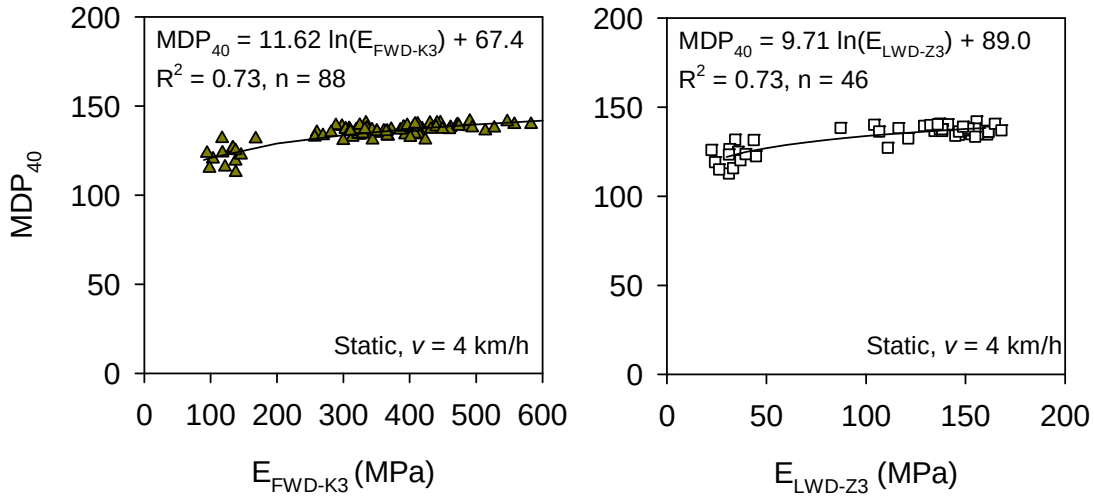

Figure 82. Regression analysis between MDP_{40} (static mode and v = 4 km/h) and Point-MVs combining data from different test beds

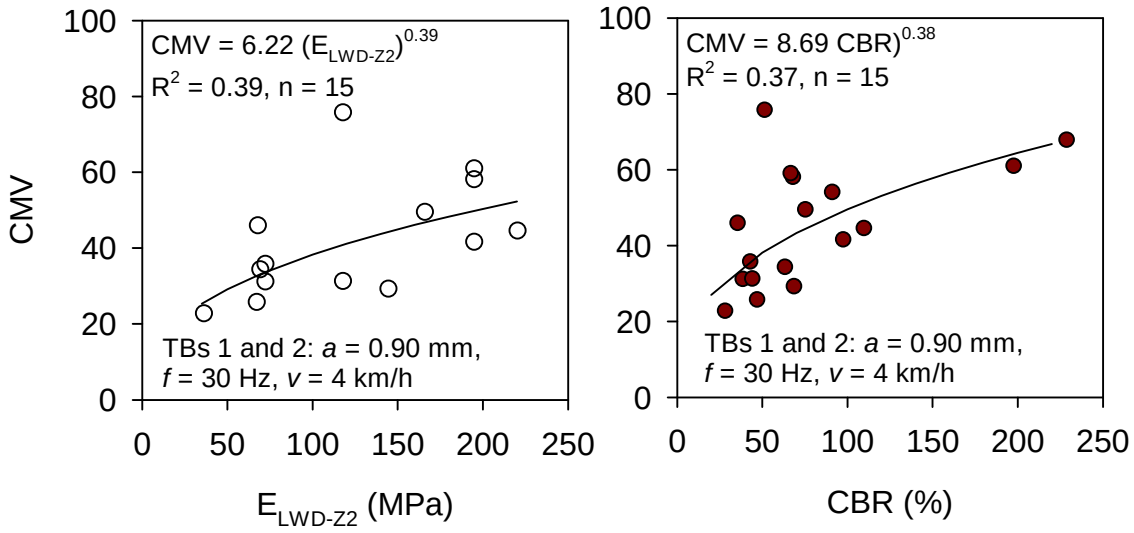

Figure 83. Regression analysis between CMV (a = 0.90 mm, f = 30 Hz, and v = 4 km/h) and Point-MVs combining data from different test beds

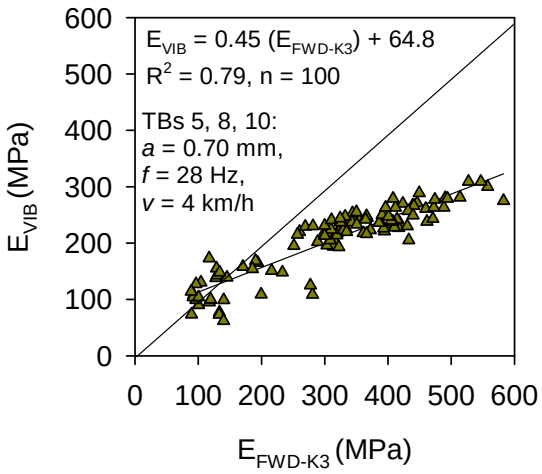

Figure 84. Regression analysis between E_{VIB} (*a* = 0.70 mm, *f* = 28 Hz, and *v* = 4 km/h) and Point-MVs combining data from different test beds

CORRELATIONS BETWEEN IN-SITU POINT MEASUREMENTS

Several different in-situ test methods were employed in this field study to determine elastic modulus, dry unit weight, and moisture content properties of the embankment subgrade and base materials. Although different in-situ test devices measure a similar property, it is important to understand how measurements from different in-situ test devices correlate with each other. This section presents relationships between modulus, dry unit weight, and moisture content measurements obtained from different test devices.

Five different test devices were used to determine elastic modulus: (a) 200 mm Zorn LWD; (b) 300 mm Zorn LWD; (c) BCD; (d) KUAB FWD; and (e) static PLT. Regression relationships between modulus measurements obtained from these five different devices are presented in Figure 85. Relationship between 200 mm and 300 mm LWD measurements indicated that E_{LWD-Z2} measurements are on average 1.3 times greater than E_{LWD-Z3} measurements. The measurements are in line with similar relationships documented by Vennapusa and White (2009). Possible reasons for this difference in modulus between E_{LWD-Z2} and E_{LWD-Z3} measurements are:

1. influence of plate diameters on E_{LWD} – decreasing plate diameter causes an increase in E_{LWD}.
2. differences is measurement influence depths between the two different plate diameters – influence depth is generally assumed to be approximately 1 to 1.5 times the plate diameter.
3. differences in applied contact stresses – applied contact stress for the 200 mm LWD = 0.2 MPa while the applied contact stress for 300 mm plate LWD = 0.1 MPa. Increasing applied contact stresses result in higher E_{LWD} values for granular materials (see Vennapusa and White 2009).

Relationship between FWD and LWD indicated that E_{FWD-K3} is on average about 3.4 times greater than E_{LWD-Z3} measurements. Possible reasons for this difference are:

1. differences in type and location of deflection measurement sensors – KUAB FWD uses geophone sensors placed on the ground through a hole at the center of the plate while Zorn LWD uses accelerometer sensor within the plate to measure deflections. Based on extensive field measurements, Vennapusa and White (2009) concluded that LWD devices that use accelerometers that measure deflection of the plate are expected to measure larger deflections compared to devices that measure deflections on the ground with a geophone.
2. differences in applied contact stresses – applied contact stress for the 300 mm FWD = 0.6 to 1.2 MPa while the applied contact stress for the 300 mm plate LWD = 0.1 MPa.

Relationships between $E_{LWD\text{-}Z3}$ vs. E_{BCD}, and $E_{FWD\text{-}K3}$ vs. E_{V1} and E_{V2} produced weak correlations (R^2 = 0.10 to 0.13). Primary reason for weak correlations between $E_{LWD\text{-}Z3}$ and E_{BCD} is attributed to the difference in the applied contact stresses. According to Briaud et al. (2006), E_{BCD} is determined using a minimum applied contact stress of about 0.01 MPa while the applied contact stress for the 300 mm plate LWD is about 10 times higher (0.1 MPa). Weak correlations between $E_{FWD\text{-}K3}$ and E_{V1} or E_{V2} is in part attributed to the limited number of measurements (n = 23) and the limited measurement range over which the tests were performed (all the tests were performed on very stiff material E_{V1} > 250 MPa).

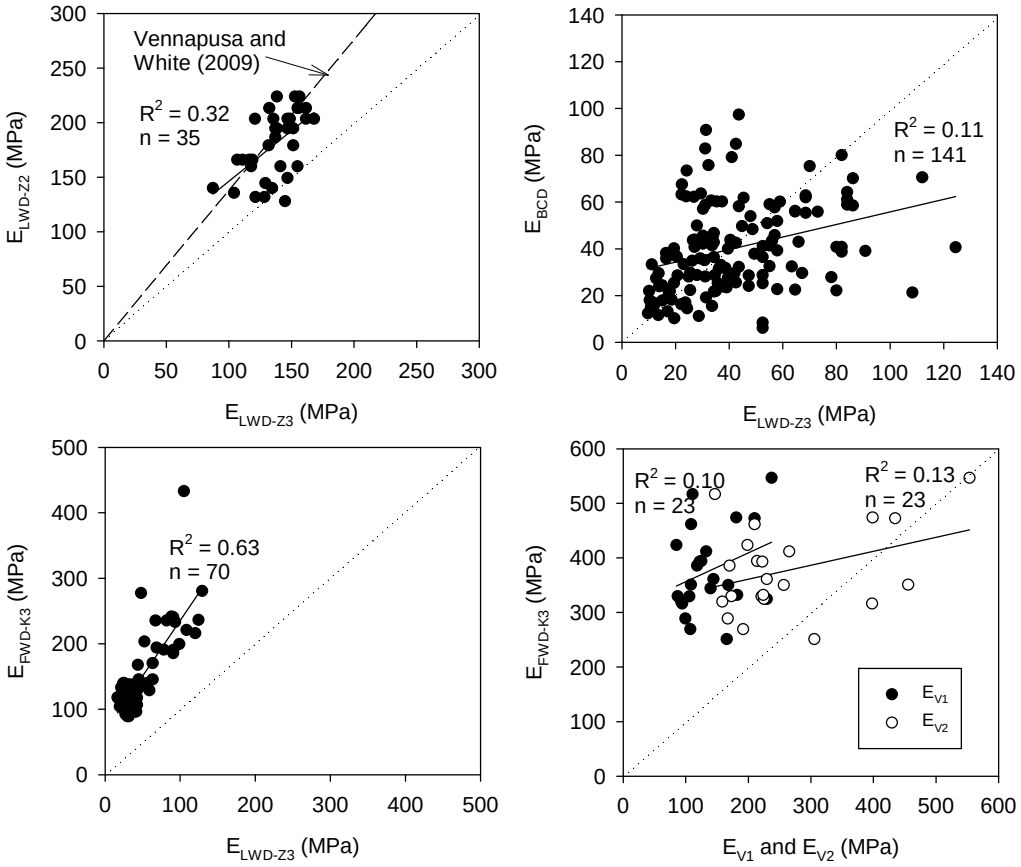

Figure 85. Correlations between modulus measurements obtained from different in-situ test devices used in this study

Three different test devices were used to determine dry unit weight (γ_d) and moisture content (w): (a) Troxler nuclear gauge; (b) Humboldt nuclear gauge; and (c) Transtech's soil density gauge. Regression relationships between dry unit weight and moisture measurements obtained from these three different devices are presented in Figure 86 and Figure 87, respectively.

Relationship between $\gamma_{d(H)}$ and $\gamma_{d(T)}$ produced strong correlation with $R^2 = 0.73$. However, on average the $\gamma_{d(T)}$ measurements were about 1.04 times greater than $\gamma_{d(H)}$ measurements. Relationship between $w_{(H)}$ and $w_{(T)}$ yielded weak correlation with $R^2 = 0.10$. On average the $w_{(H)}$ measurements were about 1.7 times greater than $w_{(T)}$ measurements.

Relationship between $\gamma_{d(H)}$ and $\gamma_{d(SDG)}$ produced weak correlation with $R^2 = 0.41$. On average the $\gamma_{d(SDG)}$ measurements were about 1.02 times greater than $\gamma_{d(H)}$ measurements. No statistically significant relationship was identified between $w_{(H)}$ and $w_{(SDG)}$. Relationship between $\gamma_{d(SDG)}$ and $\gamma_{d(T)}$ also produced a weak correlation with $R^2 = 0.27$. However, the measurements were scattered around the line of equality. Relationship between $w_{(H)}$ and $w_{(T)}$ similarly produced weak correlation with $R^2 = 0.10$. On average the $w_{(SDG)}$ measurements were about 1.2 times greater than $w_{(T)}$ measurements.

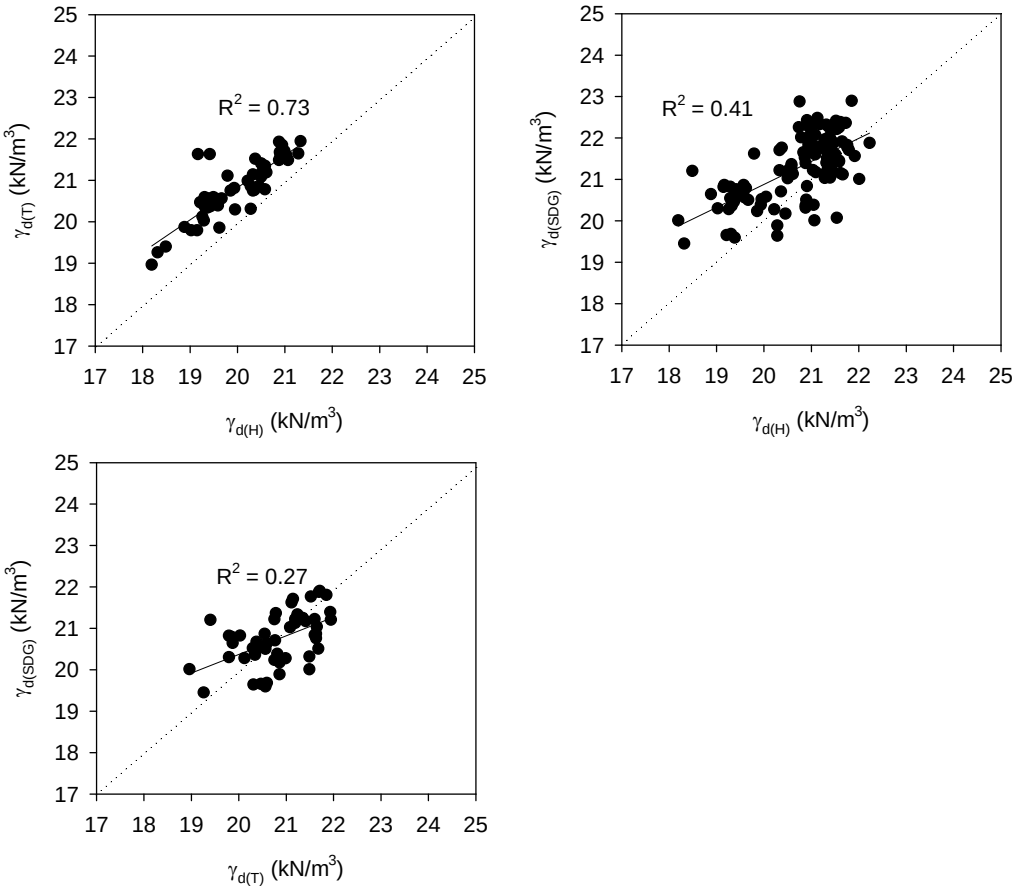

Figure 86. Correlations between density measurements obtained from in-situ test devices used in this study

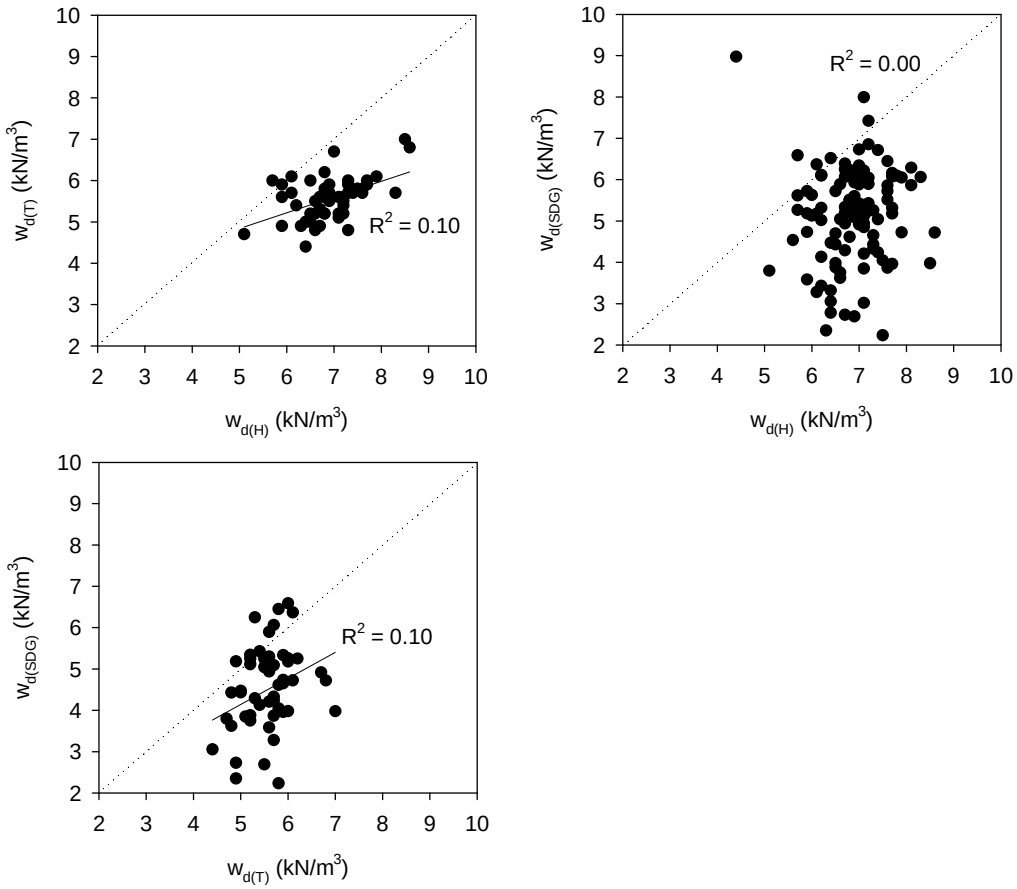

Figure 87. Correlations between moisture content measurements obtained from in-situ test devices used in this study

FIELD DEMONSTRATION – OPEN HOUSE

An open house was conducted on 05/21/2009 as part of this field investigation which included dissemination of results from previous IC field studies and results from the current field study as part of a presentation. Demonstration of the two IC rollers, a tour of the Iowa State University geotechnical mobile lab with several laboratory and in-situ testing methods were conducted at the project location. About 50 people attended the open house including New York DOT, contractor, and roller manufacturer personnel. Photographs from the open house are presented in Figure 88. Some of the attendees operated the IC rollers and received hands-on-experience.

Figure 88. Photographs from open house on the project site

SUMMARY AND CONCLUSIONS

Results from a field study conducted on the US219 project in Springville, NY from May 17–21, 2009 are presented in this report. The project involved evaluating Caterpillar CS-683 and Bomag BW213-DH IC rollers by comparing the IC-MVs with various in-situ Point-MVs (i.e., LWD, FWD, PLT, DCP, BCD, NG, and SDG). A total of 10 test beds involving calibration and production compaction operations were constructed. IC-MVs maps on the on-board computer display unit were used in selecting field QA test locations. Several NYDOT and contractor personnel received hands-on experience in operating the IC rollers and various in-situ testing methods to evaluate compaction quality of earthwork materials. On one test bed with production operations, the contractor utilized the on-board display to obtain uniform pass coverage over the test bed area.

Results obtained from various test beds contributed to developing empirical relationships between IC-MVs and various in-situ test measurements. Empirical correlations between IC-MVs and different Point-MVs generally showed weak correlations when evaluated independently for each test bed. The narrow range of measurements over which the measurements were obtained was the key factor contributing to weak correlations. When data are combined for site-wide correlations with a wide measurement range, the correlations improve. IC-MVs generally correlated better with modulus/stiffness and CBR Point MVs than with dry density Point MVs. Correlations between IC-MVs and $E_{FWD\text{-}K3}$ Point MVs strongest correlation coefficients.

Performance of AFC compaction operations in comparison with conventional operations using the Bomag IC roller were evaluated as part of this study. Following are some key observations:

- *TB 3:* Amplitude measurements along the test strip indicated that when E_{VIB} < target E_{VIB}, the amplitude is at the a_{max}, and the amplitude is effectively reduced to 0.60 mm when E_{VIB} > target E_{VIB}. However, roller jumping was still observed at several short segmented sections along the test strip.
- *TB 5:* In this test bed two side-by-side lanes were compacted in manual a = 0.70 mm mode and AFC mode (a_{max} = 1.10 mm, target E_{VIB} = 150 MPa). The average E_{VIB} values obtained in AFC mode (a = 1.0 mm on average) are on-average about 1.3 times higher than the average E_{VIB} values obtained in manual mode operation. Average $E_{LWD\text{-}Z3}$ values in the lane compacted in AFC mode were about 1.6 times higher than in the lane compacted in manual mode. However, the average relative compaction values, average $E_{FWD\text{-}K3}$ values, and CBR values are similar for the two lanes after pass 8. Although the E_{VIB} values showed low COV with AFC operations compared to COV with manual mode operations, Point-MVs did not show considerable difference in the COV values. More testing is recommended in future projects with different a_{max} and target E_{VIB} settings to further evaluate AFC mode compaction operations with variable subsurface conditions.
- *TB 10:* In this test bed, deep trenches were excavated and compacted in side-by-side lanes using manual and AFC settings. The compaction curves of average dry density, modulus, and CBR measurements generally increased with increasing passes up to pass 8 in the trench areas. However, no significant difference was measured in terms of density of the material at the surface in the trenches between lanes compacted using AFC mode and manual mode (91% relative compaction in the 1m trench and 88 to 89% relative

compaction in the 2m trench). Similarly, $E_{LWD\text{-}Z3}$ and CBR_{300} measurements did not demonstrate considerable differences between AFC mode and manual mode compacted lanes. Analysis of incremental increases in CBR with depth relative to pass 1 in the 2 m wide x 1 m deep trench did not present considerable differences between AFC mode and manual mode compaction.

To study the influence of amplitude on MDP_{40} IC-MVs, two side-by-side gravel subbase lanes were compacted in static and low amplitude modes. The average MDP_{40} values obtained in static mode are on average about 1.1 times higher than the MDP_{40} values obtained in low amplitude mode. The average $E_{LWD\text{-}Z3}$ values obtained after pass 8 in the lane compacted in static mode is about 1.6 times higher than in the lane compacted in low amplitude mode. However, the average relative compaction and CBR values are similar for the two lanes after pass 8.

Geostatistical analysis methods were utilized to analyze spatially referenced IC-MV data to assess spatial non-uniformity of compacted fill materials. Some IC-MV data sets showed nested semivariogram structures with short-range and long-range components. It is possible that the long-range components are because of differences in the underlying support conditions (i.e., shredded tire fill at depths < 1 m) while the short-range components are a result of spatial variations of soil properties close to surface. Additional studies are needed to better understand this finding.

Five different test devices were used to determine elastic modulus: (a) 200 mm Zorn LWD; (b) 300 mm Zorn LWD; (c) BCD; (d) KUAB FWD; and (e) static PLT. Regression relationships between modulus measurements obtained from these five different devices are presented in this report. Some key findings from these relationships are as follows:

- Relationships between 200 mm and 300 mm LWD measurements indicated that $E_{LWD\text{-}Z2}$ measurements are on average 1.3 times greater than $E_{LWD\text{-}Z3}$ measurements. Differences in modulus between $E_{LWD\text{-}Z2}$ and $E_{LWD\text{-}Z3}$ measurements are attributed to: (a) different plate diameters; (b) differences in measurement influence depths; and (c) differences in applied contact stresses.
- Relationship between FWD and LWD indicated that $E_{FWD\text{-}K3}$ is on average about 3.4 times greater than $E_{LWD\text{-}Z3}$ measurements. Differences are attributed to: (a) type and location of deflection measurement sensors; and (b) applied contact stresses.
- Relationships between $E_{LWD\text{-}Z3}$ vs. E_{BCD}, and $E_{FWD\text{-}K3}$ vs. E_{V1} and E_{V2} produced weak correlations (R^2 = 0.10 to 0.13). Weak correlations between $E_{LWD\text{-}Z3}$ and E_{BCD} are attributed to the difference in the applied contact stresses. E_{LWD} is determined using contact stresses that are about10 times higher than contact stresses applied to determine E_{BCD}. Weak correlations between $E_{FWD\text{-}K3}$ and E_{V1} or E_{V2} are in part attributed to the limited number of measurements (n = 23) and the limited measurement range over which the tests were performed (all the tests were performed on very stiff material E_{V1} > 250 MPa).

Three different test devices were used to determine dry unit weight and moisture content: (a) Troxler nuclear gauge; (b) Humboldt nuclear gauge; and (c) Transtech's soil density gauge.

Regression relationships between dry unit weight and moisture measurements obtained from these three different devices are presented in this report. Some key findings are as follows:

- Relationship between $\gamma_{d(H)}$ and $\gamma_{d(T)}$ produced strong correlation with $R^2 = 0.73$. However, on average the $\gamma_{d(T)}$ measurements were about 1.04 times greater than $\gamma_{d(H)}$ measurements. Relationship between $w_{(H)}$ and $w_{(T)}$ yielded weak correlation with $R^2 = 0.10$. On average the $w_{(H)}$ measurements were about 1.7 times greater than $w_{(T)}$ measurements.
- Relationship between $\gamma_{d(H)}$ and $\gamma_{d(SDG)}$ produced weak correlation with $R^2 = 0.41$. On average the $\gamma_{d(SDG)}$ measurements were about 1.02 times greater than $\gamma_{d(H)}$ measurements. No statistically significant relationship was identified between $w_{(H)}$ and $w_{(SDG)}$.
- Relationship between $\gamma_{d(SDG)}$ and $\gamma_{d(T)}$ also produced a weak correlation with $R^2 = 0.27$. However, the measurements were scattered around the line of equality. Relationship between $w_{(H)}$ and $w_{(T)}$ similarly produced weak correlation with $R^2 = 0.10$. On average the $w_{(SDG)}$ measurements were about 1.2 times greater than $w_{(T)}$ measurements.

The results from this study provided new information that demonstrates the potential advantages of implementing IC roller operations and various in-situ testing methods into earthwork construction QC/QA practice. Additional studies are needed to evaluate options for implementing these technologies into specifications.

REFERENCES

ASTM D6951. (2003). "Standard test method for use of the dynamic cone penetrometer in shallow pavement application." American Standards for Testing Methods (ASTM), West Conshohocken, Pennsylvania.

Briaud, J-L., Li, Y., Rhee, K. (2006). "BCD: A soil modulus device for compaction control." *J. of Geotech. and Geoenv. Engrg.,* ASCE, 132(1), 108-115.

Adam, D., and Kopf, F. (2004). "Operational devices for compacting optimization and quality control (Continuous Compaction Control and Light Falling Wieght Device)," *Proc., Intl. Sem. on Geotechnics in Pavement and Railway Design and Construction.,* December, Athens, Greece.

Brandl, H., and Adam, D. (1997). "Sophisticated continuous compaction control of soils and granular materials." *Proc. 14th Intl. Conf. Soil Mech. and Found. Engrg.*, Hamburg, Germany, 1–6.

Chilès, J-P., and Delfiner, P. (1999). *Geostatistics – Modeling Spatial Uncertainty.* John Wiley & Sons, Inc., New York.

Clark, I., and Harper, W. (2002). *Practical geostatistics 2000*. 3rd reprint, Ecosse North America Llc, Columbus, Ohio.

Floss, R., Gruber, N., Obermayer, J. (1983). "A dynamical test method for continuous compaction control." *Proc. 8th European Conf. on Soil Mech. and Found. Engg,* H.G. Rathmayer and K. Saari, eds., May, Helsinki, 25-30.

Hertz, H. (1895). *Über die Berührung fester elasticscher Körper*, Gesammelte Werke, Bd. 1. Leipzig.

Isaaks, E. H., and Srivastava, R. M. (1989). *An introduction to applied geostatistics*. Oxford University Press, New York.

Kröber, W. (1988). "Untersuchung der dynamischen Vorgänge bei der Vibrationsverdichtung von Böden," Ph.D. Dissertation, Schriftenreihe, Heft 11, Lehrstuhl und Prüfamt für Grundbau, Bodenmechanik und Felsmechanik der Technischen Universität München (in German).

Kröber, W., Floss, R., Wallrath, W., (2001). "Dynamic soil stiffness as quality criterion for soil compaction." *Geotechnics for Roads, Rail Tracks and Earth Structures*, A.A. Balkema Publishers, Lisse / Abingdon / Exton (Pa) / Tokyo.

Lundberg, G. (1939). *Elastische Berührung zweier Halbräume, Forschung, auf dem Gebiete des Ingenieurwesens*, Band 10, Göteborg, 201–211.

NCHRP. (2009). *Intelligent soil compaction systems – NCHRP 21-09*, National Cooperative Highway Research Program, Transportation Research Board, Washington, D.C. (in print).

Samaras, A.A., Lamm, R., Treiterer, J. (1991). "Application of continuous dynamic compaction control for earthworks in railroad construction." *Transp. Res. Rec.,* 1309, Journal of the Transportation Research Board, Washington, D.C., 42–46.

Sandström, Å. (1994). *Numerical simulation of a vibratory roller on cohesionless soil,* Internal Report, Geodynamik, Stockholm, Sweden.

Sandström Å., and Pettersson, C. B., (2004). "Intelligent systems for QA/QC in soil compaction", *Proc. TRB 2004 Annual Meeting* (CD-ROM), Transportation Research Board, Washington, D. C.

Thompson, M., and White, D. (2008). "Estimating compaction of cohesive soils from machine drive power." *J. of Geotech. and Geoenv. Engrg.,* ASCE, 134(12), 1771-1777.

Vennapusa, P., White, D.J., and Gieselman, H. (2009). "Influence of support conditions on roller-integrated machine drive power measurements for granular base.", *Intl. Found. Cong. and Equip. Expo (IFCEE) 2009*, 15-19 March, Orlando, Florida.

Vennapusa, P., and White, D. J. (2009). "Comparison of light weight deflectometer measurements for pavement foundation materials." *Geotech.Test. J.*, ASTM, 32(3), 239-251.

Vennapusa, P., White, D.J., Morris, M. (2010). "Geostatistical analysis for spatially referenced roller-integrated compaction measurements, *J. of Geotech. and Geoenv. Engrg.,* ASCE, (in print).

White, D. J., Jaselskis, E., Schaefer, V., Cackler, T. (2005). "Real-time compaction monitoring in cohesive soils from machine response." *Transp. Res. Rec., 1936*, Journal of the Transportation Research Board, Washington D.C., 173–180.

White, D.J., and Thompson, M. (2008). Relationships between in situ and roller-integrated compaction measurements for granular soils. *J. of Geotech. and Geoenv. Engrg.,* ASCE, 134(2), 1763-1770.

White, D., Thopmson, M., Vennapusa, P., and Siekmeier, J. (2008). "Implementing intelligent compaction specifications on Minnesota TH 64: Synopsis of measurement values, data management, and geostatistical analysis." *Transp. Res. Rec.,* 2045, Journal of the Transportation Research Board, Washington, D.C, 1-9.

Zorn, G. (2003). *Operating manual: Light drop-weight tester ZFG2000*, Zorn Stendal, Germany.

APPENDIX

TEST BED SUMMARY SHEETS AND EXPERIMENTAL PLAN

Accelerated Implementation of IC Technology for Embankment Subgrade Soils, Aggregate Base, and Asphalt Pavement Materials

Iowa State University Research Team Field Testing, U219, Springville, New York

Test Bed # 1 (05/17/2009)

Photos

Description: The test bed consisted of compacted embankment granular subgrade material with plan dimensions of approximately 18 m x 200 m. Reportedly, the embankment material was underlain by rubber tires at depths < 1m below the grade. The area was mapped in eight roller lanes using Caterpillar IC roller for three passes. MDP_{40} and CMV measurement values were obtained from the IC roller. Nominal machine settings during passes are provided below. In-situ point measurements (E_{LWD-Z2}, DCP-CBR) were performed at 10 test locations selected using the IC-MV map. The objectives of testing on this test bed were to obtain correlations between IC measurement values (IC-MVs) MDP_{40} and CMV and in-situ point measurements.

Machine Nominal settings:
Pass 1 (static) – v = 4 km/h
Pass 2 (low amp) – a = 0.90 mm, f = 30 Hz, v = 4 km/h
Pass 3 (low amp) – a = 0.90 mm, f = 30 Hz, v = 4 km/h

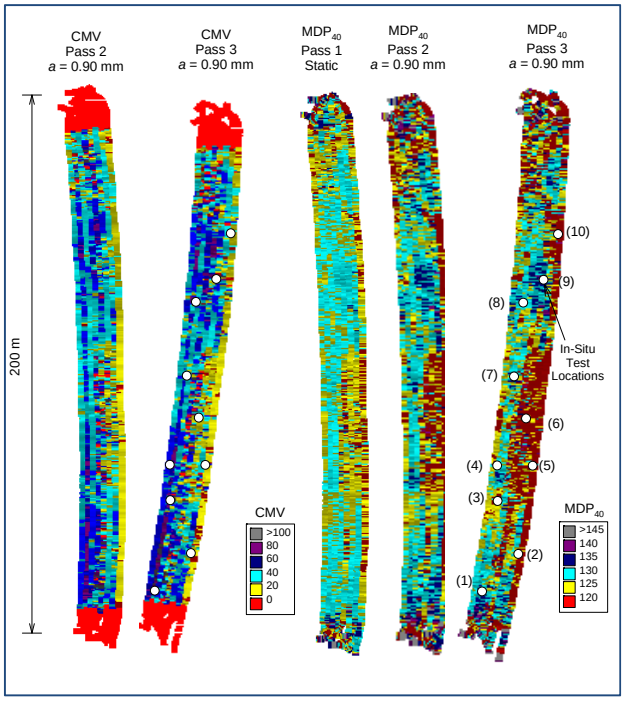

Spatial maps of IC-MVs (MDP_{40} and CMV) for passes 1, 2, and 3, and locations of in-situ point measurements

Caterpillar roller used on the test bed

Photograph of the test bed

In-situ testing methods used on the test bed: LWD (left) and DCP (right)

Accelerated Implementation of IC Technology for Embankment Subgrade Soils, Aggregate Base, and Asphalt Pavement Materials

Iowa State University Research Team Field Testing, U219, Springville, New York

Test Bed # 2 (05/18/2009)

Photos

Description: The test bed consisted of compacted embankment granular subgrade material with plan dimensions of approximately 18 m x 71 m. The test bed was connected to the south end of TB1. Reportedly, the embankment material was underlain by rubber tires at depths < 1m below the grade in the northern half of the test bed. The area was mapped in eight roller lanes using Caterpillar IC roller for two passes. MDP_{40} and CMV measurement values were obtained from the IC roller. Nominal machine settings during passes are provided below. In-situ point measurements (E_{LWD-Z2}, DCP-CBR, $w_{(H)}$, $w_{(SDG)}$, $\gamma_{d(H)}$, $\gamma_{d(SDG)}$) were performed at 7 test locations selected using the IC-MV map. The objectives of testing on this test bed were to obtain correlations between IC measurement values (IC-MVs) MDP_{40} and CMV and in-situ point measurements.

Machine Nominal settings:
Pass 1 (static) – v = 4 km/h
Pass 2 (low amp) – a = 0.90 mm, f = 30 Hz, v = 4 km/h

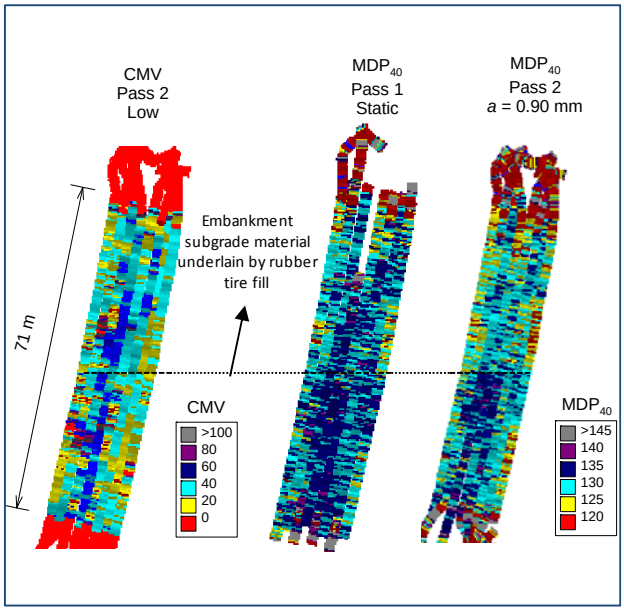

Spatial maps of IC-MVs (MDP_{40} and CMV) for passes 1 and 2

Caterpillar roller used on the test bed

In-situ testing methods used on the test bed: Humboldt NG (top left), Transtech's SDG (top right), LWD (bottom left) and DCP (bottom right)

Accelerated Implementation of IC Technology for Embankment Subgrade Soils, Aggregate Base, and Asphalt Pavement Materials

Iowa State University Research Team Field Testing, U219, Springville, New York

Test Bed # 3 (05/18/2009)

Photos

Description: The test bed consisted of compacted embankment granular subgrade material with plan dimensions of approximately 10 m x 105 m. First, the area was mapped in a manual low amplitude mode for one pass and then in an automatic feedback control (AFC) mode for one pass. In-situ point measurements (E_{LWD-Z2} and E_{LWD-Z3}) were performed along lane 3 at 62 test locations after pass 2. Following testing, Lane 3 for two more passes in different amplitude settings. The objectives of testing on this test bed were to evaluate influence of amplitude on E_{VIB} values and obtain correlations between E_{VIB} and in-situ point measurements.

Machine Nominal settings:
Pass 1 (Manual) – a = 0.70 mm, f = 28 Hz, v = 4 km/h
Pass 2 (Auto) – a_{max} = 1.90 mm, f = 28 Hz, v = 4 km/h
Pass 3 (Manual) – a = 0.70 mm, f = 28 Hz, v = 4 km/h
Pass 4 (Manual) – a = 1.50 mm, f = 28 Hz, v = 4 km/h

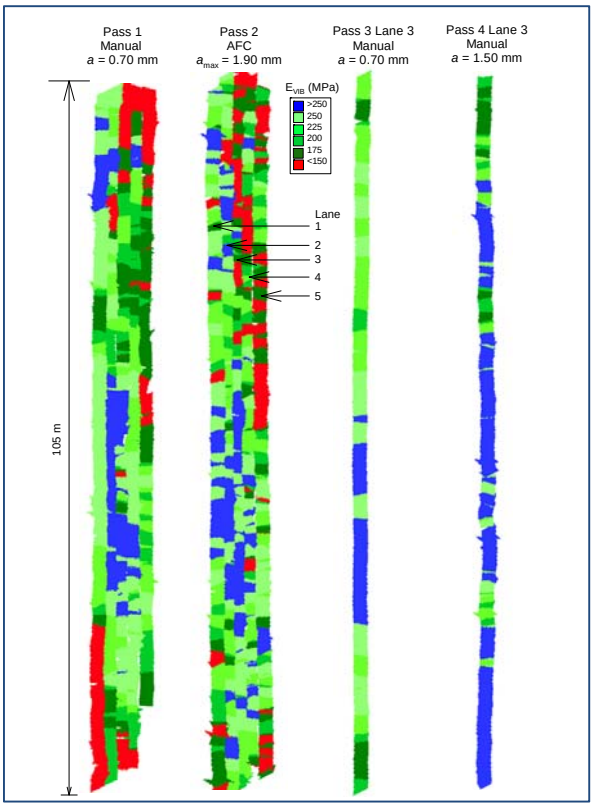

Spatial maps of IC-MVs (E_{VIB}) for different passes

Bomag roller used on the test bed

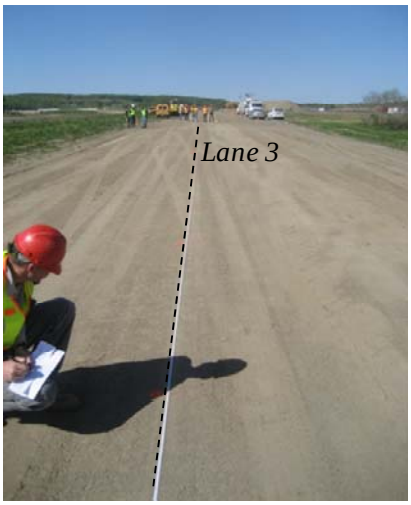

In-situ testing methods used on the test bed: 200-mm (left) and 300-mm (right) diameter LWDs

Accelerated Implementation of IC Technology for Embankment Subgrade Soils, Aggregate Base, and Asphalt Pavement Materials

Iowa State University Research Team Field Testing, U219, Springville, New York

Test Beds # 4 and 5 (05/18/2009)

Description: TBs 4 and 5 consisted of approximately 200 to 250 mm thick loosely placed aggregate subbase material over geofabric partially placed on top of TBs 1 and 2. The area was compacted in six roller lanes for eight roller passes. Lanes 1, 2, and 3 were compacted using Caterpillar IC roller and Lanes 4, 5, and 6 were compacted using Bomag IC roller using different amplitude settings. Nominal machine settings during compaction passes are provided below. In-situ point measurements ($E_{LWD\text{-}Z3}$, E_{BCD}, DCP-CBR, $w_{(H)}$, $w_{(SDG)}$, $w_{(T)}$, $\gamma_{d(H)}$, $\gamma_{d(SDG)}$, and $\gamma_{d(T)}$) were performed at 13 test locations along lanes 2, 3, 4, and 5 at passes 0 and 8. The objectives of testing on this test bed were to obtain IC-MV compaction curves and correlations between IC measurement values (IC-MVs) MDP_{40}, CMV, E_{VIB} and in-situ point measurements.

Machine Nominal settings:

Test Bed 4 (Caterpillar):
Lane 2: Pass 1 to 8 (static) – v = 4 km/h
Lane 3: Pass 1 to 8 (low amp) – a = 0.90 mm, f = 30 Hz, v = 4 km/h

Test Bed 5 (Bomag):
Lane 4: Pass 1 to 8 (AFC mode) – a_{max} = 1.10 mm, E_{VIB} = 150 MPa, f = 28 Hz, v = 4 km/h
Lane 5: Pass 1 to 8 (low amp) – a = 0.70 mm, f = 28 Hz, v = 4 km/h

Photos

Caterpillar roller used on TB4

Bomag roller used on TB5

Accelerated Implementation of IC Technology for Embankment Subgrade Soils, Aggregate Base, and Asphalt Pavement Materials

Iowa State University Research Team Field Testing, U219, Springville, New York

Construction/Testing Photos – Test Beds # 4 and 5 (05/18/2009)

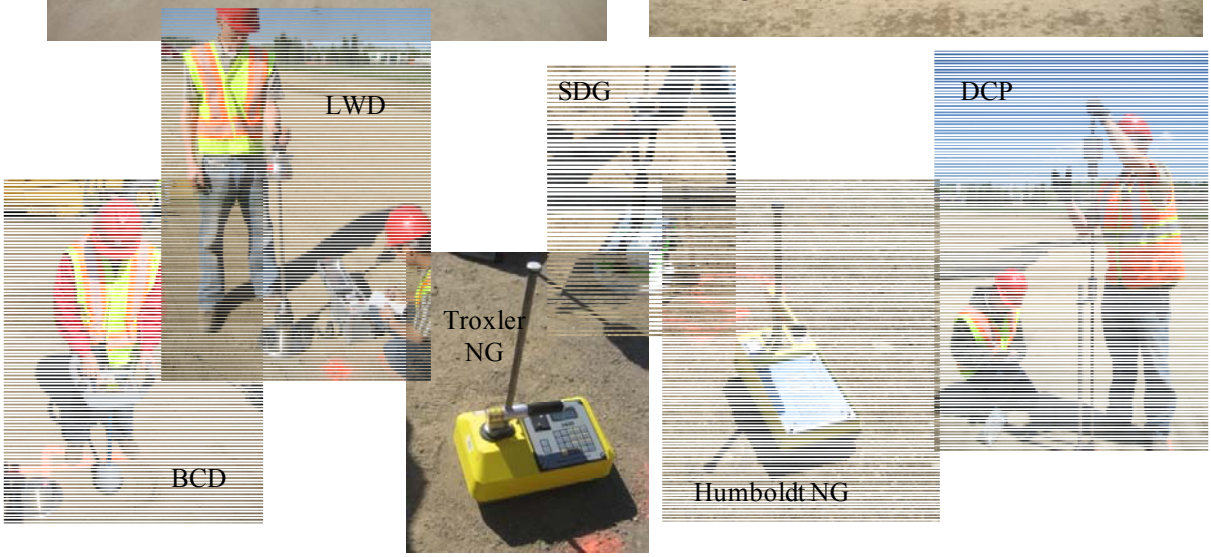

In-situ testing methods used on the test bed

Accelerated Implementation of IC Technology for Embankment Subgrade Soils, Aggregate Base, and Asphalt Pavement Materials

Iowa State University Research Team Field Testing, U219, Springville, New York

MDP_{40} and CMV spatial maps for different passes – Test Bed 4 (05/18 to 05/19/2009)

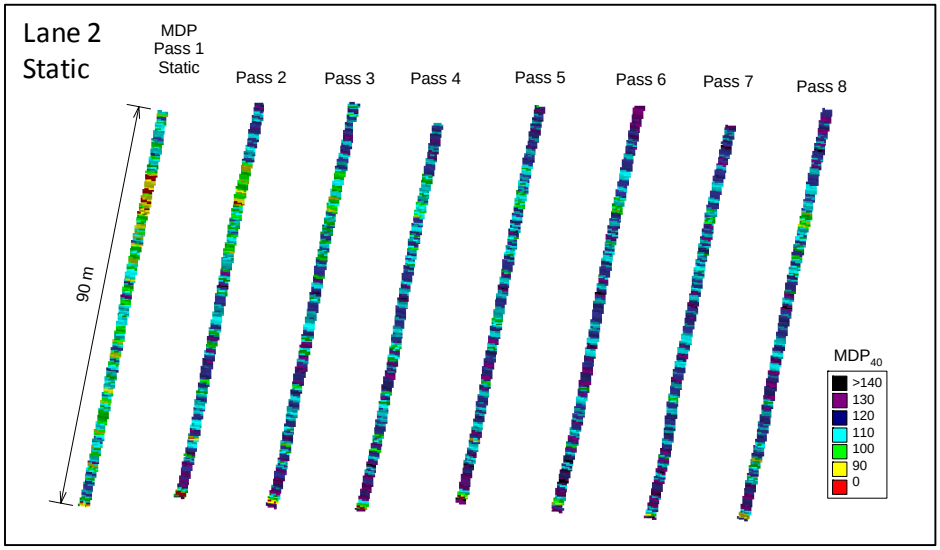

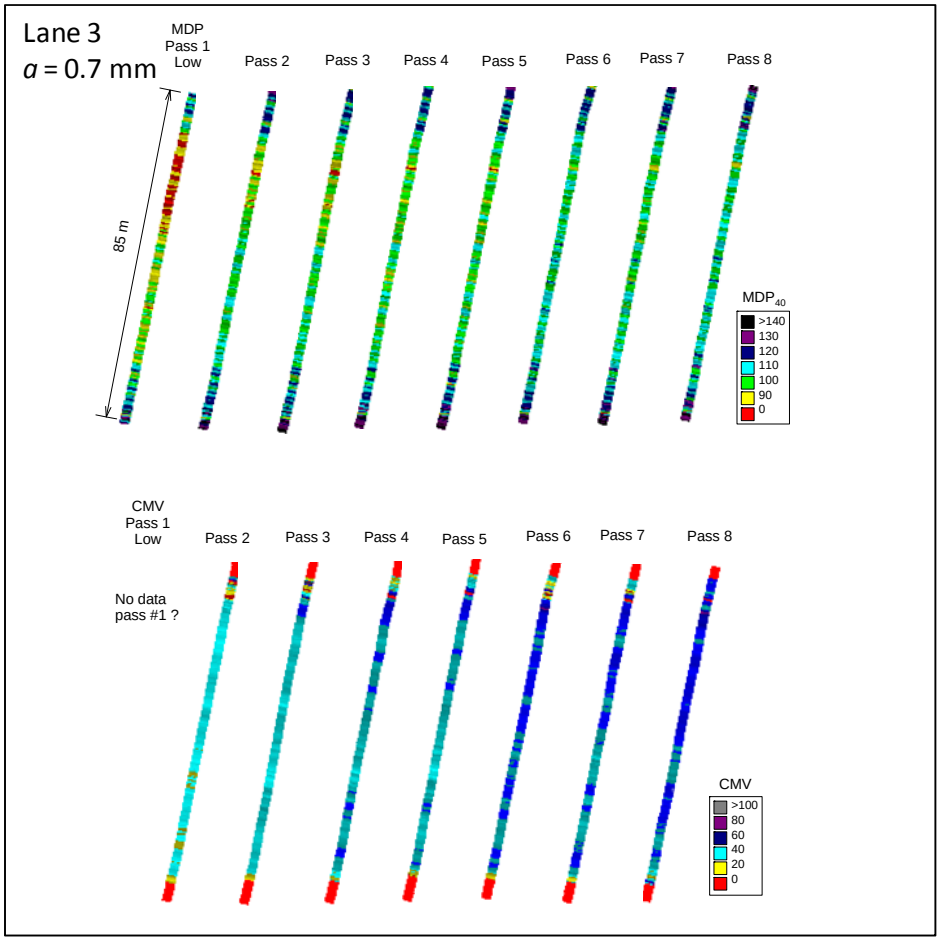

Accelerated Implementation of IC Technology for Embankment Subgrade Soils, Aggregate Base, and Asphalt Pavement Materials

Iowa State University Research Team Field Testing, U219, Springville, New York

E_{VIB} spatial maps for different passes – Test Bed 5 (05/18 to 05/19/2009)

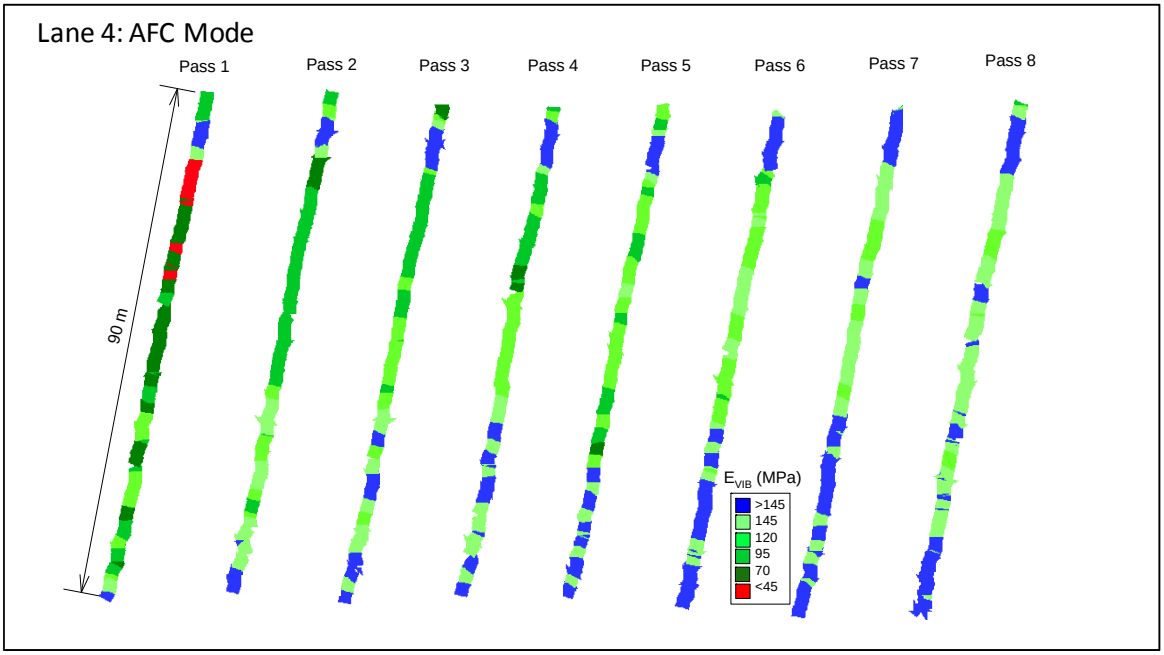

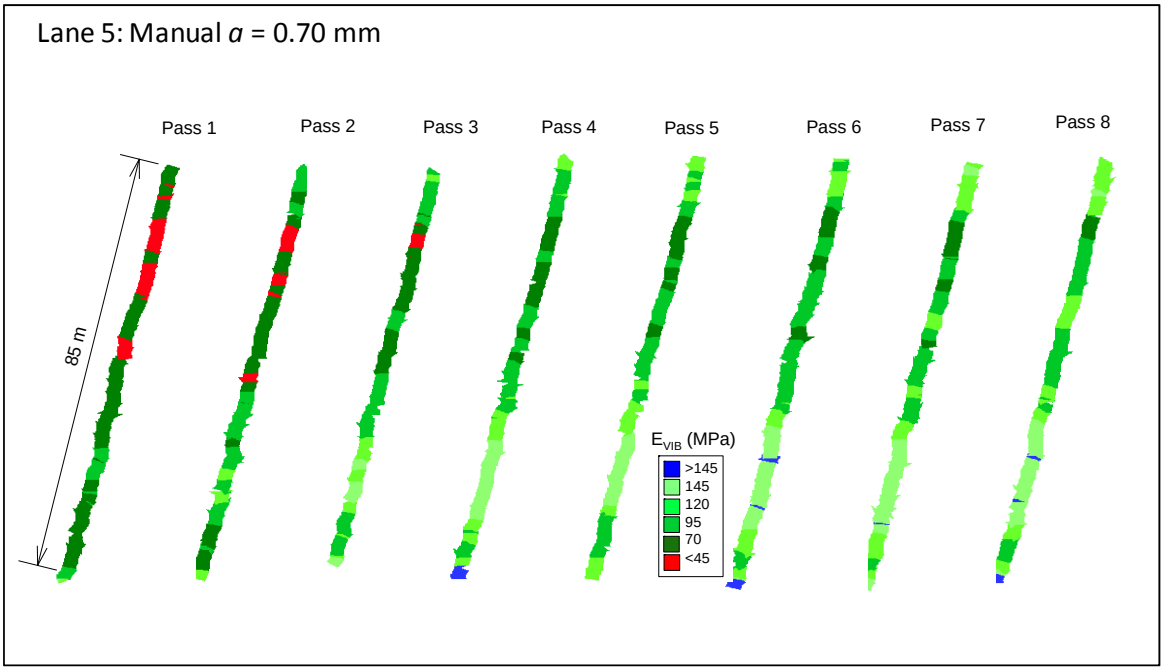

Accelerated Implementation of IC Technology for Embankment Subgrade Soils, Aggregate Base, and Asphalt Pavement Materials

Iowa State University Research Team Field Testing, U219, Springville, New York

Test Beds # 6 and 7 (05/19/2009)

Photos

Description: The test bed consisted of a production area with aggregate subbase material placed over geofabric on top of TB1 embankment material. The area was compacted using Caterpillar IC roller for two passes followed by four passes using Bomag IC roller. Nominal machine settings during compaction are provided below. After pass 6, some locations were selected for point measurements by NYDOT personnel using IC maps and were tested by ISU research team. Point measurements included E_{LWD-Z3}, E_{BCD}, DCP-CBR, $w_{(H)}$, and $\gamma_{d(H)}$. The objectives of testing on this test bed were to demonstrate the use of IC-MV maps to determine locations for testing for NYDOT personnel and obtain correlations between IC-MVs (CMV and MDP_{40}) and in-situ point measurements.

Machine Nominal settings:
Test Bed 6 (Caterpillar):
Pass 1, 2 (low amp) – a = 0.90 mm, f = 30 Hz, v = 4 km/h
Test Bed 7 (Bomag):
Pass 3 to 6 (low amp) – a = 0.70 mm, f = 28 Hz, v = 4 km/h

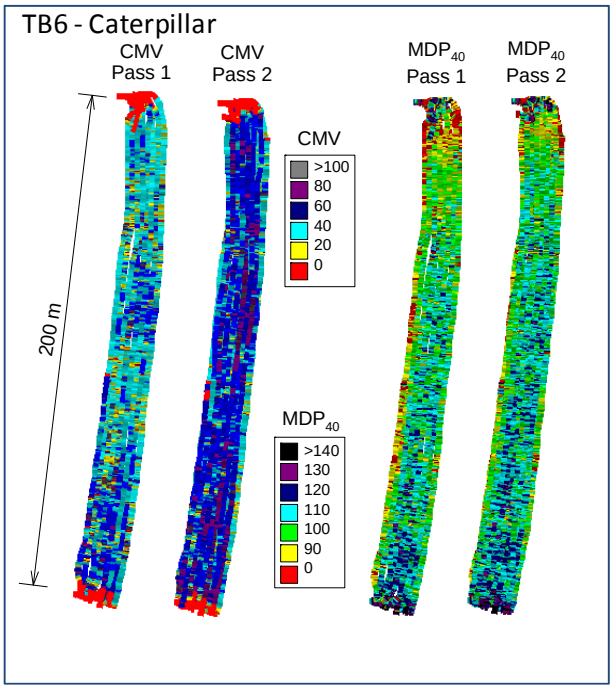

Spatial maps of IC-MVs (MDP_{40} and CMV) for passes 1 and 2

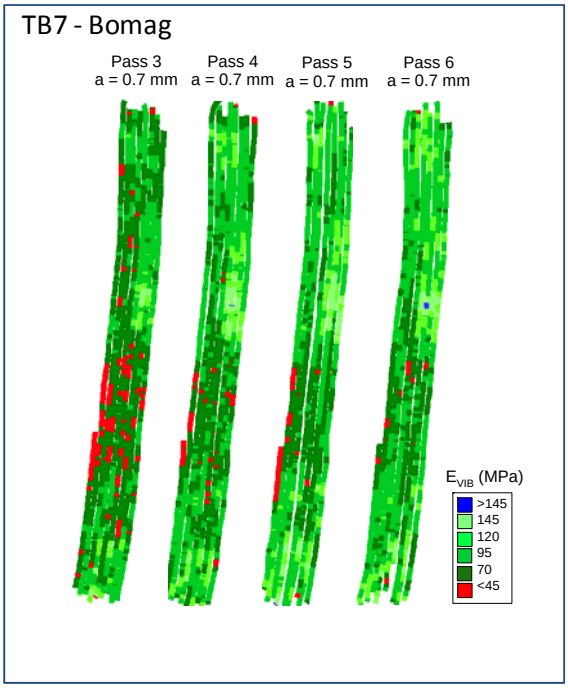

Spatial maps of E_{VIB} for passes 3 to 6

Accelerated Implementation of IC Technology for Embankment Subgrade Soils, Aggregate Base, and Asphalt Pavement Materials

Iowa State University Research Team Field Testing, U219, Springville, New York

Test Bed # 8 (05/19/2009)

Description: The test bed is located in the same area as TB 3 with compacted embankment granular subgrade material over plan dimensions of approximately 10 m x 100 m. The area was mapped in static and low amplitude settings. Just prior to mapping passes, FWD test measurements were obtained at 88 test locations and static plate load test measurements were obtained at 23 test locations along the testing lane. The objectives of testing on this test bed were to obtain correlations between IC-MVs (CMV and MDP_{40}) and in-situ point measurements.

Machine Nominal settings: (pass numbers continue from TB3

Pass 6 (low amp) – a = 0.90 mm, f = 30 Hz, v = 4 km/h

Pass 6 (static) – v = 4 km/h

KUAB FWD

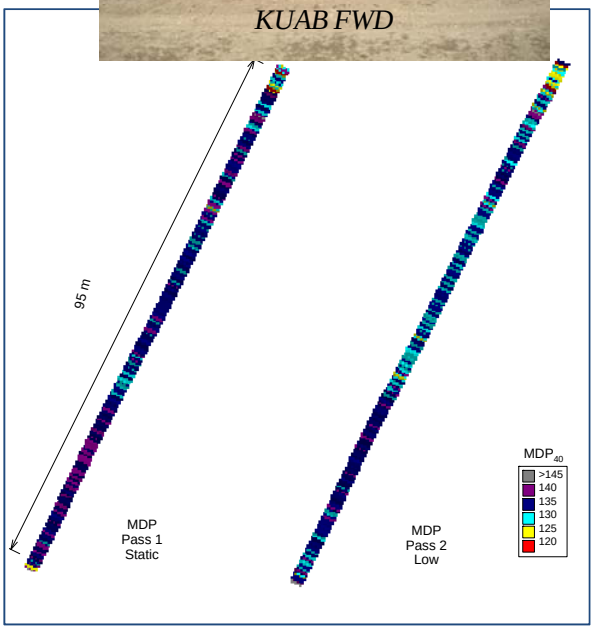

Spatial maps of MDP_{40} for passes 1 and 2

Photos

Caterpillar roller used on the test bed

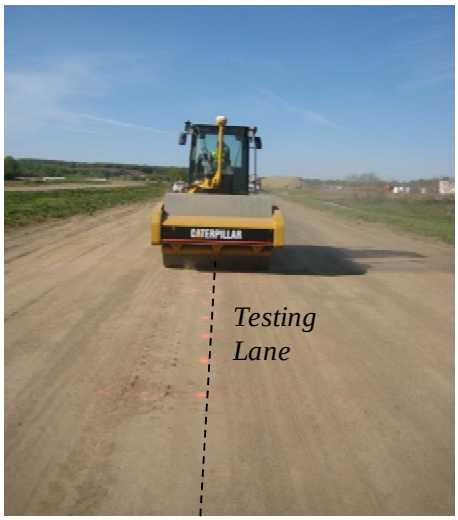

Static Plate Load Test

Accelerated Implementation of IC Technology for Embankment Subgrade Soils, Aggregate Base, and Asphalt Pavement Materials

Iowa State University Research Team Field Testing, U219, Springville, New York

Test Bed # 9 (05/19/2009)

Photos

Description: The test bed consisted of aggregate subbase material placed over geofabric on top of a compacted embankment layer. The area was compacted using Caterpillar IC roller by the Contractor personnel using low amplitude setting. The area was compacted in two different sections (TBs 9A and 9B). The dump trucks with fill material backed up to the test area, placed the fill, and returned, contributing to compaction of fill material to some extent. MDP_{40} and CMV maps after final pass are shown in the figures below. After final pass some locations were selected for $E_{LWD\text{-}Z3}$, E_{BCD}, DCP-CBR, $w_{(H)}$, and $\gamma_{d(H)}$ point measurements. The objectives of testing on this test bed were to provide hands-on experience to the Contractor and NYDOT personnel with IC technology, demonstrate the use of IC-MV maps to determine the locations for testing, and obtain correlations between IC-MVs (CMV and MDP_{40}) and in-situ point measurements.

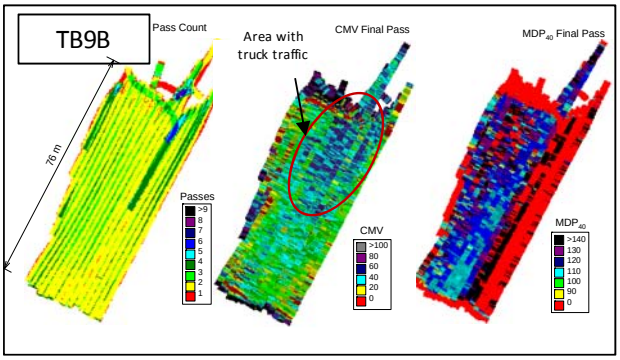

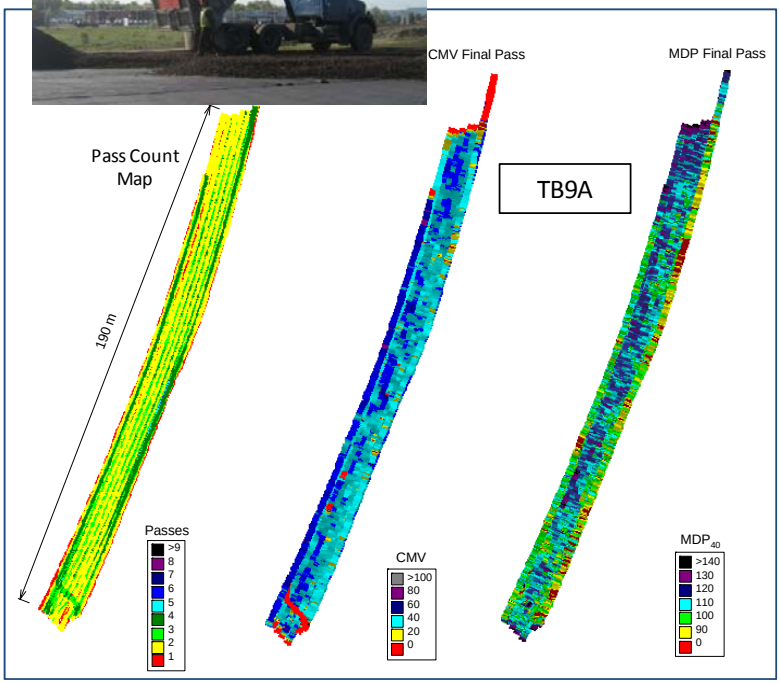

Spatial maps of IC-MVs (MDP_{40} and CMV) for final pass and pass count map

In-situ testing methods: DCP (top left), LWD (top right), Humboldt NG (bottom left), and BCD (bottom right)

Accelerated Implementation of IC Technology for Embankment Subgrade Soils, Aggregate Base, and Asphalt Pavement Materials

Iowa State University Research Team Field Testing, U219, Springville, New York

Test Bed # 10 (05/20/2009)

Photos

Description: The test bed consisted of embankment granular subgrade material with approximate plan dimensions as shown in the figure below. A 1-m wide x 1-m deep trench and a 2-m wide x 2-m trench were scarified using a backhoe to create a loose uncompacted layer of embankment fill material. Lane 1 was compacted using Caterpillar IC roller in low amplitude setting, lane 2 was compacted using Bomag IC roller in AFC mode, and lane 3 was compacted using Bomag IC roller in low amplitude setting. In-situ point measurements (DCP, LWD, NG, SDG,BCD, and FWD) were obtained after 0, 1, 2, 8, and 10 roller passes on each lane. 2-m deep DCP tests were conducted in the 2-m deep trench area. The objectives of testing on this test bed were to evaluate impact of lift thickness on IC roller values and compaction efficiency, better understand the compaction influence depth, evaluate impact of automatic feedback control (AFC) mode compaction for variable conditions, and obtain correlations between IC-MVs and point measurements.

Bomag and Caterpillar rollers used on the test bed

Plan View

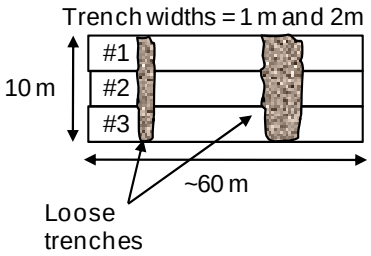

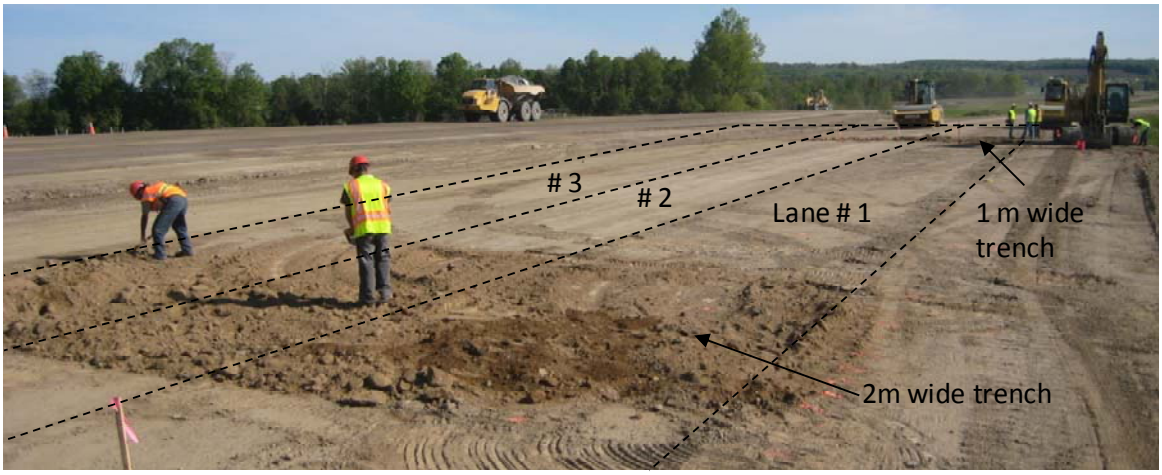

Accelerated Implementation of IC Technology for Embankment Subgrade Soils, Aggregate Base, and Asphalt Pavement Materials
US 219, Springville, NY – New York State Department of Transportation
[May 17-May 22, 2009]

THE TRANSTEC GROUP

EERC EARTHWORKS ENGINEERING RESEARCH CENTER

IOWA STATE UNIVERSITY

Embankment/Pavement Foundation Layers

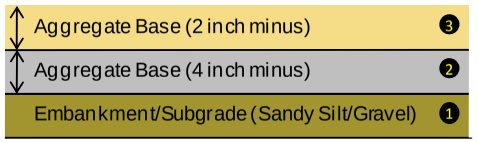

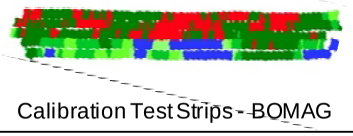

Calibration Test Strips - BOMAG

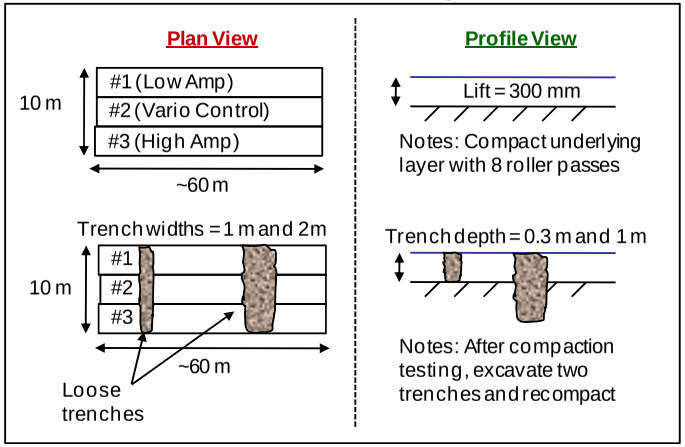

Calibration Test Strips - CAT

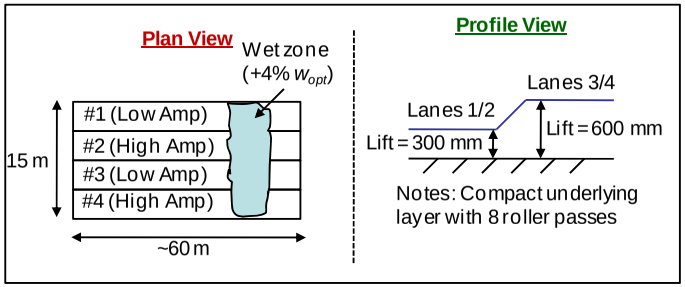

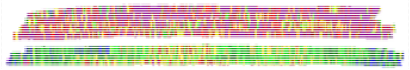

Date	TB	Machine	Amp (mm)	Spot Tests	Notes/Comments
05/17	ISU arrives at site to setup mobile lab (2pm) Setup BOMAG/CAT rollers and make trial runs with GPS (3pm) Meet with Contractor and identify potential test areas (4pm) Collect material samples for on-site laboratory characterization (5pm)				
05/18	1	BOMAG (smooth)	0.7, 2.0 Auto	DCP, LWD, NG, PLT, BCD(?)	**10 m x 60 m calibration test area.** 1. Compact foundation layer with 8 roller passes and map. 2. Place one 300 mm loose lift of silty gravel over area 3. Compact in three lanes using low, high, and vario control – 10 passes + 3 mapping passes 4. Develop compaction curves 5. Excavate trenches and repeat compaction
	2	CAT (smooth)	TBD	DCP, LWD, NG, PLT, FWD	**Roller mapping in production areas** of embankment and aggregate base. Monitor existing practice and perform in-situ tests for comparison. Use data for test run on IC QA specification.
05/19	3	CAT (smooth)	0.9 1.8	DCP, LWD, NG, PLT, BCD	**15 m x 60 m calibration test area.** 1. Compact foundation layer with 8 roller passes and map. 2. Place 300 mm loose lift of silty gravel over a area for lanes 1/2 and 600 mm loose lift lanes 3/4. 3. Create wet spot (+4%) 15 m x 10 m 4. Compact in four lanes using low and high 10 passes + 2 mapping passes 5. Develop compaction curves
	4	BOMAG (smooth)	TBD	DCP, LWD, NG, PLT, FWD	**Roller mapping in production areas** of embankment and aggregate base. Monitor existing practice and perform in-situ tests for comparison. Use data for test run on IC QA specification.
5/20 to 5/22	5/6	BOMAG (smooth)/ CAT (Smooth)	TBD	DCP, LWD, NG, PLT, FWD	Production compaction **areas** of embankment and aggregate base. Multiple lifts.
05/21	Open House –presentation of preliminary results and roller demonstrations.				

Notes:
A. Moisture condition calibration test strip areas ± 1.5% optimum except as noted.
B. NYSDOT assistance requested for FWD testing and information on project QA testing requirements.
C. As time permits repeatability passes for roller will be performed on embankment and aggregate base.

ISU Research Team Contacts:
David J. White, Associate Professor, djwhite@iastate.edu, (515) 290-1080 (cell)
Heath Gieselman, Assistant Scientist, giese@iastate.edu, (515) 450-1383 (cell)

NYSDOT - Project Goals

1. Document impact of variable feedback control on compaction uniformity
2. Document machine vibration amplitude influence on compaction efficiency
3. Evaluate impact of lift thickness on IC roller values and compaction efficiency
4. Develop correlations b/w IC roller values to traditional measurements
5. Study IC roller measurement influence depth
6. Compare IC results to tradition compaction operations
7. Study IC roller measurement values in production compaction operations
8. Evaluate IC measurement values in terms of alternative specification options